The University Of Sheffield.

DESIGN AND REAL TIME CONTROL OF A VERSATILE SCANSORIAL ROBOT

by

Mohd Abdul Hadi Hassan

A thesis submitted to The University of Sheffield for the fulfilment of the degree of

Doctor of Philosophy

Department of Automatic Control and Systems Engineering
The University of Sheffield
Mappin Street
Sheffield, S1 3JD

June 2016

Dedication

Every challenging work requires self-efforts as well as guidance of the elders especially those who were very close to our heart.

My humble effort I dedicate to my loving family

Father & Mother

Whose affection, love, encouragement and prays of day and night make me able to get such success and honor,

Along with all hardworking and respected

Lecturers

ABSTRACT

This thesis presents investigations into the development of a versatile scansorial mobile robot and real-time realisation of a control system for different configurations of the robot namely climbing mode, walking mode and steering mode. The mobile robot comprises of a hybrid leg and wheel mechanism with innovative design that enables it to interchange its configuration to perform the specific tasks of pole climbing in climbing mode, walking and step climbing in walking mode, and skid steering and inclined slope climbing in steering mode. The motivation of this research is due to the surrounding environment which is not always structured for exploration or navigation missions, and thus poses significant difficulty for the robot to manoeuvre and accomplish the intended task. Hence, the development of versatile scansorial robot with a flexible and interchangeable configuration can provide a broad range of applications and locomotion system and to achieve the mission objective successfully.

The robot design consists of four arms/legs with wheel attached at each end-effector and has two link manipulation capability. In climbing mode, the arms are configured as grippers to grip the pole and wheels accelerate to ascend or descend. The climbing angle is monitored to retain the level of the robot while climbing. However, in walking mode, the arms are configured as legs and the wheels are disabled. By implementing a periodic walking gait, the robot is capable of performing stable walking and step climbing. In steering mode, the arms are configured as suspension and the wheels are used for manoeuvring. In this mode, the skid steering system is used to enable the robot perform the turn.

The versatile scansorial robot's configurations and locomotion capabilities are assessed experimentally in real time implementation using the physical prototype. The experiments provided demonstrate the versatility of the robot and successfully fulfill the aims and objectives of the research.

ACKNOWLEDGEMENTS

First and foremost, I would like to express my gratitude and appreciation to my supervisors, Dr.M. Osman Tokhi for his invaluable guidance, assistance and support throughout the research. The level of supervision provided was exceptional, remarkably supportive and understanding during my regular academic activities as well as outside. I sincerely thankful and indebted to him for giving me the opportunity to work under his supervision.

I would also like to extend my gratitude to the current and previous Dr. Osman Tokhi's students for their support either physical or moral values to keep the momentum throughout this research process.

The financial support from Ministry of Higher Education (MOHE) in Malaysia is gratefully acknowledged. Their support has enable me to pursue my research interest to this point.

Special thanks to my parent for believing in me to further my education. Their endless trust, support and encouragement as well as advices help me to continue this journey away from home.

Table of Contents

List of Figures

List of Tables

Nomenclature

Terminology	*Description*	*Units*
θ_s	Incline slope angle	*rad*
β_i	Walking gait duty factor	
ϕ_{wi}	Walking gait transfer phase	*rad*
g_w	Walking gait	
l_0	The length of the zero link	*m*
l_1	The length of the first link	*m*
l_2	The length of the second link	*m*
W_{SR-X}	The width of the robot	*m*
H_{SR-X}	The height of the robot	*m*
L_{SR-X}	The length of the robot	*m*
m	The mass of the robot	*kg*
θ_1	Angular position of the first link to the positive Z axis	*rad*
θ_2	Angular position of the second link to the positive Z axis	*rad*
$\dot{\theta}_1$	Angular velocity of the first link to the positive Z axis	*rad/sec*
$\dot{\theta}_2$	Angular velocity of the second link to the positive Z axis	*rad/sec*
θ_{1R}	Angular position of the right first link to the positive Z axis	*rad*
θ_{2R}	Angular position of the right second link to the positive Z axis	*rad*
θ_{1L}	Angular position of the left first link to the positive Z axis	*rad*
θ_{2L}	Angular position of the left second link to the positive Z axis	*rad*
q	Generalised coordinate position of SR-X	*m*
F_x	The tractive force at the contact point of the wheel	*N*
F_y	The lateral force at the contact point of the wheel	*N*
R_x	The longitudinal resistive force of the wheel	*N*

M_r	The resistive moment around COM	*kg.m²*
W_s	The distance between centre of left and right wheels	*m*
μ_x	The friction coefficient on X axis	
μ_y	The friction coefficient on Y axis	
L	The distance between centre of front and rear wheels	*m*
a_s	The distance between centre of front wheels and COM	*m*
I	The moment inertia of the robot	*kg.m²*
$\ddot{\phi}$	Angular acceleration of the robot at Z axis	*rad/sec²*
τ	The actuator torque	
λ	Lagrange multiplier for nonholonomic constraints	
r	The radius of the wheel	*m*
v_1	The linear velocity in skid steering	*m/sec*
v_2	The angular velocity in skid steering on Z axis	*m/sec*
K_p	The proportional gain	
K_i	The integral gain	
K_d	The derivative gain	
t	The simulation time	*sec*
t_f	The final simulation time	*sec*
θ_{1f}	Final angular position of the first link on Z axis	*rad*
θ_{2f}	Final angular position of the second link on Z axis	*rad*
N_i	Normal force at the contact point	*N*
T_i	Tangential force at the contact point	*N*
C_i	Contact point between two surface	
g	The gravitational acceleration	*m/sec²*
θ	The tilt angle on Y axis	*rad*
θ_w	The foot trajectory walking angle	*Rad*
h_w	The foot trajectory path height	*cm*

v_L	The angular velocity of left wheel	*m/sec*
v_R	The angular velocity of right wheel	*m/sec*
q_r	The desired position of the steering trajectory	*m*
k_{Rp}	The proportional gain for right wheel	
k_{Ri}	The integral gain for right wheel	
k_{Rd}	The derivative gain for right wheel	
k_{Lp}	The proportional gain for left wheels	
k_{Li}	The integral gain for left wheel	
k_{Ld}	The derivative gain for left wheel	

CHAPTER 1

Introduction and Literature Review

1.1 Introduction and Motivation

Mobile service robotics has a number of applications where robustness and flexibility are the domain requirements (Sahin, 2005). A robot in this sense is designed to fulfil various kinds of tasks. In the past few decades, significant amount of research has been done in this field. To this date, a variety of mobile robots with various applications have been developed to assist humans in their daily tasks. Due to the capability of mobile robots to work around the clock, they are deployed in various places such as office buildings (Nieto-Granda et al., 2014), hospitals (Calderon et al., 2015), department stores (Ahn et al., 2013) and so on. Some of them have interactive service systems for example in applications such as entertainment and education (Murphy et al., 2015).

Over the past few years, mobile robots have been actively developed to perform tasks in diverse environments. Some environments can be dangerous and hazardous for human to carry out the tasks. Therefore, there is a need for the mobile robot to give support and assistance to perform the tasks in such environments. Recently, scientists have sent mobile robots (Figure 1.1) on exploration and navigation missions to other planets (NASA, 2009). The robots are also being used in high-risk missions such as law enforcement, military applications, nuclear radioactive site, surveillance and maintenance (Kim et al., 2010; Robotics Online, 2011). In order to execute the missions successfully, the mobile robot needs to be adaptive to manoeuvre on different types of terrains such as steps, stairs, steep hills, ditch and other unknown obstacles.

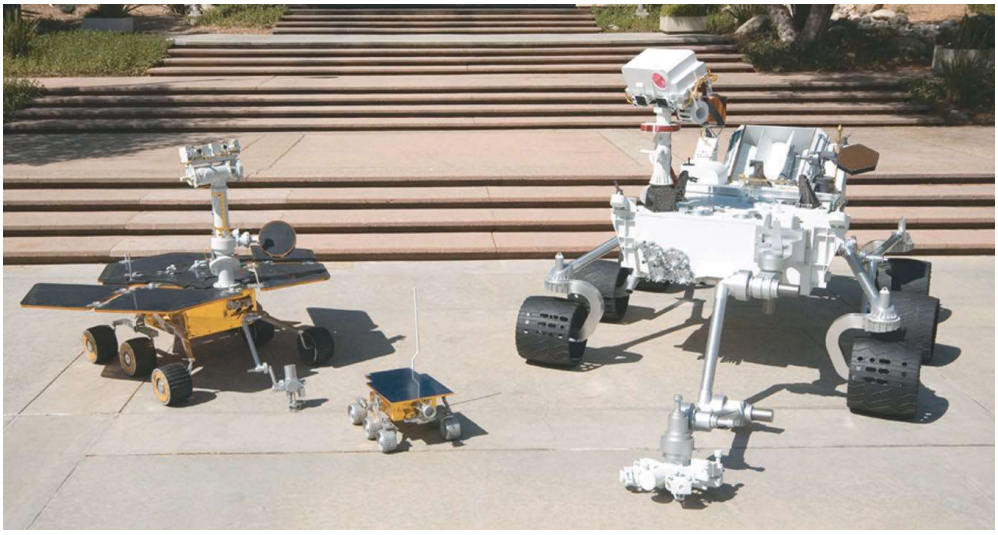

Figure 1.1: Mockups of the current family of Mars rovers: (centre) 1997 Mars Pathfinder vehicle, (left) 2004 Mars Exploration Rover vehicle, and (right) 2009 Mars Science Laboratory vehicle. (NASA, 2009)

The ability to move from one place to another with manoeuvrability is known as locomotion. It is the most basic and important aspect in robotics. In order to enable the mobile robot to move around in an unstructured environment, the form of locomotion utilised by the robot must first be carefully selected. The selection of locomotion type on basis of the environment or terrain is crucial for achieving optimum performance of the robot. Poor selection may cause significant failure for the robot to complete the task appointed. The combination of manoeuvrability and climbing makes the robot operation even more complex. A locomotion that works on defying the gravity force poses further challenges and requires the dynamics of the robot to cope with the current situation while performing the task.

In this research, the environments that are taken into consideration for the robot to perform the task are pole, step and slope surfaces. Those surfaces require the robot to implement vertical climbing for pole, step-by-step climbing for step/stair and ramp surface climbing. Therefore, a unique design that enables the robot to perform with multiple locomotion in various environments is essential.

1.2 Literature Review

Over the past few years, various designs of scansorial robots have been developed for irregular terrains and unstructured environments. The type of terrain is the main aspect that needs to be identified before the robot design process takes place. Basically, the robot design has to satisfy the surrounding environment in order to implement the locomotion properly. For instance, if the robot is designed to only climb the stairs, it is unlikely for the robot to perform pole climbing.

In addition to environment based design considerations for a climbing robot, the selection of the climbing mechanism is a further important aspect to consider. A review of the climbing mechanisms is presented in the next section and description of a suitable mechanism for the work in this project is given.

1.2.1 Climbing Robot Mechanism

The development of suitable adhesion mechanism to ensure that the robot stays on the surface during climbing manoeuvres is a central consideration in the design of a climbing robot. Previous studies have investigated four types of adhesion techniques: 1) vacuum or suction cups; 2) magnetic device for ferromagnetic surfaces; 3) gripping to the surface; 4) biomimetics inspired by the climbing animals.

1.2.1.1 Suction Forces

Passive Suction Forces

The most general adhesion mechanism for climbing robot is using vacuum suction to produce a suction force toward the surface. The vacuum adhesion mechanism is easy to control. This mechanism allows the robot to climb over arbitrary surfaces with different types of materials and allows the utilisation of different implementation strategies. More than one vacuum cup is commonly used to avoid pressure loss due to surface irregularities (Yushida et al., 2010). Figure 1.2 shows multiple vacuum cups used as adhesion mechanism for climbing.

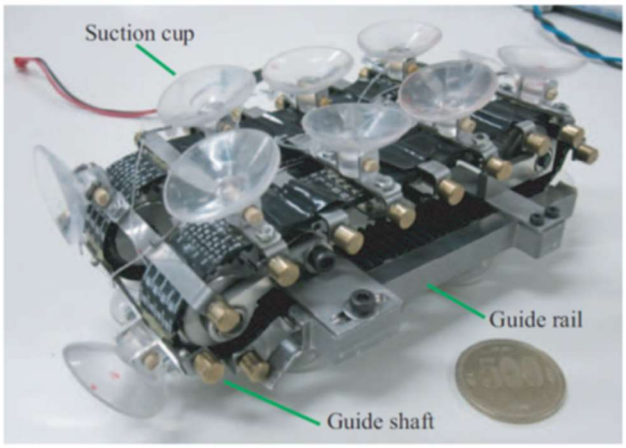

Figure 1.2: Climbing robot using suction cups (Yushida et al., 2010)

Zhu et al. (2002) designed a Cleanbot II using passive suction adhesion mechanisms for climbing. The robot deployed 52 suction cups to achieve continuous movement with maximum speed of 10 *m/min*. It is also capable of carrying a maximum payload of 25 *kg*. Zhang et al. (2007) developed Sky Cleaner 3 with the same adhesion mechanism with high payload capability of 60 *kg* and maximum travel speed of 650 *mm/s*. Kawasaki and Kikuchi (2014) developed a small legged robot with passive suction cups with just 34 *g* in weight and capable to climbed at 2.2 *cm/s*. A modular Caterpillar robot designed by Wang et al. (2009) used Unsymmetrical Phase Method (UPM) to generate reliable adhesion of the passive suction cups. Qian et al. (2006) has reported a glass-wall cleaning robot that uses vacuum suction cups as adhesion mechanism.

The weakness of climbing robots with passive suction adhesion is that the sealing of suction cup has to be perfect and it is time consuming to produce adhesion locomotion. Therefore, the robots can only manoeuvre at low speed on smooth and non-porous surfaces. Therefore, the adhesion mechanism has a significant limitation in terms of its application.

Active Suction Forces (Vortex force)

Another adhesion mechanism for climbing robot is the use of propeller to create an aerodynamic principle (Nishi and Miyagi, 1994). Longo and Muscato, (2006) designed ALICIA robots that use active suction adhesion mechanisms for climbing. ALICIA 2 has the capability to carry a payload of up to 15 *kg* in vertical direction at

a maximum travel speed of 2 *m/min*. A City-Climber robot uses has been reported that vortex force to climb the wall (Xiao et al., 2005; Elliott et al., 2007). The vortex force uses the principle of "tornado in a cup". The City-Climber robot has a robust adhesion force and high manoeuvrability by combining suction and aerodynamic attraction. It can carry additional payload of 4.2 *kg* on a brick wall. Figure 1.3 shows the City-Climber performing the climbing task on an irregular surface.

Figure 1.3: City-Climber using vortex force for adhesion (Xiao et al., 2005)

The drawback of using the vortex force is that its power consumption and noise level are high in certain applications; for example surveillance duties.

1.2.1.2 Magnetic Force

Magnetic adhesion is adopted for applications where the surface allows the adhesion force to be implemented. Magnetic attachment can be very beneficial due to its intrinsic dependability. Furthermore, the technique can create high speed locomotion but it requires heavy actuators. Despite that, magnetic attachment is functional only on ferromagnetic surfaces, and hence the mechanism will be limited to such applications (Menon et al., 2004). Permanent magnets or electromagnets have been used for climbing huge steel structures for non-destructive testing (Howlader et al., 2015) with high capacity payload of 19 *kg* and maximum adhesion forces of 205 *N*. Wang et al. (2014) develop a lightweight robot of 700 *gram* in weight for steel bridge inspection .

Leon-Rodriguez et al. (2012) have reported a mechanism which uses permanent magnets for attachment to ferromagnetic surfaces and wheels for the robot to manoeuvre. One of the benefits of this method is that energy consumption is relatively low for the adhesion (Guo et al., 2015). Furthermore, the use of magnetic wheels allows adhesion and manoeuvring on the surface at the same time (Tavakoli et al., 2013). Figure 1.4 shows an example of magnetic wheeled pipe climbing robot. It has high mobility on a ferromagnetic surface; however it can only climb a certain range of diameter of the pipe with minimum radius of 150 *mm*.

Figure 1.4: Omniclimber, magnetic wheeled climbing robot (Tavakoli et al 2013)

The main drawback to this adhesion mechanism due to the nature of magnets is that applications are restricted to ferromagnetic surfaces.

1.2.1.3 Biomimetic Inspired Adhesion Force

There has been significant amounts of studies carried out on animal behaviours in climbing surfaces so as to mimic their adhesion mechanisms. Research on gecko foot has inspired gecko climbing robots such as Waalbot II used fibrillar adhesives at Carnegie Mellon University (Murphy et al., 2011) and StickyBot at Stanford University (Kim et al., 2007; Santos et al., 2007). These robots operate by using the dry adhesive properties of gecko foot and successfully achieve the climbing (Figure 1.5).

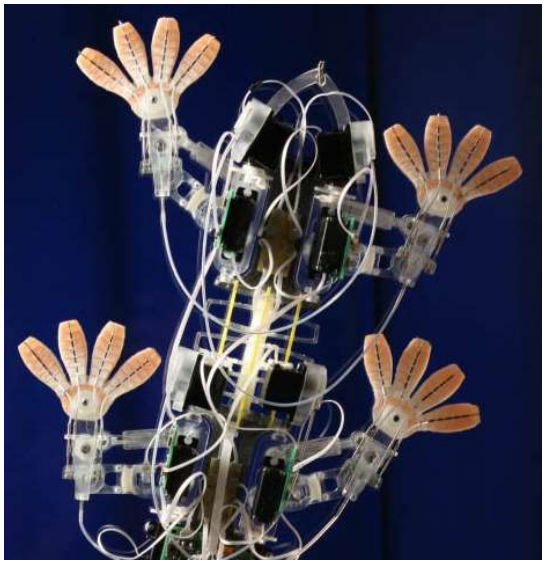

Figure 1.5: Gecko inspired climbing robot (Kim et al., 2007)

The challenge of developing the gecko foot hair is that it should be able to withstand rough handling, self-cleaning and to create a strong dry adhesive force to overcome large payloads. Further climbing inspirations from animals such as insects based on microspines have successfully been realised for bio-inspired climbing robots. Examples include SpinyBot and RiSE robot developed at Stanford University (Asbeck et al., 2006; Clark et al., 2007; Kim et al., 2005). The robots have capability to climb irregular surfaces such as concrete and brick. However, the robot has limitation for even surfaces in the absence of footholds.

1.2.1.4 Gripping on the Surface

The earlier adhesion mechanisms are only appropriate for robots to manoeuvre on walls and ceilings. However, for irregular surfaces such as wire meshes, it is almost not possible for the robot to manoeuvre.

In order to overcome such difficulty, the robot is designed to cope with the manmade structures or through natural environments. Hence, robots with gripper have been developed for climbing applications by manoeuvring while gripping the surface. The ROMA robot (Balaguer et al., 2005) (Figure 1.6) designed with grippers to climb a manmade structure, or other unique designed gripping systems on the limbs as in (Bell and Balkcom, 2006; Inoue et al., 2006).

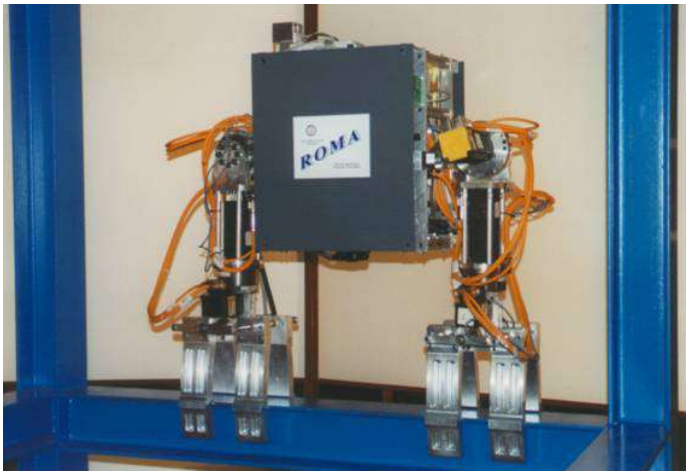

Figure 1.6: ROMA robot climbing a beam-based structure

1.2.2 Surface Climbing

Surface climbing can be divided into two categories: Climbing surface and terrain. Brick, concrete, steel, wooden surfaces fall under climbing surface category. While terrain can be further categorised into structured and unstructured terrain or environment. A flat surface is a structured surface with definite and organised conformation such as roads, rails or stairs. While unstructured terrain is a deformation structure such as fields, hills and rocky terrain.

The review of pole climbing, step climbing and slope climbing robots will be mention in following subsection due to project interest in pole, step and slope surfaces.

1.2.2.1 Pole climbing robot

Fauroux et al. (2010) has reported the design of Pobot V2 using two arms for grasping of capability to ascend poles with the cylindrical and conical shapes. The robot has capability for obstacle avoidance and passing over small collars. By manipulating the environment to create self-locking on the pole, the robot is able to climb and perform rotation around the pole. The robot can reach maximum speed of 66 *mm/s*. However, the drawback of the robot is that it suffers from slippage when it climbs over 6 meters in height. If the robot loses its self-locking position, the

possibility of falling is high and thus breaking the whole robot. Figure 1.7 shows the Pobot V2 performs the climbing task on the metal pole.

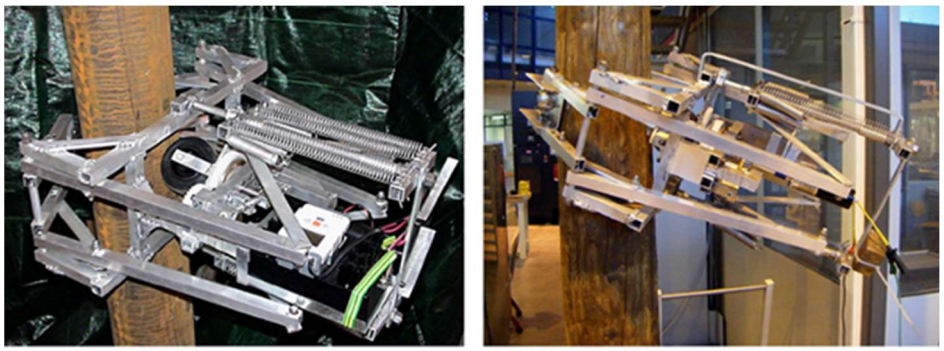

Figure 1.7: Experimental testing of Pobot (Boulevard and Renaud, 2008)

Haynes et al. (2009) has introduced the RiSE v3, which is a legged robot designed for climbing on wooden telephone poles with high speed mobility. The robot has four powerful actuated legs with claws. During the climbing, the degree of freedom (DOF) on the body is centralised to permit the robot pitch to be amended. With a flexible body as well as four actuated legs, the robot is able to climb the poles effectively due to the broad kinematic freedom and range of motion. As can be seen in Figure 1.8, the robots' legs have been designed with two degrees of freedom to allow high mobility of the robot while climbing.

The robot uses sharp claws to penetrate the wooden telephone pole. This claw design ensures a strong grip, as both the front and hind claws push downward with gravity. The claws are angled inward, and this assists in assuring a secure grip. The drawback of the robot with claw is that the probability of the claw to lose its grip is high during high speed climb.

Figure 1.8: RiSE v3 climbing robot (Haynes et al, 2009)

1.2.2.2 Steps/Stairs climbing robot

Yoneda (1987) has developed the first model of biped configuration model called "YANBO-1" that has the capability to walk on horizontal level ground as well as climb stairs. YANBO-1 has five DOF, which is considered almost minimum DOF for walking and stairs climbing robot. The research on YANBO has been continued by Ota et al. (2001a, b, 2002, 2003) with the development YANBO-2 and YANBO-3 after more than a decade. The YANBO series has similarity with ability of walking on flat surface and climbing stairs. However, the latest series of YANBO robots are equipped with two more DOF to create three ankle joint motions for improved mobility and the ability to perform manipulation. Figure 1.9 shows the YANBO series with the capability of stair or step climbing as well as manipulation.

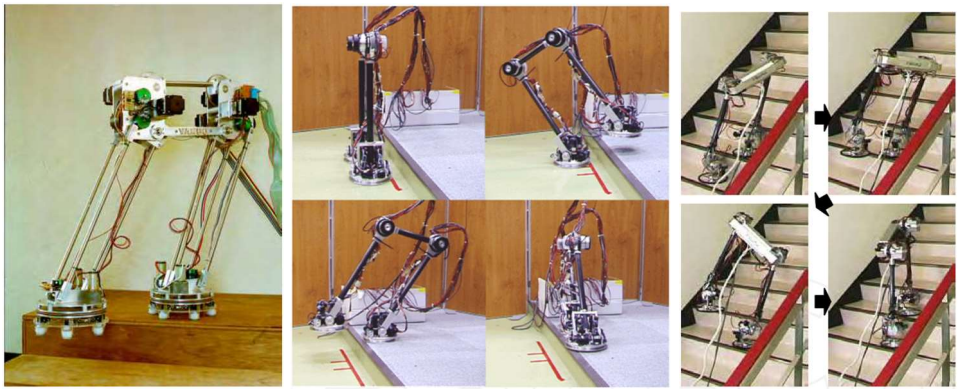

(a) (b) (c)

Figure 1.9: (a) YANBO-1 with stair climbing motion, (b) YANBO-2 with step climbing motion, (c) YANBO-3 with stair climbing motion (Yoneda et al, 2010, Ota et al., 2003)

Due to the nature of the robot design, YANBO series robot has to maintain the upper body all the time without falling over while climbing the step/stairs which consequently require longer time to perform the task. A single trajectory mistake could cause catastrophic damage because there is no other support equipped in the system.

Chen et al. (2011) has designed the leg-wheel transformable robot, *Quattroped*. This robot is designed with a unique transformation mechanism using single actuator for wheels mode and legs mode. This mechanism directly switches the morphology of the driving mechanism between wheels (full circle) and leg (combined two half circle). Figure 1.10 shows the *Quattroped* in wheel mode and leg mode.

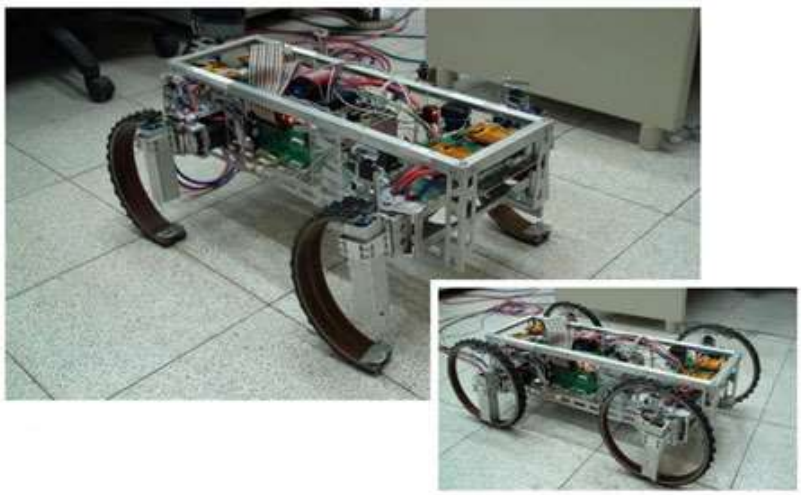

Figure 1.10: A leg-wheel hybrid mobile robot, *Quattroped* (Chen et al., 2011)

The robot is able to perform various tasks including driving and turning in wheel mode and driving, step and bar crossing, irregular terrain passing and stair climbing in leg mode. Even though the robot demonstrates excellent performance in both modes, due to the weight (14.5kg) and length (600mm), the possibility of climbing higher slope angle (> 45 degrees) beyond stairs may be impossible to be implemented.

HyTRO-I has been designed with combination of mechanically decoupled and transformable of leg and wheel mobility concepts (Lu et al., 2013). The robot has the ability to execute three motion modes: wheeled rolling, quadrupedal walking and leg-wheel hybrid mode. On the flat ground, the wheeled rolling mode is deployed for high speed manoeuvres. When the robot encounters obstacles higher than the robot itself or stairs, it transforms to quadrupedal walking mode to climb the surface. In this mode, the robot can move on rough uneven terrains by selecting stable footholds discretely, and further can climb over barriers that have vertical heights and gradients by regulating the posture to a suitable position. Figure 1.11 shows the HyTRO-I design.

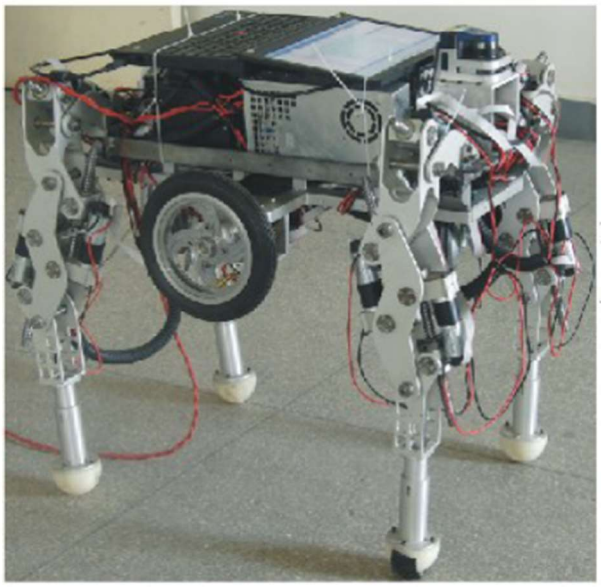

Figure 1.11: A leg-wheel hybrid mobile robot, *HyTRo-I* (Lu et al., 2013)

1.2.2.3 Slope climbing robot

YANBO-3 is a biped robot with eight DOF which is capable to walk, climb stairs and climb inclined surfaces. The three ankle joints designed in the robot allows the robot to maintain stability while climbing a slope as in Figure 1.12. The robot system uses step-by-step trajectory motion for slope climbing. This type of motion consumes a lot of energy as well as time to complete the task. Due to the inclined slope surface, the control system for the robot is much more complex in order to maintain the upright position while climbing.

HyTRo-I robot described earlier has a capability to climb steep slopes. The mode transformation of the robot permits the robot to climb the inclined surfaces in various modes i.e. wheeled rolling, quadrupedal walking and leg-wheel mode. For example, the configuration in leg-wheel mode allows the robot to climb an inclined surface by propelling the wheels with stability support from the legs. This locomotion provides high speed slope climbing as well as maintain the position on the slope without slipping downward. Figure 1.13 shows the illustration of stair and slope climbing by HyTRo-I robot.

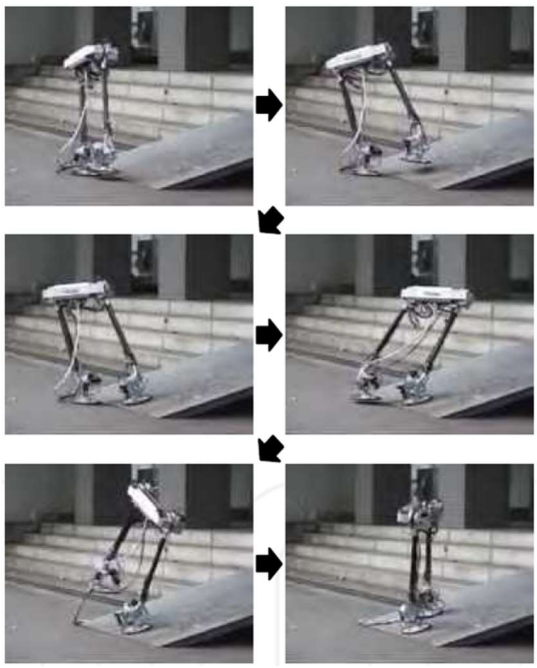

Figure 1.12: A slope climbing motion by YANBO-3 (Ota et al, 2003)

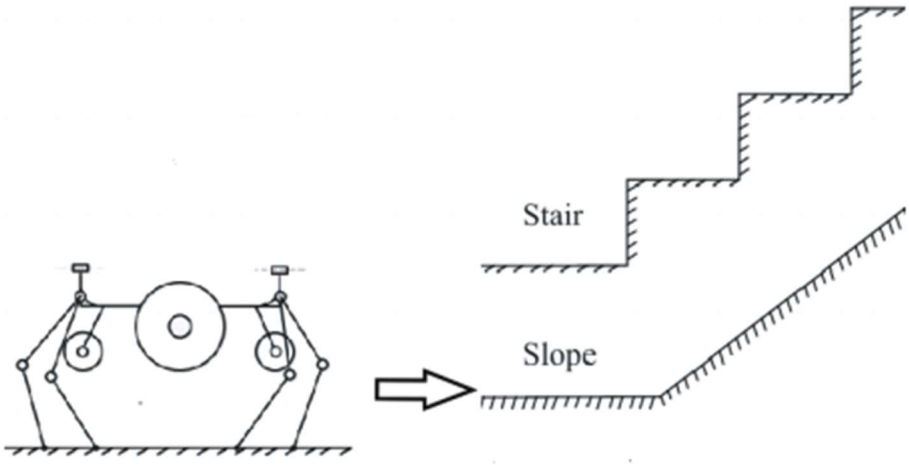

Figure 1.13: Slope climbing motion by *HyTRo-I* (Lu et al., 2013)

1.3 Statement of the Problem

Over the past few years of research in climbing robots, most of the robots only accommodate one scenario of climbing action. Due to the growing research on hybrid robots, possibilities are almost endless for the robot to perform the appointed task with different scenarios or environments. With that in mind, the design of the robot is crucial part to enable the robot to perform the task in various environments. The design of the robot has to be flexible in configuration and capable to perform multiple locomotion types in concurrence with the working surfaces.

Pole climbing is a challenging task for the robot to accomplish. In order to provide an excellent adhesion mechanism to the climbing robot, gripping toward the pole should be realised in the motion. In addition, the approach should provide a nominal force and offer significant energy saving while climbing. However, the grasping technique used in climbing robots usually incorporates grippers which definitely dependent on the surface and is time consuming. Without an effective and innovative design concept for the climbing robot, the gripping functions cannot be implemented successfully. Thus, there is a need to explore options for a new design concept that would focus on effective and efficient gripping techniques.

Step or stairs climbing imposes a different type of locomotion for the robot to be implemented. This type of locomotion is usually done by a legged robot. The robot has to climb the step or stair by using step-by-step trajectory motion. While performing the climbing task, the robot has to maintain the posture upright to avoid falling over. As a result, the performance of the robot is degraded due to the long-time consumption. Therefore, the design of the robot has to be flexible and adaptable to carry out this locomotion.

Inclined surface climbing is a further challenge for the robot to execute the climbing task. There are several types of robot that are able to implement this task, such as legged robot, wheel robot and hybrid robot. The challenge is for the robot to accomplish the task in short time. A wheel robot or a hybrid robot, for example has the ability to perform relatively faster than a legged robot. In order to achieve this, the design of the robot should be flexible to configure into those modes.

Finally, the design of the robot is the main challenge in the project in order to implement all those three different climbing task with a single robot. It has to be flexible in configuration for pole, step and slope climbing. All these tasks have to be successfully accomplished to prove the concept of versatile scansorial robot.

1.4 Research Objectives

The main aim of this work is to propose and realise a new design of scansorial mobile robot that has the capability to perform climbing locomotion in various environments, namely pole, step and slope surfaces. The aim is to increase the flexibility of the robot to work on different surfaces and is able to configure into different modes, namely climbing mode, walking mode and steering mode in conjunction with the surfaces. Ideally, the climbing mode will be used in pole climbing task, walking mode for flat terrains or step/stair climbing and steering mode for climbing on flat surfaces or slope (inclined surface) climbing.

The hypothesis of the robot design is that the interchangeability of the locomotion in accordance to the working surface will increase the functionality of the robot as well

as flexibility while working in different environments. The main objectives of this research are outlined as follows:

- Investigate the design of a versatile scansorial robot climbing task in different environments, namely pole, step and slope surfaces.
- Investigate the development of control algorithms for incorporation into the scansorial robot to perform the climbing tasks.
- Implement the developed control algorithms on an embedded real-time system platform for pole climbing in climbing mode.
- Implement the step-by-step trajectory motion for walking and step climbing task in walking mode.
- Implement the developed control algorithms for inclined slope climbing in steering mode.
- Evaluate the performance of the robot and the integrated control systems in the different climbing scenarios.

A physical prototype of the scansorial mobile robot system was developed and integrated as an experimental tool to run extensive testing to assess the robot's mobility and capabilities. The results successfully validated the hypothesis.

1.5 Contributions

The main contribution of this thesis is the design and real time control of a scansorial robot for use in various environments, namely pole, step and slope surfaces. The proposed paradigm for the mobile robot system design leads to functionality and capability that far exceeds those of state-of-the-art existing systems. The research objectives, as presented in Subsection 1.4, were achieved through the following contributions of the design, development and automation of the SR-X (the robot is named "SR-X" brief for "Scansorial Robot X").

- A new design of the scansorial mobile robot system with flexible arms that can be configured as gripper, leg or suspension for various operation modes such as pole climbing mode, walking mode and steering mode. This design approach results in a hybrid mechanism of wheeled-legged

mobile robot system that has robust design, lightweight and low production cost.

- Design and implementation of climbing mechanism for various environments such as pole, step and slope surfaces. Every environment requires a different configuration with individual climbing mechanism. For instance, climbing a pole requires the arms to work as grippers on the pole. However, for walking mode the arms are configured as legs for the robot to perform walking operation.
- Development and integration of necessary algorithms and low cost distance/proximity sensor to ensure the robot does not over climb and it avoids obstacles. The sensor will sense the obstacle distance in front of the robot. If the distance is too close, the robot will slow down and analyse the situation for next action.
- Integration of smart servo motor with daisy chain connection for communication with less wiring in the mobile robot system allowing increased system efficiency.

To achieve all the mentioned contributions, the scansorial robot has been designed so as to be flexible and reconfigured to adapt for operation in different modes.

1.6 Thesis Organisation

The organisation of the thesis reflects the sequence of steps taken through investigations for design, development and real time control of the versatile scansorial mobile robot. A brief outline of the thesis contents is given as follows:

Chapter 1: This chapter presents motivation to the research carried out in this work and the literature review of climbing robots on different surfaces. The objectives and contribution of the research are also presented in this chapter.

Chapter 2: This chapter conveys the conceptual design of climbing robot mechanism for different surfaces and the corresponding locomotion modes of operation. The walking and steering modes are also presented to ensure the final design concept accommodates the step or stairs climbing and inclined slope climbing.

Chapter 3: This chapter describes the detailed mechanical design, prototyping and assembly of the scansorial robot. From the conceptual to detailed design, Autodesk Inventor was used for 3D modelling of the designs. Using the 3D model, the length of the links were calculated and proper actuators were selected. The electronic architecture used in the robot system is also presented.

Chapter 4: This chapter presents the kinematics and dynamics of the robot system. The workspace analysis for pole climbing, step/stairs climbing and inclined slope climbing are also presented in this chapter.

Chapter 5: This chapter describes the path planning and control system for the robot system. The implementations of the robot configurations are presented in different locomotion modes.

Chapter 6: This chapter presents the real-time implementation of the scansorial robot in different modes. The experimental setup and results that corroborate the hypothesis of the research are discussed. The setup includes pole climbing, step climbing and inclined slope climbing. The results show the mobility and versatility of the robot for different setup scenarios.

Chapter 7: This chapter concludes the thesis with remarks and achievements. Recommendations for future work in this area of research are presented.

1.7 Publication

Hassan, M. A. H., Tokhi, M. O. (2013), Object grasping with dual robot manipulator using genetic algorithm. The 16th International Conference on Climbing and Walking Robots and the Support Technologies for Mobile Machines (CLAWAR 2013), University of Technology, Sidney, Australia, 14 - 17 July 2013.

Hassan, M. A. H., Tokhi, M. O. (2015), Design and implementation of a scansorial robot. The 18th International Conference on Climbing and Walking Robots and the Support Technologies for Mobile Machines (CLAWAR 2015), Zhejiang University, HangZhou, China, 6 – 9 September 2015.

1.8 Summary

A review of the literature on various climbing mechanisms and climbing surfaces of scansorial robots has been presented. The objectives of the research that has been have been established in line with motivations from the versatility of a hybrid leg-wheel robot and it functionalities.

CHAPTER 2

Conceptual Design

2.1 Introduction

The design process comprises a series of steps realising an identified idea into a functional product. Figure 2.1 shows general systematic approaches of the design process. A series of steps in the design process have to be completed in order to ensure the final product reaches the customer expectation.

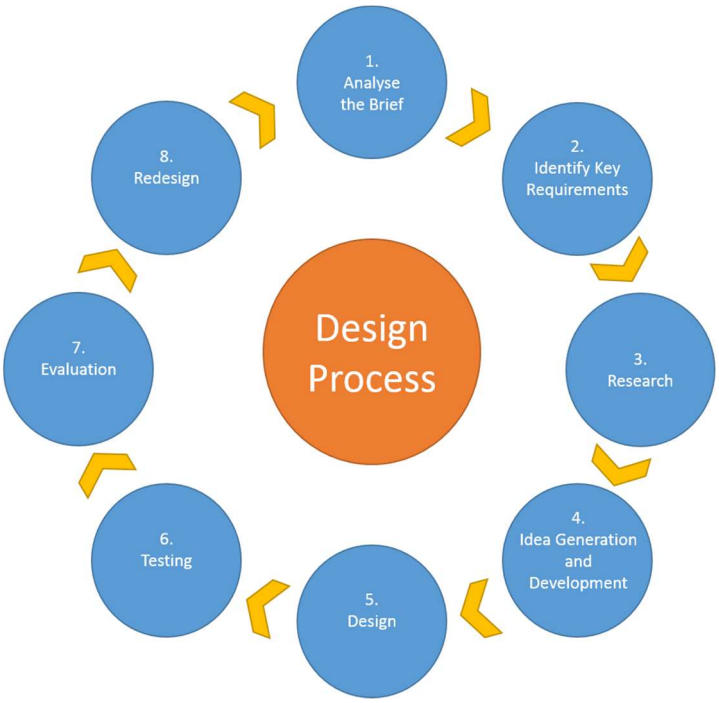

Figure 2.1: A systematic approach to design process

In this chapter some of the conceptual design ideas proposed in the project are presented. Taking into consideration the versatility of the scansorial robot, the previous concepts and various designs of the scansorial robot are studied.

As the conceptual design is the first phase of designing the scansorial robot, all objectives of the project are not taken in account. This is due to not restricting the possible innovative designs which might be adaptable to fulfil the requirements of the project with some changes.

2.2 Conceptual Designs

The term scansorial or climbing is not limited to climbing a wall, pole or other 90 degrees surface from the ground or horizontal surface. Any surface above the ground surface can be considered as a climbing surface such as step, stairs or steep surface. As the project is about a versatile scansorial robot, a few surfaces such as pole, step and steep slope are considered in this project. In this section a short overview of the proposed design is presented. Each may demonstrate the concept of individual surface climbing task that is required for final design of the robot.

2.2.1 Pole climbing design concept

Pole is a rounded, slender and long structure made of wood or metal and usually used to support something with one end placed in the ground. Pole climbing robot requires a special design to implement the climbing task. Realised from the motivation and adhesion mechanism, the most appropriate mechanism that can be used for pole climbing robot would be gripping or grasping on the surface as the pole is a man-made structure.

2.2.1.1 Grasping and multi-fingered manipulation

Multi-fingered manipulation has a significant relationship with legged locomotion. The robot hand grasps an object while a legged robot "grasps" its environment. There is a similarity between robot's fingers and legged robot on grasping object or environment by repositioning its fingers or legs. The relation between multi-fingered and legged robot also exists in climbing robot with multi-limbed.

The grasping process uses a force-closure to clutch the object. The grasp achieves force-closure if forces and torques applied to the object are resisted (Bicchi et al, 2000). In order to achieve the closure of an uninformed object, the least number of fingers are required. Various models of contact have been studied by Mason et al. (1997) and Rimon et al. (1996). However, a climbing robot, it must resist the gravity instead of achieving the force closure. Moreover, the robot must remain in

equilibrium when performing the climbing task due to the centre of the mass (COM) will be changing. In contrast with multi-fingered robot, the object has to remain in equilibrium while repositioning the finger, but its COM remains the same.

In designing the climbing robot, the COM is the main aspect to be considered. The essential aspect that will affect the drive force and the stability of the robot is the location of the COM. Moreover, for climbing, the climbing force can be improved by placing the COM closer to the pole. Simple climbing locomotion that is stated with grasping is established to emulate the motion of the COM of the arm from which values of the climbing locomotion are obtained. Figure 2.2 shows the tripod climbing design concept.

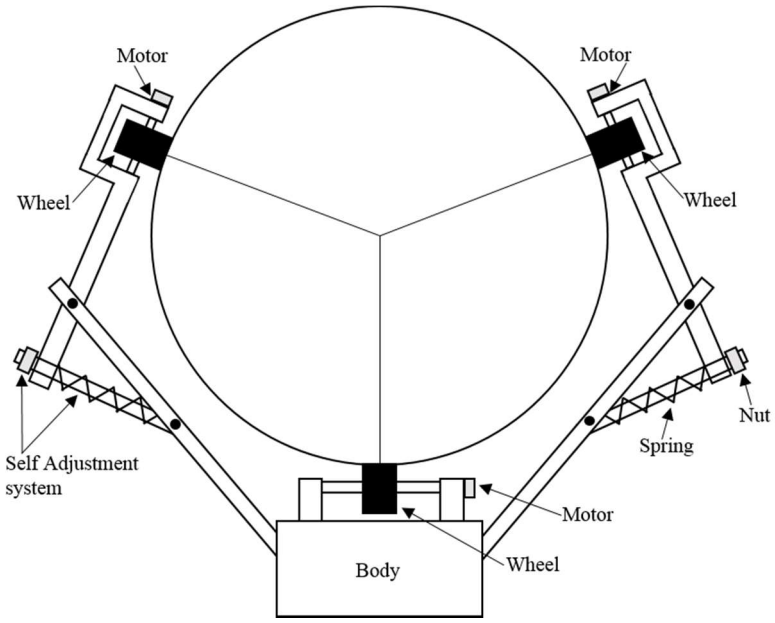

Figure 2.2: Tripod climbing concept

The gripping action in Figure 2.2 can be achieved from a self-adjustment system where the springs will push the arms toward the pole to create the grasp around the pole. Then, the climbing action for the tripod is done by the driven wheels. The main benefits of this concept are simplicity, modularity and high speed. However, this design of the robot may only perform one particular task which is pole climbing and may not be able to climb on other surfaces.

2.2.2 Step climbing design concept

Another possibility of scansorial term is performing step or stair climbing. This type of climbing can be achieved by a legged or wheeled robot (Liu et al., 2005; Miyanaka et al., 2007; Stoeter et al., 2002; Tanaka et al., 2006; Yim et al., 2000). In case of an irregular terrain, legged robots perform high mobility compared with wheeled robots. In order to perform step climbing, consideration must be given to development of higher climbing ability and design of appropriate mechanical complexity as reasonable and practical as possible. Figure 2.3 shows the design concept for step or stair climbing.

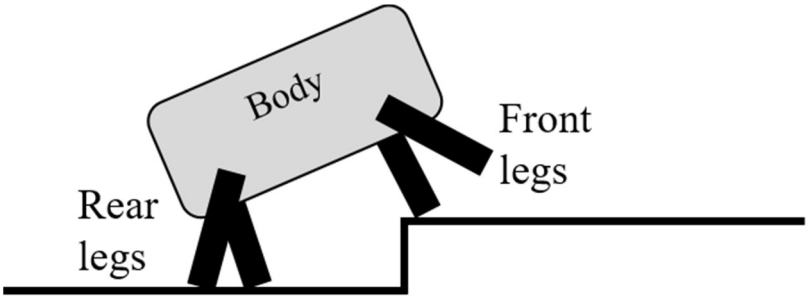

Figure 2.3: Step or stair climbing concept

A quadruped robot provides a better stability when performing step climbing. With one leg swing at a time, the other three legs support the body from falling over as long as the COM remains in the support polygon. Further explanation for support polygon will be discussed in subsection 2.4.1.

2.2.3 Sloped surface climbing design concept

Inclined slope surface is also one of the climbing surfaces for a mobile robot. Step climbing may require more time to implement the locomotion to reach the higher position, but climbing a slope takes rather less time with an appropriate locomotion mode. For inclined slope climbing, there are three types of robot that can perform the climbing task i.e. legged robot, wheeled robot and hybrid robot (Botelho et al., 2008; Duan et al., 2006; Lu et al., 2013). Due to the nature of the surface itself which is flat inclined slope, the wheeled robot performs the climbing task much better and quicker

to a legged robot in comparison. Figure 2.4 shows the conceptual design of the robot for performing the slope climbing.

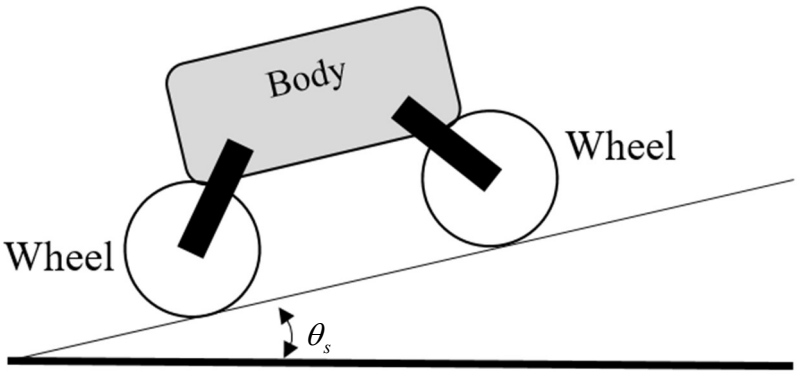

Figure 2.4: Slope surface climbing concept

The angle, θ_s, in Figure 2.4 represents the inclined slope angle of the surface. The wheels in contact with the surface create the friction force that enables the robot to climb the surface. The limitation of the inclined slope climbing is that if the angle, θ_s increases to a certain value, the friction force may reduce and the possibility of slipping will be higher. In this project, inclined slope angles of less than 30 degrees are considered.

2.3 Modes of Operation

Unstructured environment and uneven terrain are major issues for the robot in carrying the appointed task. Given the associated requirements, the locomotion of the robot has to be considered for the specific task given. With respect to the locomotion type, there are three types of locomotion that are taken into consideration: 1) Sliding Segments (Articulated body), 2) Wheel or crawler track, and 3) Leg. The hybrid type of locomotion is also considered in the new architecture to cater for the specific problems and applications.

2.3.1 Locomotion climbing surfaces using Sliding Segments (Articulated Body)

A simple mechanism to perform the climbing locomotion is sliding segments or articulated body. The most common scansorial robot that uses this type of locomotion is the robot equipped with suction cups to grab the surface. The drawbacks of such system are that it is limited to surfaces, for example, that are smooth, non-porous and non-cracked. Due to the suction adhesion mechanism, the robot requires some time to develop sufficient adhesion force and this causes delay which affects the speed of the locomotion. The worst case scenario is failure to create enough adhesion force resulting in the robot falling to the ground.

2.3.2 Locomotion climbing surfaces using Wheels

The locomotion using wheels can achieve high speed velocities. The adhesion mechanisms that can be created by wheels are suction force and friction force for scansorial robot. Similar to suction cups, the loss of pressure on the wheels equipped with suction cups may cause significant damage to the robot. For the robot using friction force to perform climbing task, the friction force generated between wheels and surfaces has to be equal to or greater than the gravitational force imposed on the robot. If the friction force is reduced while climbing, this may cause the robot to slide down and suffer a free fall damage. Another disadvantage of this type of locomotion is that the wheels have to be of certain diameter in order for the robot to perform the task on irregular terrains.

2.3.3 Locomotion using Legs

Another alternative for implementing the locomotion is the adoption of legs. Legged robots possess more advantages compared to wheeled robots such as obstacle avoidance capabilities, omnidirectional motion, variable geometry, good stability, and access to uneven terrains. Despite the benefits mentioned, such robots suffer from low speed locomotion and low energy efficiency and require complex control systems (Pedro et al., 1997). Legged robots with a larger number of legs provide redundant support increasing their payload capacity and safety on steep surfaces. However, high

number of legs lead to increase in complexity, size and weight of the robot. The control system will be more complicated to perform leg coordination.

2.3.4 Locomotion using Hybrid Leg-Wheel

Another possibility of locomotion is a hybrid locomotion by combining two or more propulsion mechanisms in achieving robust but yet flexible robot platform known as a hybrid wheel-legged robot. The locomotion offers high speed motion with wheel on flat surface and high manoeuvrability on rough terrain with leg locomotion ability. A hybrid robot of this type is an articulated robot with active internal mobility that can be used to improve stability with the wheel traction leading to global rough terrain mobility enhancement.

2.4 Climbing Mode

Climbing requires the robot to adhere continuously and ascend the surface at the same time to complete the task. In order to implement this task, the climbing motion of the robot becomes an important aspect that needs to be considered. There are two types of climbing motion namely continuous climbing motion and step-by-step climbing motion.

2.4.1 Continuous climbing concept

A pole climbing robot adopting continuous motion to ascend usually uses wheels to move along the structure. Those wheels act as a combination of both climbing mechanism and gripping module. Sara et al. (2006) have developed a wheel based nonholonomic pole climbing robot with a triangular body and six limbs. The advantage of having the wheels as climbing mechanism and gripping module is that high climbing speed is achievable. Figure 2.2 shows a conceptual robot that uses the continuous motion climbing concept.

The main advantages of continuous motion for a pole climbing robot are as follows:

- The usage of wheels provide high climbing speed.
- The design and implementation of a pole climbing robot is simple.
- The robot has possibility of modular design where wheeled modules can be connected through active or passive joints.

The main drawback are:

- Manipulation around the pole is not possible due to low manoeuvrability.
- The robot does not has the ability to pass a bent section on the pole.

2.4.2 Step-by-step based climbing concept

Step by step based climbing robot has the advantage of separate climbing mechanism and gripping modules. A minimum of two gripping modules and one form of climbing mechanism are needed for this type of robot. For this climbing concept, at least one of the grippers should grip the structure at each time while the other gripper detaches from the structure to allow the climbing mechanism extension to reach higher position of the structure. Figure 2.5 shows the concept of step by step based pole climbing robot and its climbing mechanism.

The main advantages of this concept are:

- The implementation and control of the robot are simple.
- The robot has safety and failure tolerance due to the separation of climbing mechanism and gripping modules. For example, in case of power failure the robot has the ability to maintain the last position on the structure.
- The robot is able to pass bends on the pole with climbing mechanism and gripping mechanism acting as manipulator.

The main disadvantages of such robots include:

- Due to step-by-step motion, the robot has low climbing speed.
- The robot has a low payload/weight ratio as one gripper releases the grip to make the step.

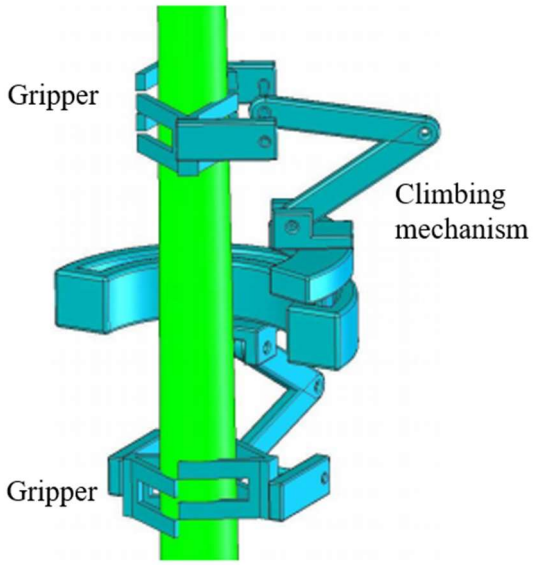

Figure 2.5: Step by step basis robot with a serial climbing configuration (Tavakoli, 2010)

2.5 Walking Mode

A robot with walking capability has a high degree of flexibility on irregular terrains. The platform allows the legs to strategically choose the contact point on the ground. This mode possesses clear advantages over wheeled mode such as obstacle climbing capability, omnidirectional motion, variable geometry, good stability, access to uneven terrain and fault tolerant locomotion (Tedeschi et al., 2014). It also has the ability to change direction without positioning the body towards the direction of motion. In addition, the legged robot can distribute the weight as well as the COM without changing the position of its supports (Arikawa et al., 2007). This advantage is desirable in cases of moving up and down a slope or stairs, or where there is a long distance between supporting objects to step on. Taking into consideration these advantages and the flexibility of robot design, it is essential to study the locomotion of the robot in walking mode.

The disadvantage of the walking mode is that the robot moves at slow speed and requires a complex control system to make sure the robot performs the task successfully.

2.5.1 Static stability and dynamic stability

Stability is a fundamental aspect of performance of the robot locomotion in walking mode. Stability is also known as balance of the robot without falling over to the ground. The fraction of time that a leg spends on the ground (duty factors) decreases to half and below with increase in speed of the robot movement (Blickhan et al., 1994). There are two categories of stability: static stability and dynamic stability.

2.5.1.1 Static Stability

A well balanced robot is said to be statically stable without falling over when it is standing. This means that the COM of the robot is within its ground contact base. The robot has the capability to create a "support polygon" in shape of triangle when one of the feet is lifted. Hence, this creates a much less stable state and if the COM shifts outside the support polygon, the chances of the robot to fall over will be high. In order to remain statically stable the robot must therefore only lift its feet in such a way that the support polygon does not shrink too much. As a result, the robot may only move a small distance (COM relative to support polygon) before it needs to modify the support polygon for the next step.

The benefit of static stability is that the demands of the control in terms of responsiveness and precision are much lower since the robot can stop at any time without requiring control for balance. Figure 2.6 shows the support polygon of a quadruped robot for achieving the static stability.

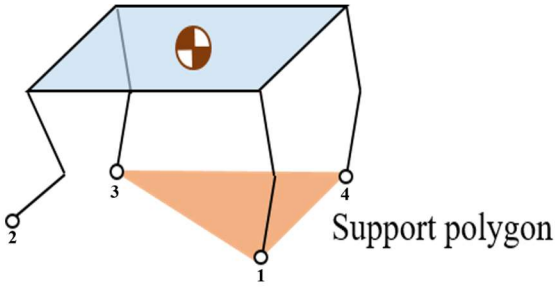

Figure 2.6: Support polygon for quadruped robot

2.5.1.2 Dynamic Stability

Dynamic stability is considered when the COM is outside of the support polygon and it requires the robot to compensate for the deviation by continuously moving to balance itself without falling over. The robot might be able to slow down or stop for a short of time, but it has to quickly counteract to avoid the COM to be outside the support polygon.

In order to realise dynamic stability, the robot requires high demand on the control. Hence, the robot has to be equipped with the following requirements:

- Equipped with sensors to measure the orientation and velocity of the robot.
- The microcontroller has to be fast enough to calculate and implement the locomotion of the limbs.
- High precision and speed in sensors measurement and counteraction of the limbs.

The advantage of this dynamic stability is that it allows the robot to rely less on the locomotion trajectory and fast action based on sensor readings.

2.5.2 Walking gaits

A walking gait is the pattern of movement involving landing and lifting of legs of a multi-legged robot to provide locomotion. The walking gait is divided into two phases: the support (stance) phase and the transfer (swing) phase. The locomotion is implemented by changing the order between support and transfer phase periodically that define the walking gait for the robot. A quadruped robot requires at least three legs for statically stable gaits and two legs for dynamically stable gaits in contact with the ground at all times (Hardt et al., 2000). The walking gait can be categorised into two types: Non-periodic gait and periodic gait.

2.5.2.1 Non-Periodic Gait

A non-periodic gait is one that does not rely on time or period to implement the locomotion. The advantage of this gait is that it can be used on an irregular terrain or unknown environment.

2.5.2.2 Periodic Gait

A periodic is gait when is the motions of the legs are implemented with same behaviour and periodically. There are a few types of periodic gait such as wave gait, crawl gait, crab-walking, turning gait, creeping gait, tripod and tetrapod gaits (Hirose, 1984). The advantage of periodic gait is that it only requires limited computation due to its repeating nature. McGhee et al. (1985a, b) have devised a structured framework for regular gait specification and analysis. They introduced the concept of a gait formula, which consists of a collection of parameters that uniquely define a periodic gait. Further explanation of the gait formula usage has been presented by Song et al. (1989) and Santos et al. (2006).

In periodic gait, the robot body is continuously in motion at constant speed that requires the sequence and timing of the steps. The simplest possible case is to step with only one leg at a time that requires specification of the step sequence. The most common gait used in walking robot is wave gait where it is moving one side of the

leg from back to front followed by the other side in the same manner. In the context of McGhee's framework, the sequence and timing are encoded by two parameters:

Duty factor (β_i): The fraction of a gait cycle that leg, i, is in contact with the ground (i.e. in the support phase).

Transfer phase (φ_{wi}): The fraction of a gait cycle by which the *placement* of the leg i lags behind the placement of leg 1. Here leg 1 is the actual physical number of the leg on the robot and not the first leg that takes a step. This mean that a transfer phase may be negative if its placement occurs before that of leg 1, or positive is it happens after leg 1.

By considering both parameters above, the simplest specification of a gait for a robot with *n* legs given by the gait formula.

$$g_w = \{\beta_1,...,\beta_n,\phi_{w1},...,\phi_{wn}\} \tag{2.1}$$

It is possible for all the legs to have the same duty factor, in which case only one value of β is specified. For instance, if a walking robot as in Figure 2.7 executes the sequence of steps (1-2-3-4) in the transverse walk with one step at a time, the gait can be distinguished (4 - 1)! = 6 different gaits. The touchdown time of leg i is measured from the touch down of leg 1 and therefore the first phase is equal to zero ($\phi_{w1} = 0$). By using $3/4$ duty factor, Equation (2.1) can be written as follows:

$$g_w = \left\{\beta = 3/4, \phi_{w1...4} = 0, \frac{1}{4}, \frac{1}{2}, \frac{3}{4}\right\} \tag{2.2}$$

Note that all legs spend the same amount of time in the support phase. Since the duty factor (β_i) and transfer phase (φ_{wi}) are dimensionless fractions of the time to implement the gait cycle, the speed of the robot is independent from any changes in the gait formula.

Equation (2.2) represents the optimal wave gait with the most crucial feature in phase three at the moment when leg 4 in contact with the ground, leg 1 initiates the lift-off

as in Figure 2.7. The statically stable condition can be achieved by choosing the possible range of duty factor ($0.75 \leq \beta < 1$).

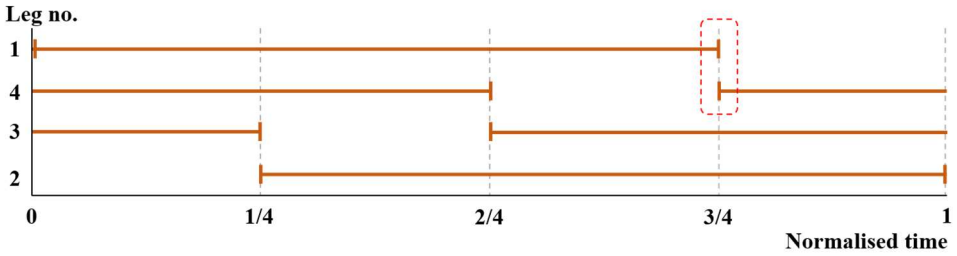

Figure 2.7: Wave gait for leg robot in walking mode ($\beta = 0.75$)

2.6 Steering Mode

Wheels have always been the choice in robots for high speed mobility. Realisation of mobility with a wheeled system is often very simple and does not require advanced control techniques or additional joints to get the robot moving. In fact, mobility with wheeled systems is the most energy efficient with regard to the speed of the robot. Such method of transverse is commonly selected for continuous surfaces with rough terrains. Wheeled systems are commonly chosen for exploration rovers due to the stability, manoeuvrability and simple control offered. Examples of robots using passive linkage mechanisms are Micro5 (Kubota et al. 2003), CRAB (Thueer et al. 2006), and Zaurus (Sato et al. 2007). Robots using active linkage mechanisms include SpaceCat (Lauria et al. 1998) and Nanokhod (Winnendael et al. 1999). Wheeled systems operate by maintaining continuous contact with the surface in order to drive the vehicle forward. They are therefore most effective on flat and even terrains where high speeds can be achieved without collision.

2.6.1 Stability

The minimum number of wheels required for static stability is two. A robot with a two wheeled differential drive can achieve stability if the COM is below the wheel axle or if there is a third point of contact striking the floor. For instance, Segway Human Transporter (Kamen, 2001) uses a two wheeled system that achieves balance

(stability) and has become a popular commercial product in the market. Under normal circumstances a wheeled robot needs at least three wheels with ground contact to achieve static stability, additionally the COM has to be completely within the support polygon, formed by the three wheels with ground contact (Roland, 2004).

A four wheeled system is the most stable considering that the support polygon is created by the wheels in each corner either in rectangular or square shaped platform. This system offers more flexibility to the robot to implement skid steering in terms of turning in differential or point turn.

2.6.2 Manoeuvrability

The crucial aspect that needs to be considered in a wheeled system is the manoeuvrability of the robot to carry out its tasks. A robot capable of moving in any direction on the ground plane (x – axis, y – axis) is classified omnidirectional. This type of mobility usually requires active powered wheels that can manoeuvre in more than one direction such as Swedish (Indiveri, 2009) or spherical wheels. However, in contrast to the omnidirectional robot, Ackermann steering configuration, is used in cars, which enable achieving the correct turning angle of steering wheels (two or four wheel drive). The vehicles that use this configuration usually have a larger turning radius than its size. Moreover, the vehicle is not able to move sideways (steering in any axis direction), and this restricts the movement especially in side parking. In order to achieve this task, the vehicle requires several parking manoeuvres consisting of repeated changes in wheel direction and forward and backward movement. This steering technique is commonly used in robotic systems, because it is simple and robust system as well as supports mobility at high speed manoeuvres (Roland, 2004)].

2.6.3 Controllability

The benefit of omnidirectional designs is that the robot is able to perform high manoeuvrability. However, this design imposes a complex and difficult control system to be implemented in the robot system. For instance, in driving a robot with four wheels on straight forward trajectory, all wheels must be driven with exactly the

same speed in order to manoeuvre in a perfect straight line. A slight error of the speed in one of the wheels will cause deviation from the desired travel path of the robot.

In comparison to omnidirectional steering, Ackermann steering has a greater advantage on simpler and easier control system implementation. For straight forward driving, the steerable wheels are locked and the motorized wheels drive the robot forward. Hence, the steering is much easier, hence a simpler control system.

Based on the considerations discussed it can be concluded that there is in general an inverse correlation between controllability and manoeuvrability. The easier the control system, it is more likely to have less manoeuvrability and vice versa (Roland, 2004).

2.7 Selection of the final design category

Three design categories for different locomotion were introduced in the last subsection. The final design should include all those three previous conceptual designs and locomotion modes to fit the objective of the project. For this purpose, the design requirements based on the objectives of the project which were discussed in the last section will comprise the following:

1. The scansorial robot should be able to perform the climbing task on pole, step and inclined slope surface.
2. The robot to be configurable into three locomotion modes based on the climbed surface i.e. climbing mode for pole climbing, walking mode for step climbing and wheeled steering mode for inclined slope climbing.
3. The control system for each configuration should be simple to implement.

From the consideration above, in order to achieve all the objectives the final design should include the leg and wheel as a hybrid robotic system. For the climbing pole, the legs (or arms) should act as a gripper on the pole while the drive wheels are used to ascend or descend the pole. For step climbing, the leg should be used for walking and the wheels should be disabled. Finally, for inclined slope climbing, the leg will be configured as a suspension for the wheels to implement the steering mode for inclined slope climbing. Table 2.1 shows the locomotion mode and associated status of the legs and wheels.

Table 2.1: Locomotion mode and leg-wheel status

Mode	Legs (Arms)	Wheels
Climbing Mode	Active	Active
Walking Mode	Active	Passive
Steering Mode	Active (Suspension)	Active

As the pole climbing robot carries the weight up during climbing, it is very important to optimise the robot design with suitable mechanism to decrease the weight of the robot. The designed robot mechanism should also have the capability to be configurable into walking mode and steering mode. Based on this fact, the designer should consider the flexible design in all steps of the design process including materials and actuators to reduce the weight and the size as much as possible. The most crucial optimisation step takes place in the conceptual design step. Hence, this early step should be considered as a critical step to ensure the objectives of the project are achievable.

2.8 The final conceptual design

To design the climbing mechanism for pole climbing robot, the COM position should be considered as well as the contact points on the pole. Multiple contact points increase the friction force generated to adhere on the pole while climbing. The closer the position of COM toward the pole, the greater fiction force generated by the contact points. Further explanation on pole climbing using friction force will be given in Chapter 4. Figure 2.8 shows an illustration of the pole climbing.

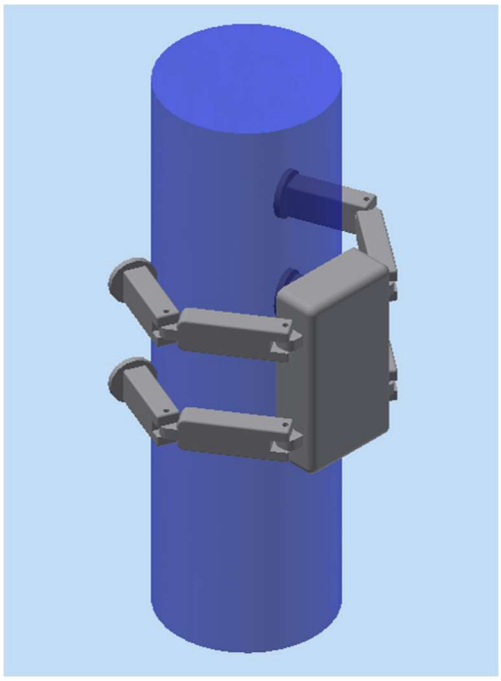

Figure 2.8: Pole climbing design concept

The arms in the robot are connected using revolute joints and the wheels contact points provide a grip using friction force between the pole and wheels. In order to create a minimum stable grip around the pole, at least three contact points are needed as in Figure 2.2. Figure 2.9 shows the top view with the third wheel on the robot's body.

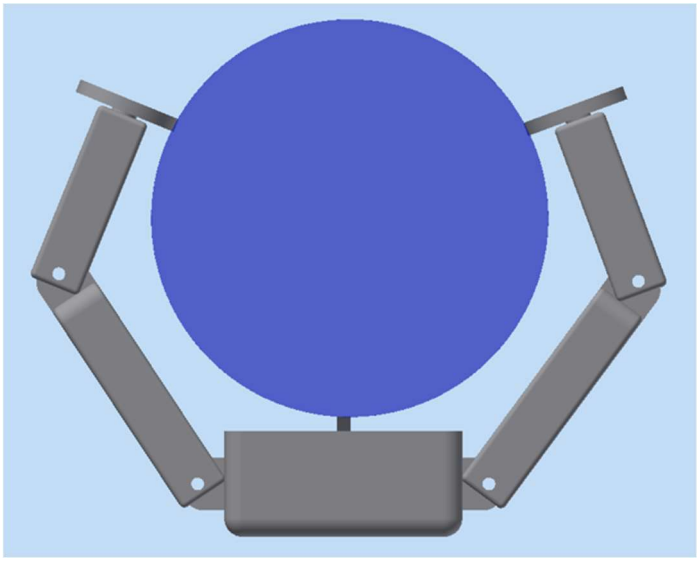

Figure 2.9: Top view pole climbing design concept

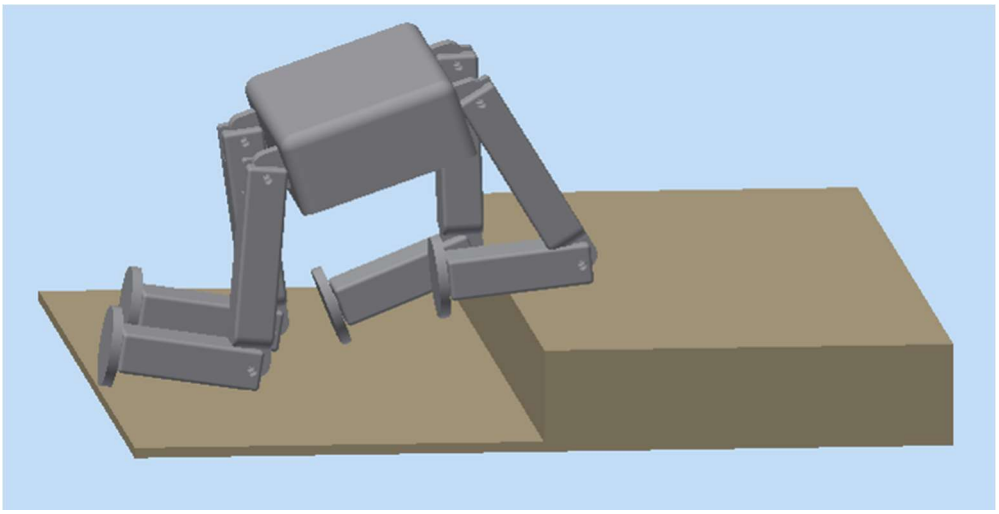

Figure 2.10: Step climbing concept

Since the arms of the robot from Figure 2.8 are configurable, it is possible to configure them to become legs in walking mode. Figure 2.10 shows the legs (or arms) configuration of the robot for step climbing. It may be possible to extend both links on the leg to make the robot stand taller. However, due to the angle restriction on link one with the body, the second link is configured as a whole foot in this mode. Further description of this configuration will be given in chapter 4. All the wheels that are attached to the robot are disabled in this mode because the orientation of the wheels face perpendicular to the forward motion.

In steering mode, the configuration of the robot is set up as in Figure 2.11. The arms (or legs) are configured as suspension and the wheels will drive the robot forward. In this configuration, the robot adopts the skid steering system due to the no steerable wheels to change the direction on the ground plane or slope surface. However, it is possible to make the turn by using differential skid steering and point turn skid steering. Further details of the skid steering will be presented in chapter 4. The wheels attached to the body are disabled in this configuration because there is no contact established between the robot and the surface.

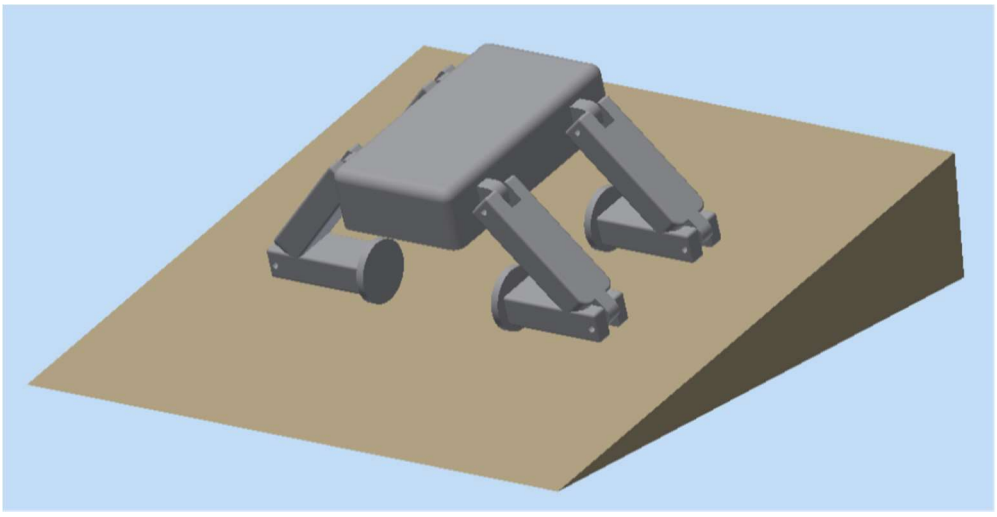

Figure 2.11: Inclined slope surface climbing concept

Based on the illustration given in Figure 2.8, Figure 2.10 and Figure 2.11, it is possible to realise multiple locomotion in a single robot given that innovative robot design is configurable into respective modes. In order to realise the conceptual design into actual robot, it is necessary to study the capability of the actuators that may be used in the system. The limitation that may occur in the hardware may prevent to achieve the objectives of the project. Further details on the hardware will be given in chapter 3.

2.9 Summary

The design and development of a versatile scansorial robot is systematically approached through the proposed conceptual design and climbing mechanism. The first phase is to ensure that all the necessary step are taken to achieve the objectives of the project by considering the gripping and climbing mechanism with different locomotion modes. The combination of a few design concepts enable the final innovative design with high flexibility to give rise for an enormous set of possible robot configurations.

CHAPTER 3

Mechanical Design, Sensors and Electrical Architecture

3.1 Introduction

This chapter describes the details of mechanical design, sensors and the electrical architecture of SR-X. Designing the scansorial robot requires hardware that is lightweight, precise and robust. The climbing robot platform consists of several servo motors, sensors, robot frames and microcontroller. This chapter will cover the hardware and electrical components of the scansorial robot.

3.2 Mechanical Design Architecture

3.2.1 3D model design of the robot

The 3D model has been designed in Autodesk Inventor Professional 2014 Student version (Autodesk, 2014). The individual parts are designed to replicate the corresponding actual hardware parts. When choosing the parts, the designer should opt from what is available in the market with appropriate budget available for the project. After a comprehensive survey of the available commercial products, the Robotis Company (Robotis, 2006) from Korea was chosen to supply the parts needed for the project. The main purpose of 3D model design is to simulate the robot with the proposed configuration modes that were discussed in conceptual design section previously without spending the money upfront. With limited budget available, this method can avoid unnecessary cost that may occur during the building of the actual hardware.

It follows from the conceptual design of the scansorial robot in chapter 2 that at least a minimum of 14 DOF are required. Each arm contains three DOF, two of which are set to joint mode and the other one is set to wheel mode. The SR-X has a total of four arms, resulting in 12 DOFs in total. Another two DOFs are set to wheel mode, and located on the robot body. An extra joint has been included in the SR-X body between upper body and lower body parts. However, in this project the joint has been set as

static to configure both body parts as one structure. Figure 3.1 shows the 3D model of the final design from front perspective view and Figure 3.2, the rear perspective view of SR-X.

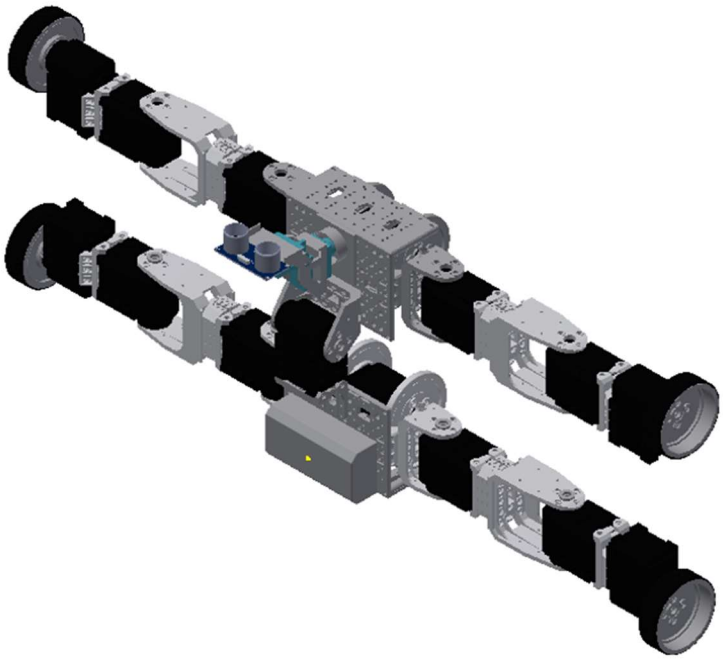

Figure 3.1: Front perspective view of SR-X design

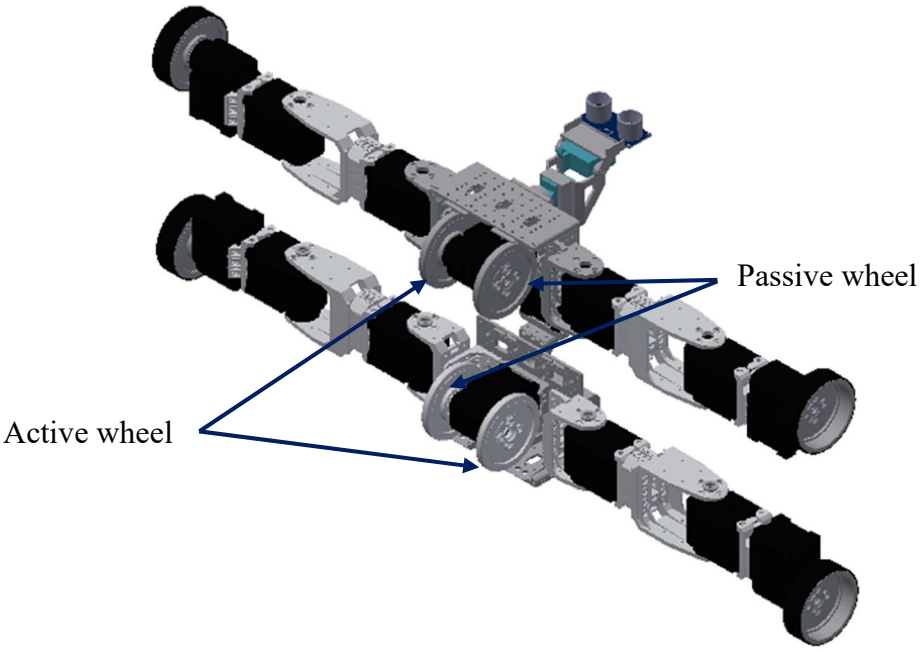

Figure 3.2: Rear perspective view of SR-X design

The design includes two identical body parts (upper and lower body) connected using servo motor as a passive joint to configure both body parts as one structure. Figure 3.3 shows the main body part of SR-X robot. Each arm has two links consisting of three servo motors two of which are set as revolute joints and the third servo motor as wheel joint. There are eight revolute joints and six wheel joints resulting in a total of 14 active servo motors in SR-X. Table 3.1 shows the dimensions of complete SR-X robot and each link length.

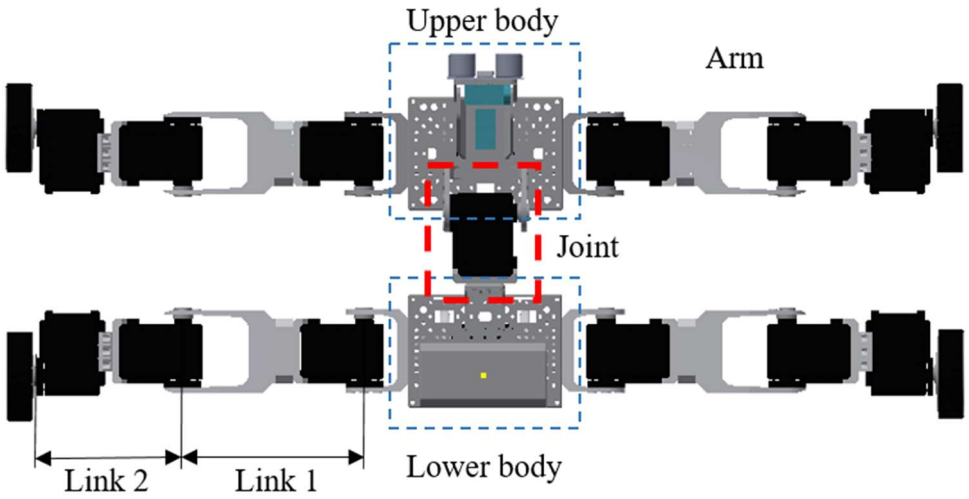

Figure 3.3. Main part on SR-X robot

Table 3.1 The SR-X design parameters' values

Sign	Description	Value
W_{SR-X}	Robot width	112.0 mm
H_{SR-X}	Robot height	181.0 mm
L_{SR-X}	Robot length	558.0 mm
l_0	l_0 Link length	28.85 mm
l_1	l_1 Link length	105.5 mm
l_2	l_2 Link length	83.50 mm
m	Robot weight	2.7 kg

3.2.2 Detailed assembly of SR-X

Along with the challenge and effort to realise the concept into feasible, simple and robust design, most of the components considered in this design are off-the-shelf components. The servo motor used in SR-X is a smart servo motor (Dynamixel AX-12A) that has a capability to configure into joint mode or wheel mode in one small package. Hence, it has significantly reduced the overall size of the robot compared to a conventional servo motor.

3.2.3 Assembly of main SR-X body

There are two body parts in SR-X, upper body and lower body as in Figure 3.3. The lower body is assembled to mirror the upper body of SR-X. The upper SR-X body consists of nine components as shown in Figure 3.4. SR-X body is designed to be symmetrical with the servo motor is mounted in the middle and the L bracket on either side of the base frame. Notice that the servo motors on the body parts contain two wheels as in Figure 3.4. Due to the nature of the servo motor (section 3.2.2) with one movable/active side, a passive wheel has to be added on the other side in order to create a symmetrical grip when implementing the pole climbing. Further explanation on this system will be presented in chapter 4. The set of components needed to assemble upper and lower body parts is listed in Table 3.2.

Table 3.2: Components of main SR-X body

Item no.	Description	Quantity
1	Base Frame	1×2
2	L bracket	2×2
3	Servo side mounting frame	1×2
4	Servo motor AX-12A	1×2
5	Bushing	1×2
6	Washer	1×2
7	Wheel	2×2

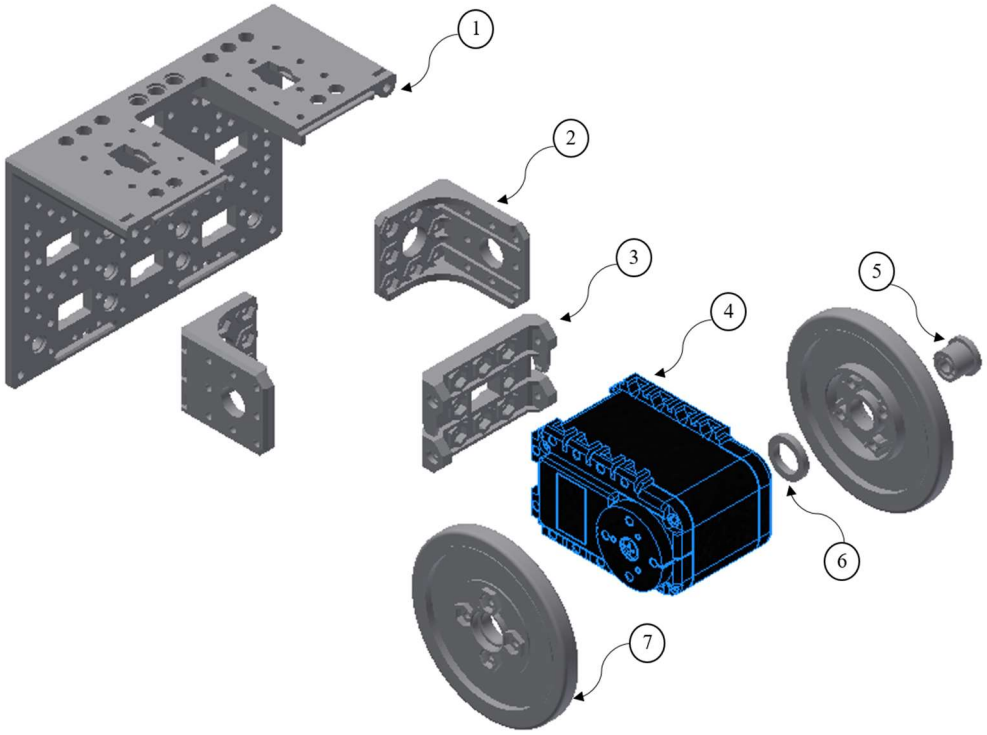

Figure 3.4: Assembly of main SR-X body in exploded view

3.2.4 Assembly of SR-X body joint

The SR-X body joint is assembled as in Figure 3.5. This joint is designed to mount the upper and lower body in place as shown in Figure 3.3. The upper body is mounted to the servo 45° frame (item no. 1 in Table 3.3) and the lower body is mounted to L bracket (item no. 6 in Table 3.3) on SR-X body joint. Table 3.3 shows the components needed to assemble SR-X body joint. The initial purpose of this joint is to provide the flexibility between upper and lower bodies. However, the joint has been set to static joint in this project for the sake of simplicity and robust control. Hence, from this point forward the SR-X body joint, upper body and lower body is considered as one big part of SR-X.

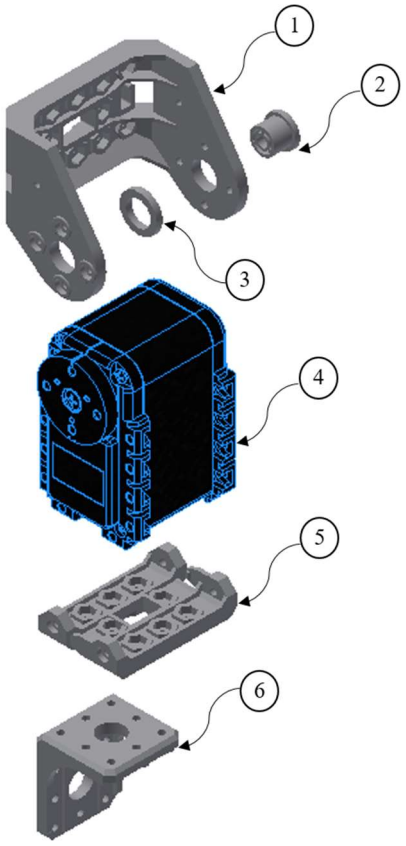

Figure 3.5: Assembly of SR-X body joint in exploded view

Table 3.3: Components of main SR-X body joint

Item no.	Description	Quantity
1	Servo 45° U frame	1
2	Bushing	1
3	Washer	1
4	Servo motor AX-12A	1
5	Servo side mounting frame	1
6	L bracket	1

3.2.5 Assembly of SR-X arm

The SR-X arm is assembled as in Figure 3.6. The arm contains three servo motors two of which are set to be revolute joints in joint mode and the third one is set to wheel mode. There are four arms in SR-X as in Figure 3.3. The total number of components used for each arm is shown in Table 3.4

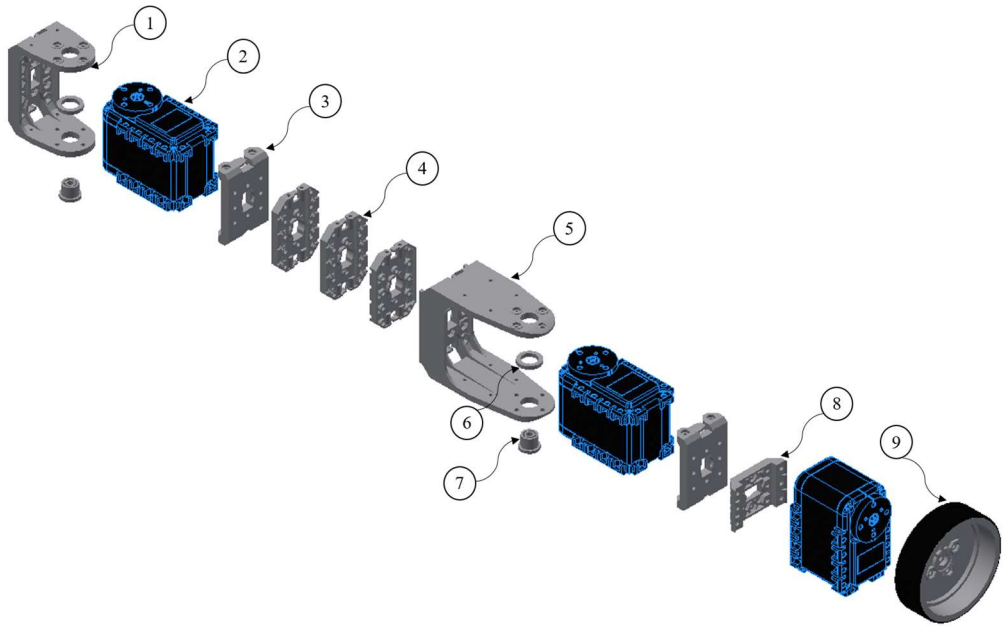

Figure 3.6: Assembly of SR-X arm in exploded view

Table 3.4: Components of SR-X arm

Item no.	Description	Quantity
1	Servo U frame	1×4
2	Servo motor AX-12A	3×4
3	Servo side mounting frame	2×4
4	Spacer	3×4
5	Servo long U frame	1×4
6	Washer	2×4
7	Bushing	2×4
8	Servo short side mounting frame	1×4
9	Wide wheel	1×4

3.3 Electrical Hardware Architecture

3.3.1 Microcontroller

The microcontroller utilised in SR-X is OpenCM9.04 B-type as in Figure 3.7. The OpenCM9.04 is an embedded board based on STMicroelectronics STM32F103CB 32 bit Cortex-M3 processor. The board has 26 I/O pins (10 input analog, 8 timer), a pair dedicated 3-pin connectors for Dynamixel XL-series, a pair dedicated 3-pin TTL Dynamixel connectors, a type-B micro USB connector, 2 2-pin connector for lithium polymer (Li-Po) batteries, JTAG header, and reset switch. The OpenCM9.04 is a platform with open-source hardware and software. Table 3.5 shows the full specification of the microcontroller.

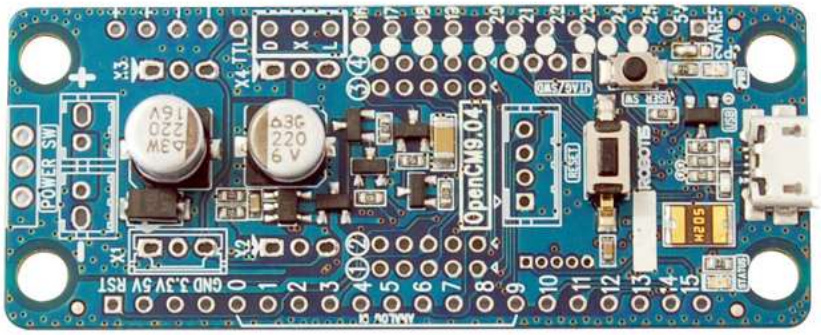

Figure 3.7: Robotis Dynamixel OpenCM9.04-B microcontroller

Table 3.5: Robotis Dynamixel OpenCM9.04-B specification

Controller Model	**OpenCM9.04-B**
CPU	STM32F103CB (ARM Cortex-M3)
Operating Voltage	7-16 V (5 V programming only over USB)
External I/O Pins	26
Timers	8
Analog In Pins (ADC)	10 (12 bit)
Flash	128 kB
SRAM	20 kB
Clock Speed	72 MHz
USB 2.0 Full Speed Ports	1
CAN	1
USART	3
SPI	2
I^2C (TWI)	2
Debug	JTAG & SWD
TTL Port (3-Pin)	4
External Sensor Ports (5 Pin)	4
Dimensions	27 x 66.5 mm
Weight	13 g

3.3.2 Servo Motor

The Dynamixel AX-12A servo actuator in Figure 3.8 is an all in a single package and consists of a reduction speed gear, a DC motor and electronics with networking functionality. The actuator has been designed with high quality of material to withstand huge external force and it also can produce high torque despite its compact size. The actuator also has the capability to sense and react to changes in internal temperature or supply voltage.

Figure 3.8: Dyamixel AX-12A servo motor (Robotis, 2006)

The servo motor has the ability to control the position and speed precisely with a 10 bits resolution. It provides feedback for angular position, angular velocity, and load torque. The servo motor has an alarm system which can warn when parameters diverge from operator defined ranges with the LED to indicate the error status. With the daisy chain connection for communication in the servo motor, it is able to use a distributed control for position, velocity, compliance and torque from the main processor to control many motors at once. The bearing used in the motor is to avoid degradation in motor efficiency when using high external loads. Table 3.6 shows the detailed specification of Dynamixel AX-12A.

Table 3.6: Dynamixel AX-12A specification (Robotis, 2006)

AX-12A Stats	
Operating Voltage	12V
Stall Torque	15.3 kg·cm
No-load Speed	59 RPM
Weight	55g
Size	32 x 50 x 40 mm
Resolution	0.29°
Reduction Ratio	1/254
Operating Angle	300° or Continuous Turn
Operating Voltage	9-12V (Recommended Voltage 11.1V)
Max Current	900 mA
Standby Current	50 mA
Operating Temp	-5°C ~ 85°C
Protocol	TTL Half Duplex Async Serial
Module Limit	254 valid addresses
Com Speed	7343bps ~ 1Mbps
Position Feedback	Yes
Temp Feedback	Yes
Load Voltage Feedback	Yes
Input Voltage Feedback	Yes
Compliance/PID	Yes
Material	Plastic Gears and Body
Motor	Cored Motor
Position Sensor	Potentiometer

3.3.3 Sensors

Sensors system can be categorized into two types: 1) Proprioceptive sensors and 2) Exteroceptive sensors. Proprioceptive sensors provide the internal state of the system part relative to an internal frame of reference. For instance, encoders, potentiometer, accelerometer and gyroscope are proprioceptive sensors that are sensing the internal status. On the other hand, exteroceptive sensors provide the current state of the working environment. For example, light sensors, touch sensors, ultrasonic sensors and proximity sensors. Both type of sensors are used in SR-X.

Accelerometer and Gyroscope

The MPU-6050 sensor in Figure 3.9 contains a gyroscope and an accelerometer with an onboard Digital Motion Processor™ (DMP™) capable of processing complex 9-axis MotionFusion algorithms (InvenSense, 2013). It is very accurate as it contains 16-bits analog to digital conversion (ADC) hardware for each channel. Therefore, it can capture the x, y and z channels at the same time. The master I^2C bus is used to access the signal sensor through MotionFusion algorithm's intervention from the system processor. Figure 3.10 shows the MPU6050 system diagram using I^2C bus communication.

Figure 3.9: MPU 6050 Six axis Gyro + Accelerometer (InvenSense, 2013)

Figure 3.10: MPU-6050 system diagram (InvenSense, 2013)

Calibration of the accelerometer is necessary for absolute inclination measurement of the robot body and arm at the same level. Any change in the angle will cause a change on the effect of gravitational force along the *z* axis and thus change the output voltage of the accelerometer. MPU 6050 sensor as in Figure 3.9 consists of both accelerometer and gyroscope on the same chip. The accelerometer has slow response and corrupted with noise and the gyroscope has fast response but undergoes time drift error due to accumulated error by integration to obtain angle information. Figure 3.11 shows the angle measurements of both accelerometer and gyroscope. The initial orientation of the accelerometer was set at zero degrees.

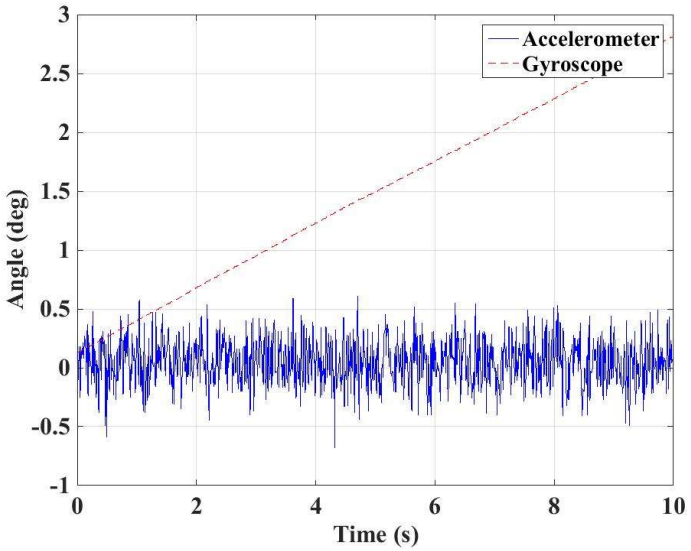

Figure 3.11: Accelerometer angle measurements

Kalman Filter

The Kalman filter offer recursive calculation to estimate the state $x \in R^n$ of a discrete-time controlled process,

$$x_k = Ax_{k-1} + Bu_{k-1} + w_{k-1} \tag{3.1}$$

with a calculation of $z \in R^n$,

$$z_k = Hx_k + v_k \tag{3.2}$$

Where x_k is the signal with current step k, u_k is the control input, w_k is a process measurement and v_k is noise measurement. The noise is assumed to be white noise, with normal probability distribution and independent,

$$p(w) \sim N(0, Q) \tag{3.3}$$

$$p(v) \sim N(0, R) \tag{3.4}$$

A and *B* represent the $n \times n$ matrices related to current signal and control inputs and *H* is constant. While *Q* is the process noise covariance and *R* is the measurement noise covariance. Figure 3.12 shows a flow chart of Kalman filter.

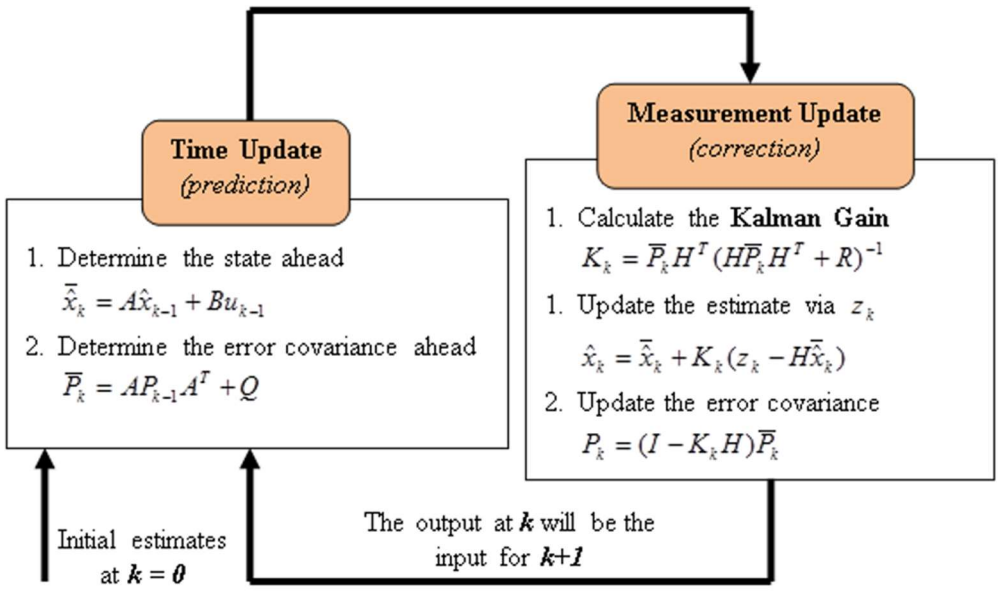

Figure 3.12: Process of iteration of Kalman filter

The Kalman filter was implemented for the angle measurement with the Q and R set to 0.001 and 0.003 respectively. Figure 3.13 shows the output for filtered angle measurement thus obtained. From this point, the filtered angle reading will be the angle that is taken into consideration while implementing on the SR-X in real time.

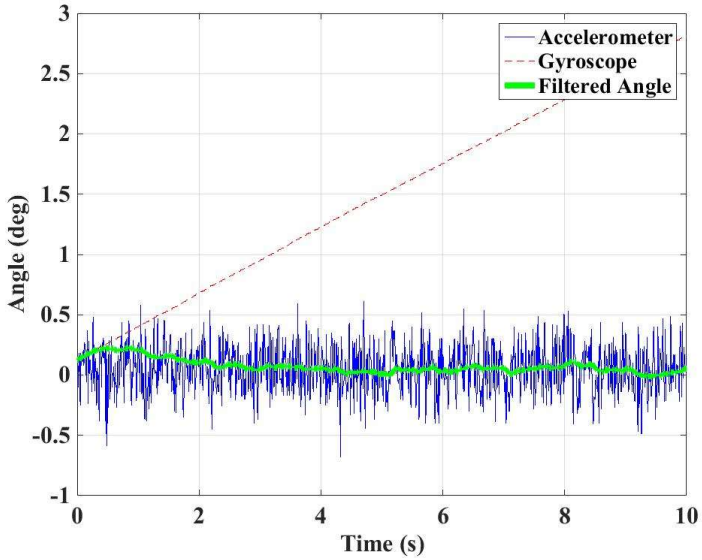

Figure 3.13: Kalman filter angle measurement

Ultrasonic Sensor

Ultrasonic sensor is a non-contact distance measurement sensor. The ultrasonic wave is emitted from transmitter in one direction and the emitted time is recorded. The echo on the sensor is monitored in the incoming ultrasonic wave after it has bounced back from the obstacles and the reflection time is recorded. The principle of ultrasonic distance measurement used is based on the measurement of the emitted time to reflection time with the speed of sound (340 m/s). The distance calculation for the ultrasonic sensor is given as:

$$d_{obstacle} = V_{soundspeed} \times T_{reflectiontime} \tag{3.5}$$

where $d_{obstacle}$ is the distance of the obstacle from the sensor, $V_{sounspeed}$ is the speed of sound (340 m/s) and $T_{reflectiontime}$ is the time taken from emitted time to reflection time. Figure 3.14 shows the ultrasonic sensor used in the SR-X system and Figure 3.15

shows the principle of measuring the distance. Table 3.7 shows the ultrasonic specification.

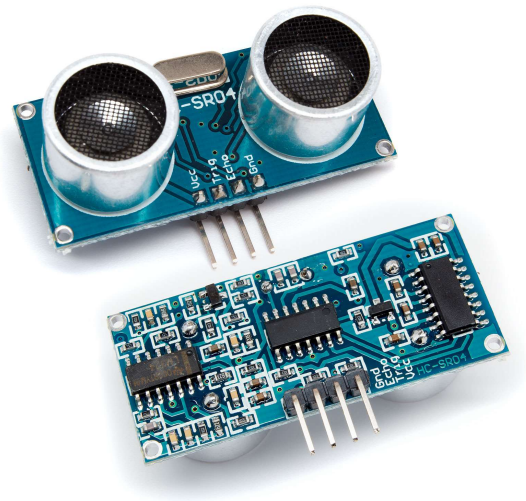

Figure 3.14: Ultrasonic sensor

Table 3.7: Ultrasonic sensor specifications

Electrical parameters	**HC-SR04 Ultrasonic Module**
Operating Voltage	DC-5V
Operating Current	15 mA
Operating Frequency	40 kHz
Farthest Range	400 cm
Nearest Range	2 cm
Measuring Angle	15 Degree
Input Trigger Signal	10 μs TTL pulse
Output Echo Signal	Output TTL level signal, proportional with range
Dimensions	4.5 x 2.0 x 1.5 cm

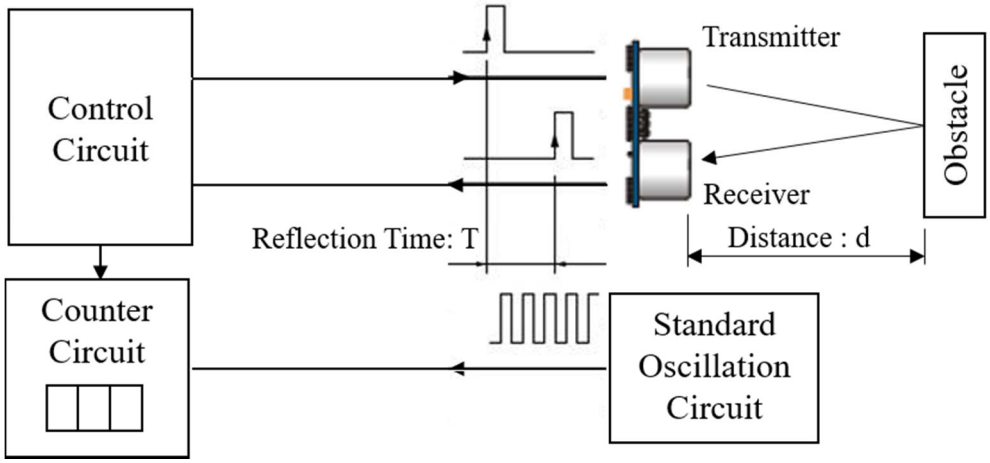

Figure 3.15: Principle of measuring distance using Ultrasonic sensor

Proximity Sensor

The proximity sensor used in SR-X is SHARP GP2Y0A21 optical triangulation sensor as shown in Figure 3.16. It is an infrared proximity sensor that shines a beam of infrared light and measures the intensity of the light that is bounced back using a phototransistor in the module. Due to the sensor is sensing the intensity of the infrared light, the range of distance measurement is limited and non-linear as in Figure 3.17. The geometry of the object in front of the sensor also affects the measurement as a non-flat surface may be different to flat surface at the same distance. Table 3.8 shows the specification of the sensor.

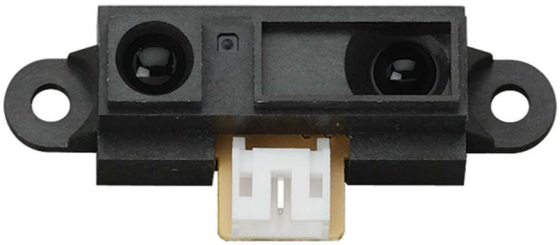

Figure 3.16: Proximity sensor

Table 3.8: Proximity Sensor Specification

Electrical parameters	**SHARP GP2Y0A21 Module**
Operating Voltage	DC 4.5V – 5.5V
Operating Current	30 mA
Farthest Range	80 cm
Nearest Range	10 cm
Measuring Angle	15 Degrees
Dimensions	2.95 x 1.30 x 1.35 cm

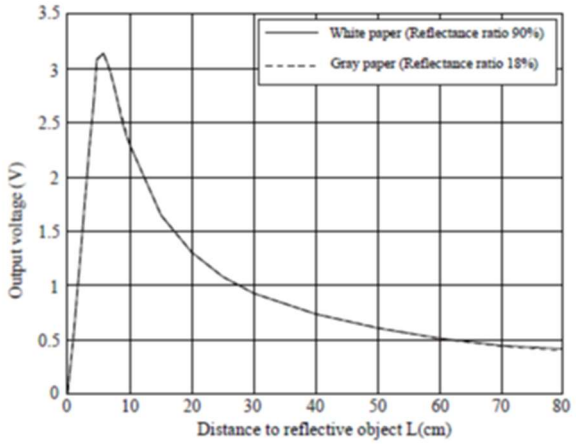

Figure 3.17: The output voltage of the proximity sensor against the distance of gray and white paper.

Power Supply System

One of the constraining factors for small mobile robot design is generally the power system. Having several servo motors running at the same time requires tremendous amount of energy to ensure the robot implements the motion successfully. Hence, the robot needs to be equipped with large capacity battery on board. The size and weight of the battery have to be small enough in order to fix the battery on the robot. SR-X has been equipped with Lithium-Polymer available from Robotis Company. The battery has protection circuit to protect it from over charge, over discharge and excess

current supply. Figure 3.18 shows the battery utilised in SR-X system and Table 3.9 shows the specification of the battery.

Figure 3.18: Lithium-Polymer 11.1V battery

Table 3.9: Lithium-polymer (Li-Po) battery specification

Li-Po parameter	**Value**
Voltage	11.1V
Capacity	1000 mAh
Discharge	10 C
Weight	83 g
Dimensions	70 x 35 x 15 mm

3.4 Electronics Architecture

The electronics architecture of SR-X is illustrated as in Figure 3.19. There are 15 Dynamixel servo motors connected in daisy chain for communication with the microcontroller. Eight of the Dynamixel servos are used in joint mode for the arms, and the rest are used in wheel mode. The ultrasonic sensor is mounted in front of the robot for obstacle detection. While the proximity sensor is mounted on the rear of the robot for reversing or descending applications.

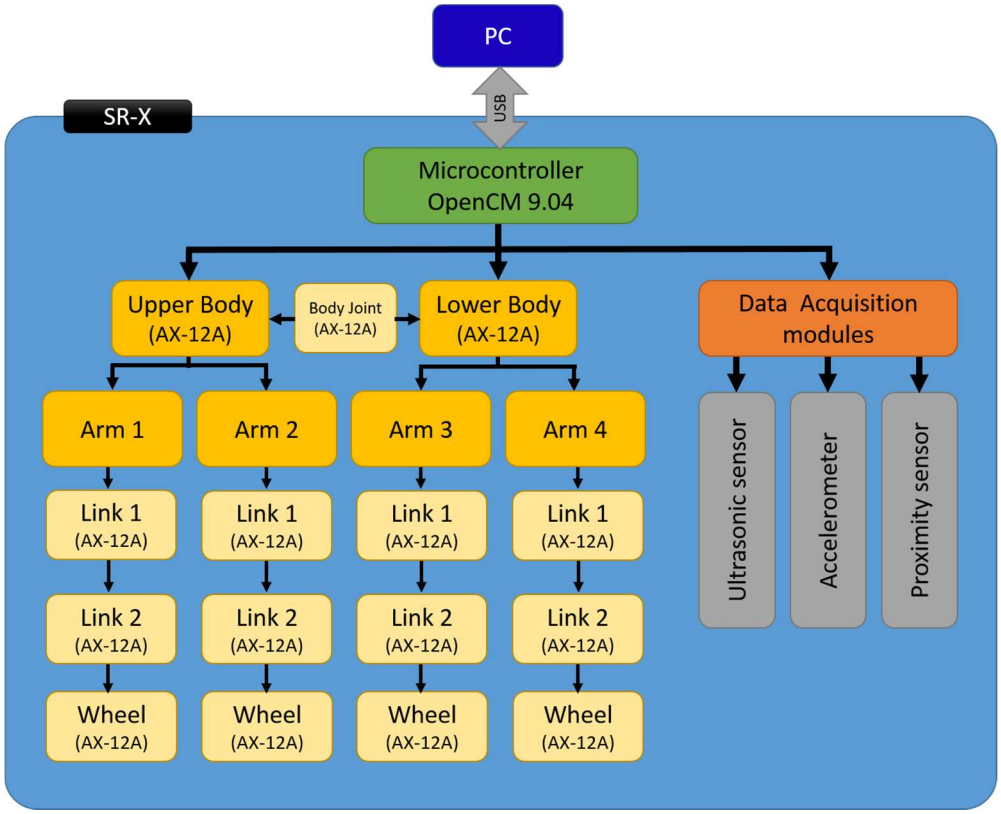

Figure 3.19. Electronics Architecture of SR-X robot

3.5 Summary

The detailed design of scansorial robot (SR-X) and the electronics components were described in this chapter. For the sensors, the resolution and accuracy of the readings were discussed for the purpose of real time implementation. Finally the global view of the electronics architecture was presented.

CHAPTER 4

Kinematics, Dynamics and Workspace Analyses

4.1 Introduction

The kinematics and dynamics analyses are necessary to realise the conceptual design phase for optimum performance of SR-X robot. These analyses are necessary beforehand so that the control system can be implemented in the robot later. Furthermore, the workspace analysis also has to be carried out in order to determine the limitation poses in the robot. This chapter will discuss the kinematics, dynamics and workspace analyses for SR-X robot.

4.2 Kinematics Analysis

The key aspect for designing the locomotion of the robot is to investigate its kinematics. A systematic analytical method was used to obtain the robot's arm orientation. As discussed in Chapter 2, SR-X robot arm contains three DOFs where two of them are revolute joints and the third is in wheel mode. Hence, the arm is considered as two links manipulator in planar coordinates (x – y axes). Figure 4.1 represents the arm of the robot with two links. The link parameters are shown in Table 4.1.

Table 4.1: Two-link manipulator parameters.

Link	a_i	α_i	d_i	θ_i
1	l_1	0	0	θ_1
2	l_2	0	0	θ_2

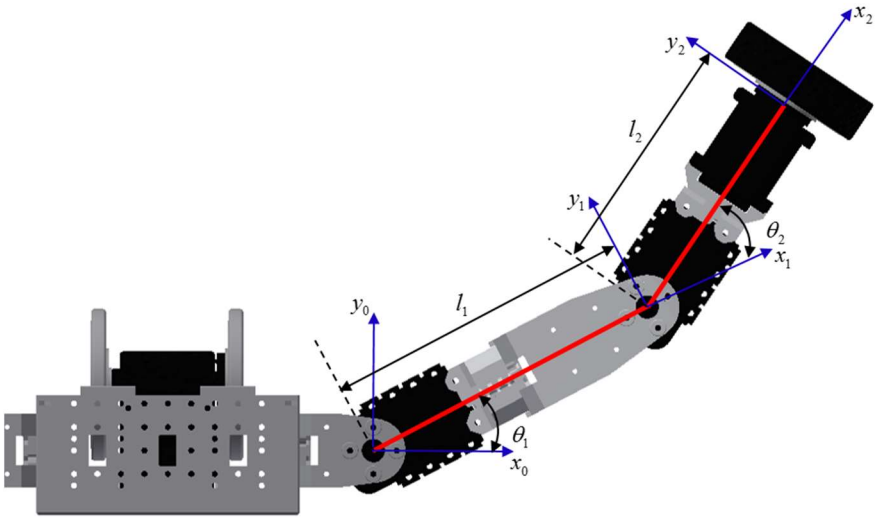

Figure 4.1: Coordinate frames attached to the SR-X arm. The z-axes all point out of the page, and are not shown in the figure.

4.2.1 Forward Kinematics

Denavit and Hartenberg standardized the way to represent the modelling of robotic motion (Niku et al., 2001). Through the use of a series of transformation matrices to move to each reference frame of each joint, the motion of a robot can be represented by a matrix. As the robot moves, so do the local reference frames. The local reference frame of each joint uses the z-axis to represent the motion of either rotational or linear movement, according to the right-hand rule for rotation.

The following abbreviation notations are used in kinematics analysis:

c_1 represents $\cos\theta_1$.

s_1 represents $\sin\theta_1$.

c_{12} represents $\cos(\theta_1 + \theta_2)$.

s_{12} represents $\sin(\theta_1 + \theta_2)$.

The A-matrices are determined from (Appendix) as

$$A_1 = \begin{bmatrix} c_1 & -s_1 & 0 & l_1 c_1 \\ s_1 & c_1 & 0 & l_1 s_1 \\ 0 & 0 & 1 & 0 \\ 0 & 0 & 0 & 1 \end{bmatrix} \tag{4.1}$$

$$A_2 = \begin{bmatrix} c_2 & -s_2 & 0 & l_2 c_2 \\ s_2 & c_2 & 0 & l_2 s_2 \\ 0 & 0 & 1 & 0 \\ 0 & 0 & 0 & 1 \end{bmatrix} \tag{4.2}$$

The transformation T-matrices are represented as

$$T_1^0 = A_1 \tag{4.3}$$

$$T_2^0 = A_1 A_2 = \begin{bmatrix} c_{12} & -s_{12} & 0 & l_1 c_1 + l_2 c_{12} \\ s_{12} & c_{12} & 0 & l_1 c_1 + l_2 s_{12} \\ 0 & 0 & 1 & 0 \\ 0 & 0 & 0 & 1 \end{bmatrix} \tag{4.4}$$

The *x* and *y* components of the origin O_2 in the base frame are the first two elements in the last column of T_2^0;

$$x = l_1 c_1 + l_2 c_{12} \tag{4.5}$$

$$y = l_1 c_1 + l_2 s_{12} \tag{4.6}$$

Equations (4.5) and (4.6) are the coordinates of the end-effector in the base frame.

4.2.2 Inverse Kinematics

The inverse kinematics is expensive and usually requires a long duration to solve in real time applications. The manipulator implements the tasks in Cartesian space, while the actuators use joint space. Position vector and orientation matrix are part of

Cartesian space. However, the joint angles are defined from joint space. The inverse kinematics is a conversion of the position and orientation from Cartesian space to joint space of a manipulator end-effector as in Figure 4.2.

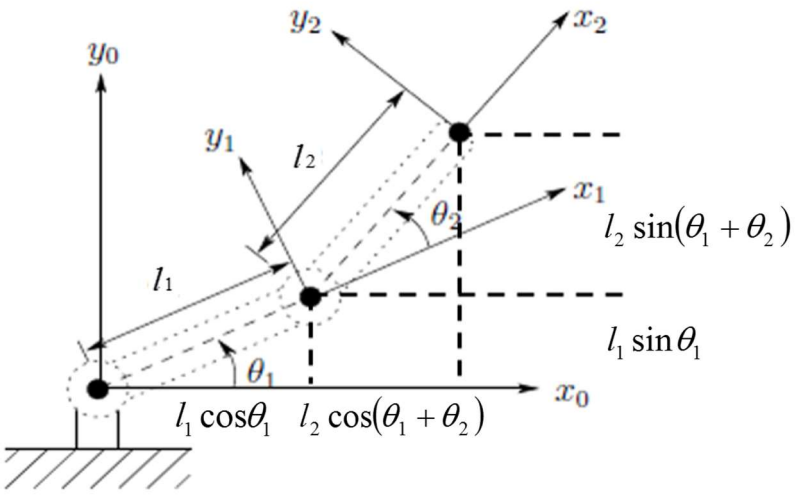

Figure 4.2: Two-Link planar manipulator. The z-axes all point out of the page, and are not shown in the figure.

By using the trigonometry, the inverse kinematics can be solved from equations (4.5) and (4.6). The solution of θ_2 can be calculated by adding the squares of both equations.

$$x^2 = l_1^2 c_1^2 + l_2^2 c_{12}^2 + 2 l_1 l_2 c_1 c_{12} \tag{4.7}$$

$$y^2 = l_1^2 s_1^2 + l_2^2 s_{12}^2 + 2 l_1 l_2 s_1 s_{12} \tag{4.8}$$

$$x^2 + y^2 = l_1^2 (c_1^2 + s_1^2) + l_2^2 (c_{12}^2 + s_{12}^2) + 2 l_1 l_2 (c_1 c_{12} + s_1 s_{12}) \tag{4.9}$$

Since $c_1^2 + s_1^2 = 1$, $s_{12} = s_1 c_2 + c_1 s_2$ and $c_{12} = c_1 c_2 - s_1 s_2$, equation (4.9) is simplified as follows

$$x^2 + y^2 = l_1^2 + l_2^2 + 2 l_1 l_2 (c_1 [c_1 c_2 - s_1 s_2] + s_1 [s_1 c_2 + c_1 s_2]) \tag{4.10}$$

$$x^2 + y^2 = l_1^2 + l_2^2 + 2 l_1 l_2 (c_1^2 c_2 - c_1 s_1 s_2 + s_1^2 c_2 + c_1 s_1 s_2) \tag{4.11}$$

$$x^2 + y^2 = l_1^2 + l_2^2 + 2 l_1 l_2 (c_2 [c_1^2 + s_1^2]) \tag{4.12}$$

$$x^2 + y^2 = l_1^2 + l_2^2 + 2l_1 l_2 c_2 \tag{4.13}$$

From equation (4.13),

$$c_2 = \frac{x^2 + y^2 - l_1^2 - l_2^2}{2l_1 l_2} \tag{4.14}$$

Since $c_i^2 + s_i^2 = 1$ where $(i = 1,2,3,...)$, s_2 is given as

$$s_2 = \pm\sqrt{1 - \left(\frac{x^2 + y^2 - l_1^2 - l_2^2}{2l_1 l_2}\right)^2} \tag{4.15}$$

Lastly, the angle, θ_2 has two solutions that can be written as

$$\theta_2 = atan2\left(\pm\sqrt{1 - \left(\frac{x^2 + y^2 - l_1^2 - l_2^2}{2l_1 l_2}\right)^2}, \frac{x^2 + y^2 - l_1^2 - l_2^2}{2l_1 l_2}\right) \tag{4.16}$$

The angle, θ_1 can be determined by multiplying each side of equation (4.5) by c_1 and equation (4.6) by s_1 and adding the resulting equations with previous calculation of angle, θ_2 yielding

$$c_1 x = l_1 c_1^2 + l_2 c_1^2 c_2 - l_2 c_1 s_1 s_2 \tag{4.17}$$

$$s_1 y = l_1 s_1^2 + l_2 s_1^2 c_2 - l_2 s_1 c_1 s_2 \tag{4.18}$$

$$c_1 x + s_1 y = l_1(c_1^2 + s_1^2) + l_2 c_2 (c_1^2 + s_1^2) \tag{4.19}$$

The simplified equation is obtained as follows

$$c_1 x + s_1 y = l_1 + l_2 c_2 \tag{4.20}$$

Then, multiplying both sides of equation (4.5) by $-s_1$ and equation (4.6) by c_1 and then summing the resulting equations yield

$$-s_1 x = -l_1 s_1 c_1 - l_2 s_1 c_1 c_2 + l_2 s_1^2 s_2 \tag{4.21}$$

$$c_1 y = l_1 c_1 s_1 + l_2 c_1 s_1 c_2 - l_2 c_1^2 s_2 \tag{4.22}$$

$$-s_1 x + c_1 y = l_2 s_2 (c_1^2 + s_1^2) \tag{4.23}$$

The simplified equation is given by

$$-s_1 x + c_1 y = l_2 s_2 \tag{4.24}$$

Now, equation (4.20) multiplies by x and equation (4.24) multiplies by y and sums the resulting equations to get c_1.

$$c_1 x^2 + s_1 xy = x(l_1 + l_2 c_2) \tag{4.25}$$

$$-s_1 xy + c_1 y^2 = y l_2 s_2 \tag{4.26}$$

$$c_1 (x^2 + y^2) = x(l_1 + l_2 c_2) + y l_2 s_2 \tag{4.27}$$

From equation (4.7),

$$c_1 = \frac{x(l_1 + l_2 c_2) + y l_2 s_2}{x^2 + y^2} \tag{4.28}$$

Since $c_i^2 + s_i^2 = 1 \ \ (i = 1,2,3,...)$, s_2 is obtained as

$$s_1 = \pm \sqrt{1 - \left(\frac{x(l_1 + l_2 c_2) + y l_2 s_2}{x^2 + y^2} \right)^2} \tag{4.29}$$

Finally, the angle, θ_1 has two solutions and can be written as

$$\theta_1 = atan2\left(\pm \sqrt{1 - \left(\frac{x(l_1 + l_2 c_2) + y l_2 s_2}{x^2 + y^2} \right)^2}, \frac{x(l_1 + l_2 c_2) + y l_2 s_2}{x^2 + y^2} \right) \tag{4.30}$$

The two solutions will represent the right and left arm of the robot.

4.2.3 Jacobian Matrix and Singularity Analysis

The Jacobian matrix is a first-order partial derivatives matrix. In a robotic arm, the Jacobian matrix relates the end-effector velocity to the joint velocity. To calculate the Jacobian matrix, the forward kinematics of two links, revolute joint manipulator from equation (4.5) and equation (4.6) are taken into time derivative to form the following equations.

$$\dot{x} = -l_1 s_1 \dot{\theta}_1 - l_2 s_{12} \dot{\theta}_1 - l_2 s_{12} \dot{\theta}_2 \tag{4.31}$$

$$\dot{y} = l_1 c_1 \dot{\theta}_1 + l_2 c_{12} \dot{\theta}_1 + l_2 c_{12} \dot{\theta}_2 \tag{4.32}$$

Expressing equation (4.31) and equation (4.32) in matrix form,

$$\frac{d}{dt}\begin{bmatrix} x \\ y \end{bmatrix} = \begin{bmatrix} \frac{\partial x}{\partial \theta_1} & \frac{\partial x}{\partial \theta_2} \\ \frac{\partial y}{\partial \theta_1} & \frac{\partial y}{\partial \theta_2} \end{bmatrix} \begin{bmatrix} \dot{\theta}_1 \\ \dot{\theta}_2 \end{bmatrix} \tag{4.33}$$

$$= \begin{bmatrix} -l_1 s_1 - l_2 s_{12} & -l_2 s_{12} \\ l_1 c_1 + l_2 c_{12} & l_2 c_{12} \end{bmatrix} \begin{bmatrix} \dot{\theta}_1 \\ \dot{\theta}_2 \end{bmatrix} \tag{4.34}$$

$$\begin{bmatrix} \dot{x} \\ \dot{y} \end{bmatrix} = \mathbf{J}(\theta) \begin{bmatrix} \dot{\theta}_1 \\ \dot{\theta}_2 \end{bmatrix} \tag{4.35}$$

where $\mathbf{J}(\theta)$ is the Jacobian matrix. To understand the relation between end-effector velocity and joint velocity, equation (4.34) is expanded to form the following equation,

$$\frac{d}{dt}\begin{bmatrix} x \\ y \end{bmatrix} = \begin{bmatrix} -l_1 s_1 - l_2 s_{12} \\ l_1 c_1 + l_2 c_{12} \end{bmatrix} \dot{\theta}_1 + \begin{bmatrix} -l_2 s_{12} \\ l_2 c_{12} \end{bmatrix} \dot{\theta}_2 \tag{4.36}$$

rearrange equation (4.36) yields,

$$\frac{d}{dt}\begin{bmatrix} x \\ y \end{bmatrix} = \begin{bmatrix} -s_1 \\ c_1 \end{bmatrix} l_1 \dot{\theta}_1 + \begin{bmatrix} -s_{12} \\ c_{12} \end{bmatrix} l_2 \left(\dot{\theta}_1 + \dot{\theta}_2 \right) \tag{4.37}$$

In equation (4.37), the first part is the velocity of the joint itself. The second part shows the velocity of end-effector as related to the velocity of the joint.

4.2.4 Singularity Analysis

Singularities occur whenever one or more DOFs are lost (Lung, 1999) and commonly indicate a position where a particular mathematical formulation fails. Singularities of serial arms are either boundary or interior. Boundary singularities occur when the tool tip is on the surface of the robot's workspace. Interior singularities occur inside the work envelope when two or more of the axes of the robot form a straight line, i.e., collinear. In two links robot manipulator, a configuration where determinant of $\mathbf{J}(\theta) = 0$ is called a singularity of the robot. In this configuration, the forces in the arm of the robot may go to infinity, causing a breakdown of the robot. By calculating the determinant of $\mathbf{J}(\theta)$ leads to:

$$\det\begin{bmatrix} -l_1 s_1 - l_1 s_{12} & -l_2 s_{12} \\ l_1 c_1 + l_2 c_{12} & l_2 c_{12} \end{bmatrix} = 0 \tag{4.38}$$

$$l_1 s_{12} c_1 - l_1 s_1 c_{12} = l_2 s_{12} c_{12} - l_2 s_{12} c_{12} \tag{4.39}$$

$$l_1 (s_{12} c_1 - s_1 c_{12}) = 0 \tag{4.40}$$

Using the trigonometry identities of $s_{12} = s_1 c_2 + c_1 s_2$ and $c_{12} = c_1 c_2 - s_1 s_2$ and substituting into equation (4.40) yields:

$$\sin(\theta_2) = 0 \tag{4.41}$$

Therefore, $\theta_2 = 0$ or $\theta_2 = \pi$ (180°). This singularity configuration for robotic arm happens at the border of the workspace. Hence, the two links manipulator does not have singularity inside its workspace except on the borders. This facilitates the singularities avoidance in the motion algorithms.

4.3 Workspace Analysis

Understanding the movement of SR-X arm is the key to form the configuration modes, namely climbing mode, walking mode and steering mode discussed in Chapter 2. Workspace in robotic arm is defined by the combination of all points reachable by the end-effector of the robot. By setting the restrictions on the workspace, it constrains the possible arm configuration and allows certain modes to be implemented in SR-X robot. Furthermore, understanding the workspace is the key to establish a relationship between workspace and algorithms for all configuration modes. This section will discuss the workspaces for individual configuration mode of SR-X.

4.3.1 The General Workspace

The general workspace is the volume containing all reachable points of the arm joints and the information on the size of a space in which the robot can work safely. In general workspace, an assumption has been made on the range operation of SR-X arms' joint. This assumption allows the workspace analysis to be simpler based on 3D model designed in chapter 3. Figure 4.1 shows the visualisation of the workspace in 2-D (x – y axes) which is two links planar manipulator. By employing the full range of motion of revolute joint 1 and revolute joint 2, the arm joint tip is capable of moving to any point within the range shown in Table 4.2.

Table 4.2: SR-X arm range of operation

Revolute Joint Angle	Joint Operable Range in Degrees	Axis of Rotation
θ_1	-100 to 100	z_1
θ_2	-135 to 135	z_2

However, this assumption has limitation based on the SR-X design especially revolute joint 2. If the angle of θ_1 is set to maximum value, 100°, the value of θ_2 can only reach maximum value of 100° instead of the assumption value in Table 4.2. Figure 4.3 shows the condition where the limitation occurs in SR-X arm. Therefore,

when developing the algorithms this condition has to be taken into account to avoid malfunction during the operation in any configuration mode.

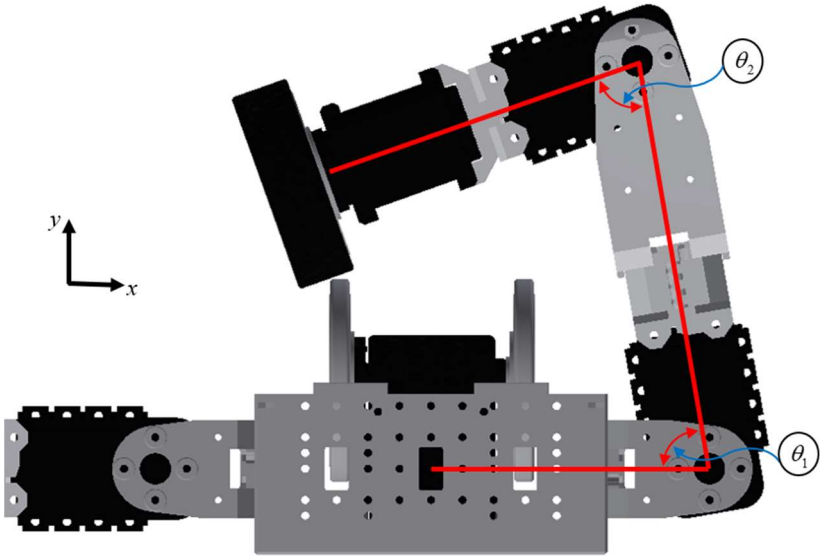

Figure 4.3: Limitation of angle, θ_2. The z-axes all point out of the page, and are not shown in the figure.

4.3.2 Workspace Analysis for Climbing Mode

In climbing mode, the workspace reachability by end-effectors are very important for the robot to create a grip on the pole to climb. The dimension of the pole is also another important factor for the robot to provide a proper grip while climbing. The dimension of the pole used in this project is 110 *mm* in diameter. For a proper grip on the pole, at least a minimum of 120° angle in between the contact points is required (Chen et. al., 2011). If the angle is lower than that the robot will suffer an insufficient grip and the possibility of slipping from the pole is higher. Figure 4.4 shows that the SR-X arms are gripping the pole at 120° angle.

This configuration has been simulated in MATLAB to validate the reachability workspace of SR-X arms. Figure 4.5 shows the result of the simulation for both left and right arms. The red area in Figure 4.5 is the reachable area for SR-X arm to perform the gripping mechanism on the pole.

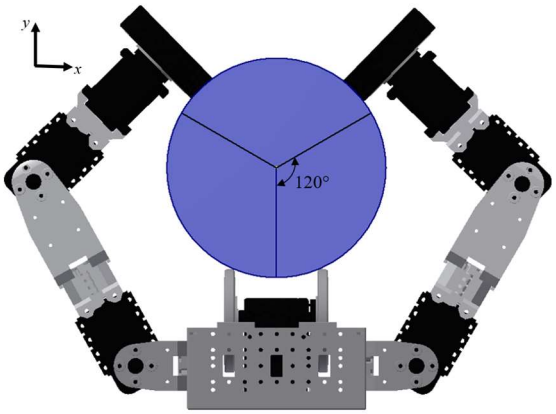

Figure 4.4: Limitation of θ_2 angle. The z-axes all point out of the page, and are not shown in the figure.

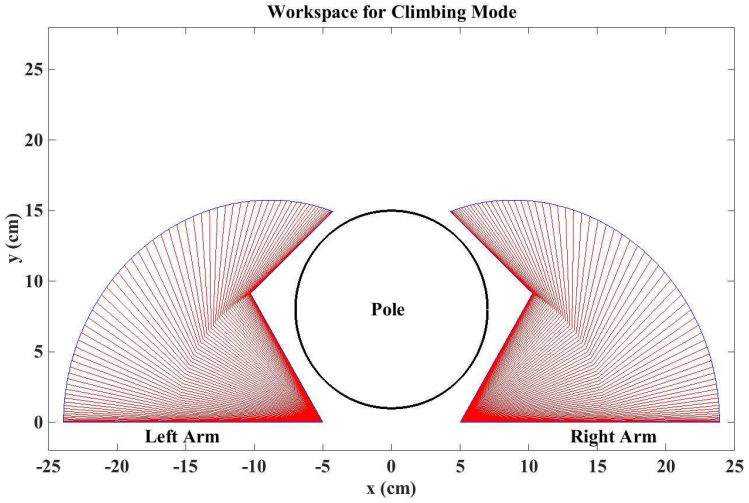

Figure 4.5: Simulation of workspace for SR-X arm around the pole.

The initial position and final position of link 1 and link 2 angles are shown in Table 4.3.

Table 4.3: Climbing mode workspace

Revolute Joint Angle	Initial Angle Position	Final Angle Position	Axis of Rotation
θ_{1R}	0°	60°	z_{1R}
θ_{2R}	0°	76°	z_{2R}
θ_{1L}	180°	120°	z_{1L}
θ_{2L}	180°	104°	z_{1L}

4.3.3 Workspace Analysis for Walking Mode

In walking mode, all SR-X arms are configured to be legs for the robot. All the wheels in this mode are disabled as not used while implementing the walking operation. Figure 4.6 shows the walking configuration mode for SR-X from side view and Figure 4.7 shows the same configuration from perspective view. The leg's geometry for four legs is similar and the locomotion is the same except the robot uses diagonally opposite legs to walk as discuss in Chapter 2. For simplicity of the system in walking mode, the following assumptions have to be considered:

- The model of each leg is a planar two-link manipulator.
- The tracking line of the hip joint of the proposed walking configuration is planned as a straight line which is parallel with the ground.
- The hip joint has a linear motion with constant angular velocity.

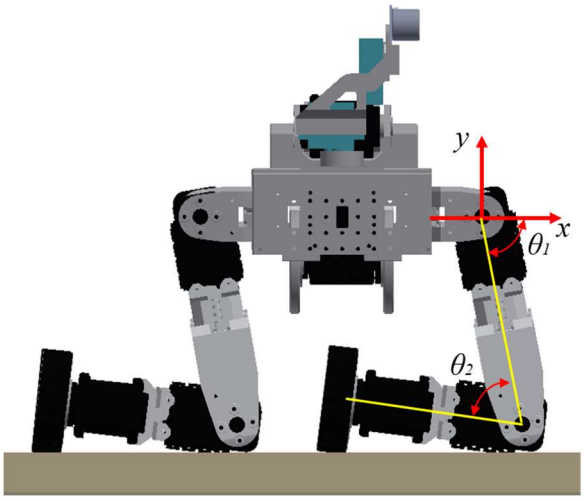

Figure 4.6: SR-X in walking mode configuration from side view. The z-axes all point out of the page, and are not shown in the figure.

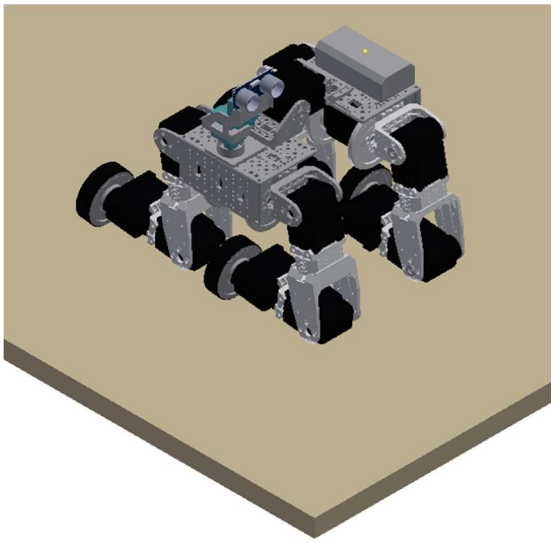

Figure 4.7: SR-X in walking mode configuration from perspective view.

Table 4.4: Initial leg position of walking mode

Revolute Joint Angle	**Front Leg Angle**	**Rear leg Angle**	**Axis of Rotation**
θ_1	90°	90°	z_1
θ_2	180°	180°	z_2

The inverse kinematic of SR-X in walking mode can be solved to find the joint variables as illustrated in Figure 4.8.

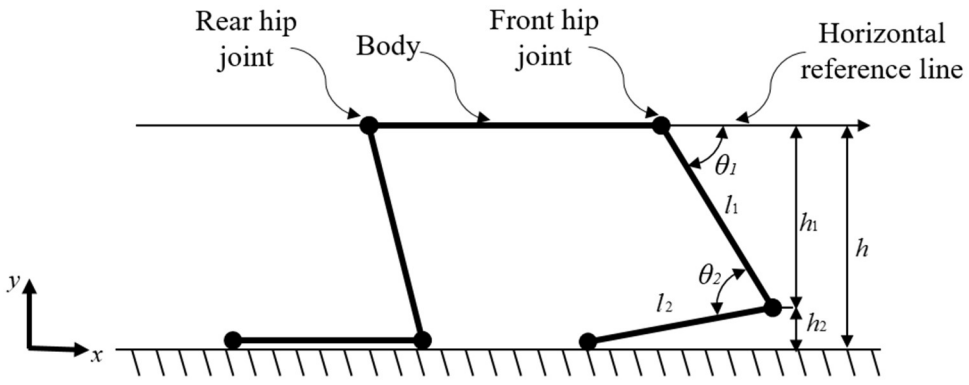

Figure 4.8: Inverse kinematics for SR-X in walking mode configuration.

From Figure 4.8, the link lengths are represented by l_1 and l_2, the height of the hip joint to the floor is represented by h. The values of h_1 and h_2 can be calculated as follows:

$$h_1 = l_1 \sin\theta_1 \tag{4.42}$$

$$h_2 = l_2 \sin(\theta_2 - \theta_1) \tag{4.43}$$

From Figure 4.8, equation (4.42) and equation (4.43), h can be obtained as,

$$h = l_1 \sin\theta_1 + l_2 \sin(\theta_2 - \theta_1) \tag{4.44}$$

The θ_2 angle can be obtained from equation (4.44) as follows:

$$\theta_2 = \sin^{-1}\left(\frac{h - l_1 \sin\theta_1}{l_2}\right) + \theta_1 = f(\theta_1) \tag{4.45}$$

Equation (4.45) is the kinematic model for control of knee joints. If h, l_1 and l_2 are constant, knee joint angle, θ_2 depends on hip joint angle, θ_1. From the assumption, while the actuator of hip joint rotates with constant angular velocity, the actuator of knee joint is controlled by equation (4.45).

The workspace for SR-X in walking mode configuration has a limitation subject to general workspace (section 4.3.1) as well as the limitation shown in Figure 4.3. This limitation has to be taken into consideration when generating the algorithm for walking trajectory planning.

4.3.4 Workspace Analysis for Steering Mode

In steering mode, SR-X robot is configured as a skid steering type of wheel robot. The skid steering is considered as all-terrain vehicle and has many advantages over other off-road robots in terms of high manoeuvrability, high power and an ability of working in hard environmental conditions but possess a simple mechanism to operate (Dang et. al., 2010). It navigates by the angular velocity difference between left

wheels and right wheels to make a turn (Caraciolo et. al., 1999). This method is also called differential drive to implement the skid steering turn. Figure 4.9 shows the SR-X configuration in steering mode.

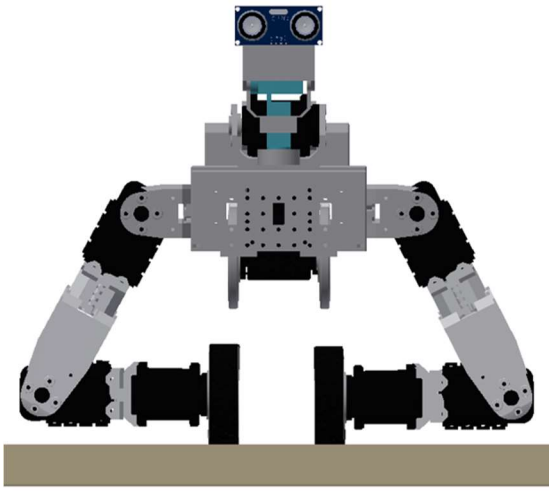

Figure 4.9: SR-X in walking configuration mode from side view

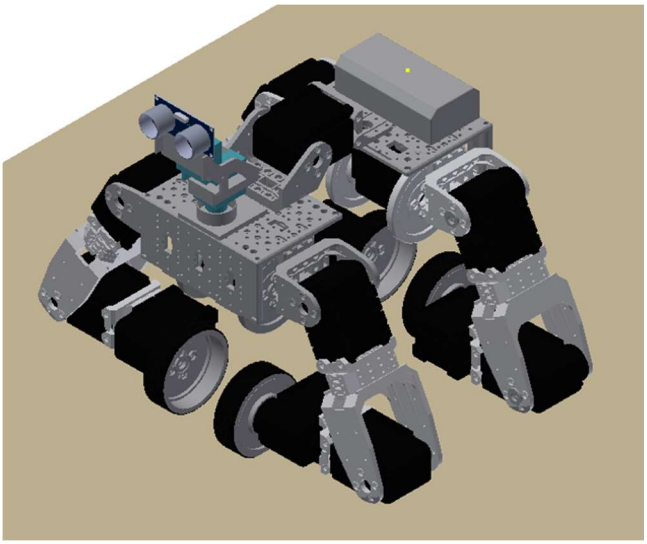

Figure 4.10: SR-X in walking configuration mode from side view

The SR-X robot in steering mode has a constant orientation workspace. This workspace is defined as the region that can be reached by the reference point on the moving platform, when the orientation of the moving platform is kept constant. When the robot is configured in this mode, the angles for link 1 and link 2 are kept constant throughout the operation. Table 4.5 shows the fixed angle values for θ_1 and θ_2.

Table 4.5: Link angles setting in steering mode

Revolute Joint Angle	Left Arm Angle	Right Arm Angle	Axis of Rotation
θ_1	-100°	-80°	z_1
θ_2	0°	180°	z_2

4.3.4.1 Kinematic and Dynamic Modelling for Steering Mode

In order to consider the kinematic model of SR-X robot in steering mode, the following assumptions were made for simplicity:

- The SR-X robot is placed on a plane of the X-Y coordinate.
- The point contact occurs between the wheels and the plane surface.
- The thickness of the wheel is neglected.
- The longitudinal wheel slippage is neglected.
- The speeds of the two wheels on each side are the same.
- The mechanical system is subject to nonholonomic constraints.

A free body diagram of SR-X in steering mode is shown in Figure 4.11 with the fixed coordinate system set to $q = [X, Y, \phi]$, where ϕ is the heading angle of the platform which is the same yaw angle for the moving coordinate system $[x_1, y_1, \phi]$ to be placed at the centre of mass (COM) of the platform.

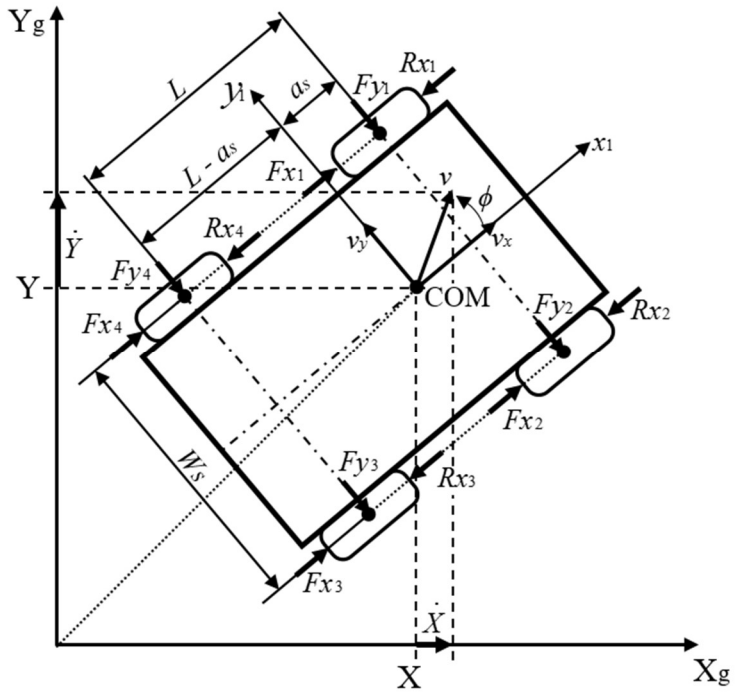

Figure 4.11: A schematic model of free body diagram.

Based on the schematic model illustrated in Figure 4.11 and the given assumptions of $F_{x4} = F_{x1}$ and $F_{x3} = F_{x2}$, the equations of motion can be obtained as (Caracciolo et al., 1999):

$$m\ddot{x} = 2F_{x1} + 2F_{x2} - R_x \tag{4.46}$$

$$m\ddot{y} = -F_y \tag{4.47}$$

$$I\ddot{\phi} = W_s\left(F_{x1} - F_{x2}\right) - M_r \tag{4.48}$$

where,

F_x is the tractive force at the contact point of the wheel.

R_x is the longitudinal resistive force of the wheel.

F_y is the lateral force at the contact point of the wheel.

M_r is the resistive moment around COM.

W_s is the distance between centre of left and right wheels.

By considering friction coefficients (μ_x, μ_y), the resistive force, lateral force and resistive moment at the COM can be calculated as:

$$R_x = \sum_{i=1}^{4} R_{xi} = \mu_x \frac{mg}{4} \sum_{i=1}^{4} \mathrm{sgn}(\dot{x}_i) \tag{4.49}$$

$$F_y = \sum_{i=1}^{4} F_{yi} = \mu_y \frac{mg}{L} (\mathrm{sgn}(\dot{y}_1) + \mathrm{sgn}(\dot{y}_3)) \tag{4.50}$$

$$M_r = a_s (F_{y1} + F_{y2}) - (L - a_s)(F_{y3} + F_{y4}) + \frac{W_s}{2}(R_{x2} + R_{x3} - R_{x1} - R_{x4}) \tag{4.51}$$

The nonholonomic constraints characteristic can be represented as:

$$A(q)\dot{q} = 0 \tag{4.52}$$

where q is the n dimensional generalised coordinates. $A(q)$ is an $m \times n$ dimensional matrix. Since the constraints are assumed to be nonholonomic, equation (4.46) is not integrable. Hence, the constraints are assumed to be independent or in other words, $A(q)$ has rank m.

The dynamic model of SR-X as the generalised coordinates is given by:

$$\mathbf{M}(\mathbf{q}, \ddot{\mathbf{q}}) = \mathbf{E}(\mathbf{q})\tau + \mathbf{A}^{\mathrm{T}}(\mathbf{q})\lambda - \mathbf{F}(\mathbf{q}, \dot{\mathbf{q}}) \tag{4.53}$$

where,

$\mathbf{M}(\mathbf{q}, \ddot{\mathbf{q}})$ is the $n \times n$ dimensional positive definite inertia matrix.

$\mathbf{F}(\mathbf{q}, \dot{\mathbf{q}})$ is the n dimensional velocity dependent force vector.

$\mathbf{E}(\mathbf{q})$ is the $n \times r$ dimensional matrix mapping the actuator space into generalised coordinate.

τ is the r dimensional vector of actuator force/torque.

λ is the Lagrange multiplier for nonholonomic constraints.

The dynamic model of the platform with generalised coordinates, $q = (X, Y, \phi)$ can be expressed in matrix notation by:

$$\mathbf{M}(\mathbf{q}, \ddot{\mathbf{q}}) = \begin{bmatrix} m & 0 & 0 \\ 0 & m & 0 \\ 0 & 0 & I \end{bmatrix} \tag{4.54}$$

$$\mathbf{F}(\mathbf{q}, \dot{\mathbf{q}}) = \begin{bmatrix} R_x \cos\phi - F_y \sin\phi \\ R_x \sin\phi + F_y \cos\phi \\ Mr \end{bmatrix} \tag{4.55}$$

$$\mathbf{E}(\mathbf{q}) = \begin{pmatrix} \cos\phi & \cos\phi \\ \sin\phi & \sin\phi \\ W_s/2 & -W_s/2 \end{pmatrix} / r \tag{4.56}$$

$$\mathbf{A}(\mathbf{q}) = \begin{bmatrix} -\sin\phi & \cos\phi & 0 \end{bmatrix} \tag{4.57}$$

$$\tau_i = 2rF_{xi} \quad (i = 1,2) \tag{4.58}$$

where, r is the radius of the wheel, τ_1 and τ_2 are the torques produced by the left and right side motors.

In order to accomplish the skid steering by creating a differential velocity between the left and right side of the wheels, the kinematic equation concerning the platform velocity, *v*, can be written by:

$$\dot{q} = \mathbf{S}(\mathbf{q})\mathbf{v}, \ \ v \in \Re^2 \tag{4.59}$$

$$\mathbf{S}(\mathbf{q}) = \begin{bmatrix} \cos\phi & 0 \\ \sin\phi & 0 \\ 0 & 1 \end{bmatrix} \tag{4.60}$$

where, $\mathbf{v} = \begin{bmatrix} v_{linear}, v_{angular} \end{bmatrix}^T = \begin{bmatrix} v_1, v_2 \end{bmatrix}^T$ refers to linear velocity, $v_{linear} = v_1 = \begin{bmatrix} v_x & v_y \end{bmatrix}$ and angular velocity, $v_{angular} = v_2$ vector at the platform COM and $\mathbf{S}(\mathbf{q})$ is coordinate transformation matrix.

Since the velocity front and rear left wheel have the same speed, similarly to front and rear right wheels, the four-wheel skid-steering platform can be considered as a two-wheel differential driven mobile platform. Therefore, the equation of motion for the platform with nonholonomic constraint can be presented as:

$$\mathbf{M}(\mathbf{q},\ddot{\mathbf{q}}) = \mathbf{E}(\mathbf{q})\tau + \mathbf{A}^{\mathrm{T}}(\mathbf{q})\lambda - \mathbf{F}(\mathbf{q},\dot{\mathbf{q}}) = \mathbf{E}(\mathbf{q})\tau - \mathbf{F}(\mathbf{q},\dot{\mathbf{q}}) \tag{4.61}$$

$$\because \mathbf{A}(\mathbf{q},\dot{\mathbf{q}}) = \begin{bmatrix} -\sin\phi & \cos\phi & 0 \end{bmatrix} \begin{bmatrix} \dot{X} \\ \dot{Y} \\ \dot{\phi} \end{bmatrix} = 0 \tag{4.62}$$

Equation (4.62) eliminates the Lagrange multiplier, λ due to nonholonomic constraint is zero. From equation (4.59) and equation (4.61), the state feedback control law becomes:

$$\boldsymbol{\tau} = \left(\mathbf{S}^{\mathrm{T}}\mathbf{E}\right)^{-1}\left(\mathbf{S}^{\mathrm{T}}\mathbf{M}\mathbf{S}\mathbf{u} + \mathbf{S}^{\mathrm{T}}\mathbf{M}\dot{\mathbf{S}}\mathbf{v} + \mathbf{S}^{\mathrm{T}}\mathbf{F}\right) \tag{4.63}$$

where $\mathbf{u} = \dot{\mathbf{v}} = \left[\dot{v}_1, \dot{v}_2\right]$ refers to the control input. Further explanation of the control system will be discussed in Chapter 5.

4.4 Summary

The kinematics and dynamics of the SR-X arm were derived from two links manipulator as well as Jacobian matrix and singularities and the related equations obtained. By manipulating the arms, SR-X can be configured into different configurations namely climbing mode, walking mode and steering mode.

CHAPTER 5

Path Planning and Controller Design

5.1 Introduction

This chapter describes the path planning and control system for the SR-X in various modes of operation. The low level and high level controls of the system are described, where the low level control is designed for Dynamixel servo motor and high level control for the motion planning algorithm.

5.2 Control system

The control system of the robot can be divided into two parts. The first part comprises the low-level servo motor control, while the second part comprises a high-level robot motion-planning algorithm. In the low level control, the Dynamixel servo motor with specific identification number (ID) gets its set points via a serial communication bus through the daisy chain connection. These set points are then processed to drive the Direct Current (DC) electric motor. In most servos a gearbox is attached to increase the output torque. This output has a position sensor to measure its position for feedback to the on-board controller. From this a schematic of the servo motor can be derived, which is shown in Figure 5.1. Table 5.1 shows the parameters of the Dynamixel servo motor.

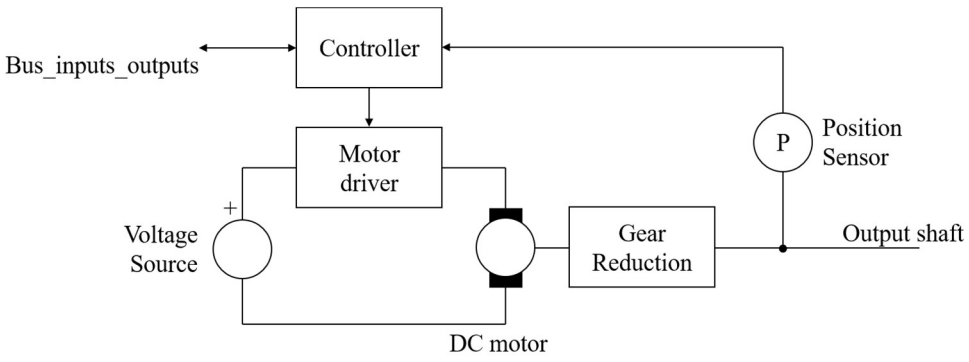

Figure 5.1: Schematic of the Dynamixel servo motor

Table 5.1: Parameters of the Dynamixel AX-12A servo motor (Robotis, 2006)

Parameters	**AX-12A**	
Gear Reduction Ratio	1/254	
Input Voltage (V)	7V	10V
Final Max Holding Torque (Nm)	1.18 Nm	1.62 Nm
Sec / 60 degrees	0.269 s	0.196 s

The Dynamixel servo motor specification in Table 3.6 from chapter 3 shows that the servo has an operating angle of 300°(joint mode), or an endless turn (wheel mode). For operating angle 300° (joint mode) with the number of positions 1024 (10 bits value), the resolution is given as follows:

$$\frac{Max\_operating\_angle}{Number\_of\_position} = \frac{300°}{2^{10}-1} = 0.29° \tag{5.1}$$

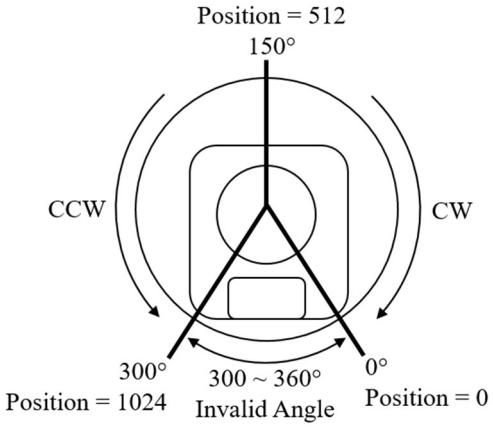

Figure 5.2: Dynamixel servo motor operating angle in joint mode (Robotis, 2006).

Figure 5.2 shows the position of the servo motor shaft within the operating range angle of 300°. In order to ensure the Dynamixel servo motor operates properly, a real time testing was carried out to analyse the performance of the servo motor. Figure 5.3 shows the result of the real time implementation of the servo with initial position of zero degrees to final position (step input) of 90°. The servo took about 1.3 seconds to reach the set point of 90°.

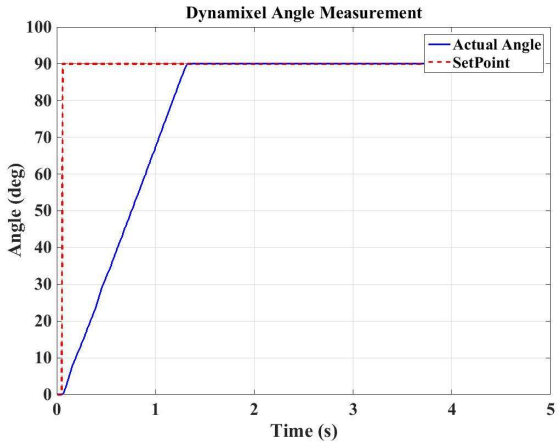

Figure 5.3: Dynamixel servo motor angle measurement from 0 to 90°.

The second part of the control system is the high level control system which comprises the motion planning algorithm of SR-X. In this project, a controller design based on Proportional-Integral-Derivative (PID) control is implemented in the robot system. Generally, PID control is simple to implement and produces adequate results, therefore it is the most commonly used control mechanism in industry. The main objective of the PID controller is to minimise the error between the desired and the actual output of the system.

The PID controller consists of three main parameters which are proportional, integral and derivative gains (*Kp*, *Ki* and *Kd*). The parameters are tuneable and associated with the proportional error, integral of the error and the change of error respectively as illustrated in Figure 5.4. The first part is proportional part that acts to reduce the error and the rise time of the output so as to reach the desired value. The second part is the integral which is used to eliminate the steady state error of the response. Finally, the derivative part is used to reduce the overshoot in the response due to the change of error in the system. By combining all three terms weighted by their gains, the error associated with the control signal can be eliminated or minimised significantly. There are a few methods to tune the controller gains such as Cohen-Coon, Ziegler-Nichols and software tools.

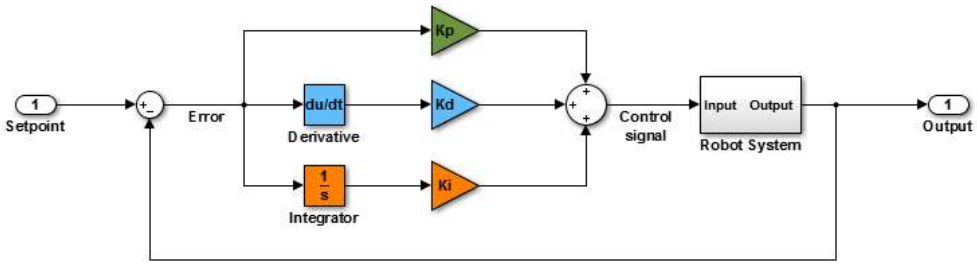

Figure 5.4: PID controller structure diagram

Practically, the PID controller can be implemented with the absence of some part such as PI, PD, P, or I controller depending on the application and the required system response. PI controllers are more common in the industry for two reasons: first, having the integral part will ensure that the system will reach its target and there is no steady state error. Second, the derivative part of the controller has high sensitivity to measurement noise and may produce oscillation in the output of the system that may cause mechanical damage (Ogata, 2002).

5.3 Path planning of climbing mode operation

SR-X arm has two links connected by two joints: a shoulder joint and an elbow joint described as in Figure 4.1 in chapter 4. In climbing mode, the problem is to determine how to control the joint angles with the servo motors to move the arm from one position to another. The arm is at the rest position and moves to a desired position with zero start and stop velocity and acceleration. The path planning for climbing mode is to ensure the elbow joint initialises first before the shoulder joint. This technique is used to avoid the shoulder joint colliding with the pole before the end-effector reaches the desired position. Figure 5.5 shows an illustration of path planning for the SR-X arm.

In order to control the arm with proper motion, polynomial expressions are used for controlling the motion by generating commands sent to the joint motor controllers.

$$\theta_1(t) = \theta_1(0) + a_1 t^5 + a_2 t^4 + a_3 t^3 + a_4 t^2 + a_5 t \tag{5.2}$$

$$\theta_2(t) = \theta_2(0) + b_1 t^5 + b_2 t^4 + b_3 t^3 + b_4 t^2 + b_5 t \tag{5.3}$$

where $\theta_1(0)$ and $\theta_2(0)$ are the initial angle values at time $t=0$ and coefficient vectors $\mathbf{a}=[a_1 \quad a_2 \quad a_3 \quad a_4 \quad a_5]^T$ and $\mathbf{b}=[b_1 \quad b_2 \quad b_3 \quad b_4 \quad b_5]^T$ are determined to provide the desired motion. For given values of $\theta_1(0)$, $\theta_1(t_f)$, and final coordinates time, t_f, matrix equations are set up and solved for coefficient vector **a.** Similarly, for given values of $\theta_2(0)$, $\theta_2(t_f)$, and t_f, matrix equations are set up and solved for coefficient vector **b**. These results are used for path planning of the arm.

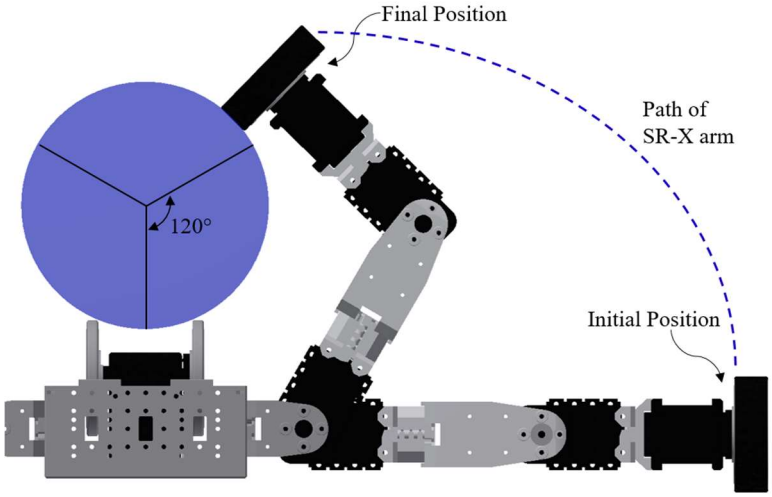

Figure 5.5: Illustration of path planning for SR-X arm. The z-axes all point out of the page, and are not shown in the figure.

The remaining constraints in the arm motion are the velocity and acceleration of the links and are zero at the known starting location and the desired final location. This implies that the angular velocity and angular acceleration of the two joints will be zero at time $t=0$ and $t=t_f$. The angular velocity of the first link at time t is the derivative of the angle $\theta_1(t)$ with respect to time,

$$\theta_1'(t)=5a_1t^4+4a_2t^3+3a_3t^2+2a_4t+a_5 \tag{5.4}$$

The velocity at $t=0$ is

$$\theta_1'(0)=a_5=0 \tag{5.5}$$

and thus, coefficient $a_5=0$. The angular acceleration is the second derivative of the angle $\theta_1(t)$ with respect to time

$$\theta_1'' = 20a_1t^3 + 12a_2t^2 + 6a_3t + 2a_4 \tag{5.6}$$

The acceleration at $t = 0$ is

$$\theta_1'' = 2a_4 = 0 \tag{5.7}$$

and thus, coefficient $a_4 = 0$. Rearrange the three constraints on $\theta_1(t)$ and it derivatives at time $t = t_f$ in matrix form:

$$\begin{bmatrix} t_f^5 & t_f^4 & t_f^3 \\ 5t_f^4 & 4t_f^3 & 3t_f^2 \\ 20t_f^3 & 12t_f^2 & 6t_f \end{bmatrix} \begin{bmatrix} a_1 \\ a_2 \\ a_3 \end{bmatrix} = \begin{bmatrix} \theta_1(t_f) - \theta_1(0) \\ 0 \\ 0 \end{bmatrix} \tag{5.8}$$

Similarly, for $\theta_2(t)$:

$$\begin{bmatrix} t_f^5 & t_f^4 & t_f^3 \\ 5t_f^4 & 4t_f^3 & 3t_f^2 \\ 20t_f^3 & 12t_f^2 & 6t_f \end{bmatrix} \begin{bmatrix} b_1 \\ b_2 \\ b_3 \end{bmatrix} = \begin{bmatrix} \theta_2(t_f) - \theta_2(0) \\ 0 \\ 0 \end{bmatrix} \tag{5.9}$$

Equation (5.8) and equation (5.9) have three equations and three unknowns for each angle and its two derivatives. The equations can be solved by using the elimination method or substituting method to make three equations with three variables. Hence, this is the purpose for selecting a fifth-degree polynomial to control the motion. The lower degree three terms (t^2, t^1, t^0) have coefficients with value zero to meet the constraints at $t = 0$. While, the higher degree three terms (t^5, t^4, t^3) and corresponding three unknown coefficients. If an additional higher degree terms applies, the additional constraint has to be added to the equation in order to solve the corresponding coefficients.

A MATLAB simulation was performed to validate the trajectory of SR-X arm. Figure 5.6 shows the simulation result of path planning trajectory. The simulation parameter for SR-X arm path planning is shown in Table 5.2.

Table 5.2: Simulation parameter for SR-X arm path planning

Sign	Description	Value
t	Initial time	0 s
t_f	Final time	2 s
θ_1	Initial shoulder joint angle	0°
θ_2	Initial elbow joint angle	0°
θ_{1f}	Final shoulder joint angle	60°
θ_{2f}	Final elbow joint angle	76°
l_1	Length of link 1	10.55 cm
l_2	Length of link 2	8.35 cm

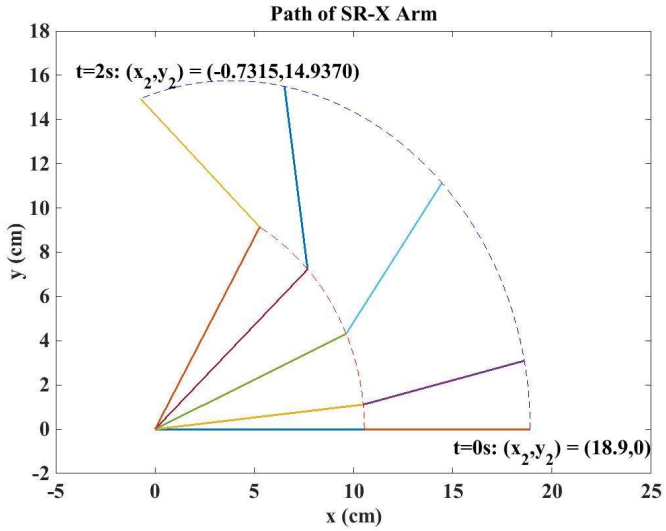

Figure 5.6: Simulation of path planning for SR-X arm in MATLAB. The x – y axis unit are in centimetre (cm)

From the simulation, the coefficient for θ_1 motion and coefficient for θ_2 motion are obtained as follow:

$$\mathbf{a} = \begin{bmatrix} 0.1963 & -0.9817 & 1.3090 \end{bmatrix}^T \tag{5.10}$$

$$\mathbf{b} = \begin{bmatrix} 0.2487 & -1.2435 & 1.6581 \end{bmatrix}^T \tag{5.11}$$

As noted in Figure 5.2, the initial position of end-effector was at $\begin{bmatrix} x & y \end{bmatrix} = \begin{bmatrix} 18.9 & 0 \end{bmatrix}$ (all in *cm* unit) which is the total length, $(l_1 + l_2)$ of SR-X arm on the *x* axis. The final

position of the end-effector from the graph was $[x \quad y] = [-0.7315 \quad 14.9370](cm)$. The simulation has been verified with the actual hardware to ensure the system is working properly when implementing in real time. The results of angle measurement for θ_1 and θ_2 were obtained as in Figure 5.7 and Figure 5.8. The final position of the end-effector obtained from the real time implementation was $[x \quad y] = [-0.8106 \quad 14.9449](cm)$ as in Figure 5.9.

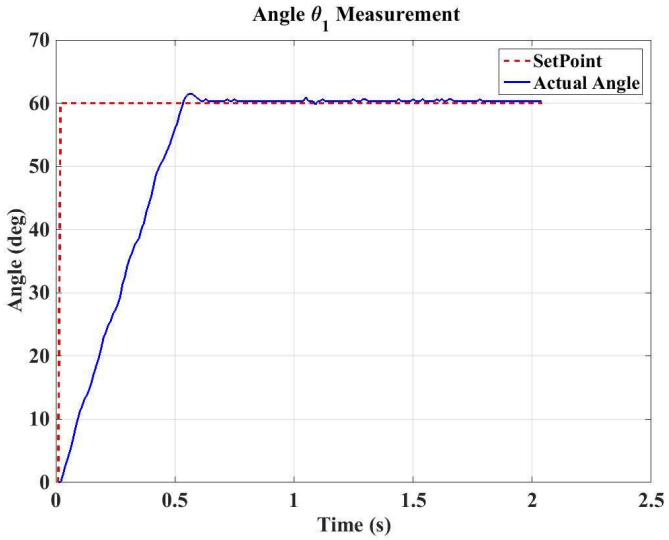

Figure 5.7: Real time implementation of link 1 for SR-X arm.

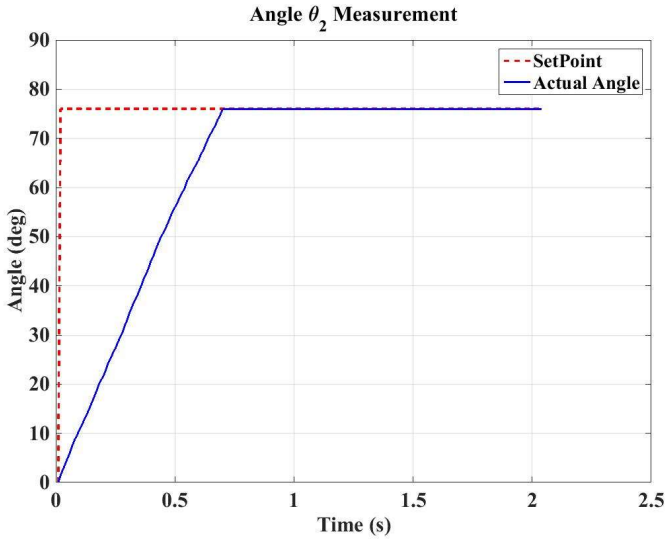

Figure 5.8: Real time implementation of link 2 for SR-X arm.

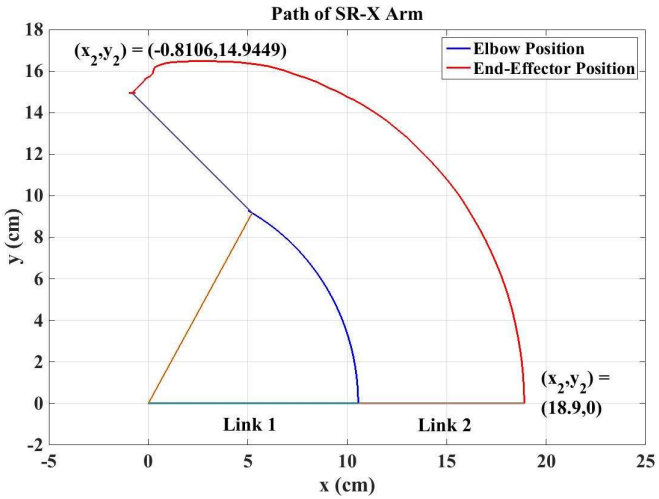

Figure 5.9: Real time implementation of path planning for SR-X arm. The x – y axis unit are in centimetre (cm)

5.3.1 Pole climbing based on self-locking

Friction force is a main property for every climbing robot to perform the climbing task. The higher the friction force applied toward the surface the better the mobility of climbing locomotion. This property allows the robot to attach to the surface and is called the self-locking condition. Self-locking can be obtained by friction and sufficient amount of external forces to create a locking condition (Lenormand et al., 1990; Spenle′ and Gourhant, 1993). This feature allows the robot to maintain its position on the pole with less power consumption.

The motion of a mechanical system can be described by the kinematic equations without considering the torques and forces generating that motion, whereas the relation between torques/forces and motion is clearly described by the dynamic equations. The importance of the equations of motion lie in simulation of the system and design of the drivers, motors and control algorithms.

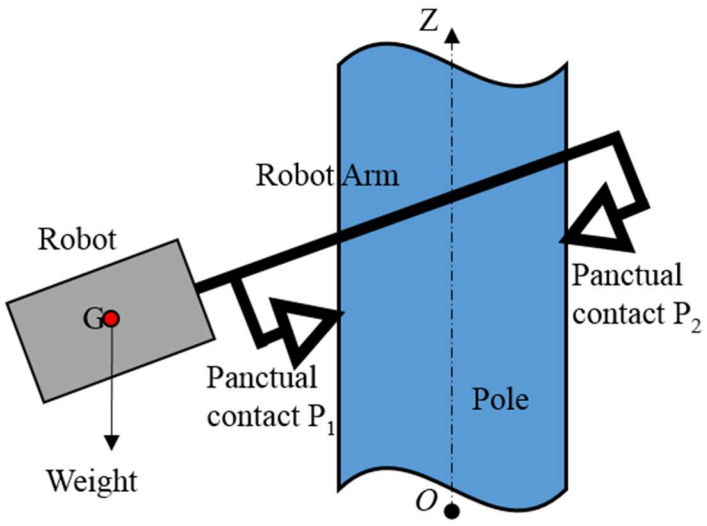

Figure 5.10: Self-locking on the pole for the robot

The robot has to obey the locking criterion in order to stay in position. Figure 5.10 shows the contact points P_1 and P_2 allowing the centre of mass G to be shifted according to friction conditions. Self-locking on climbing robot can be produced by adopting the locking mechanism as in Figure 5.10. However, for a climbing robot, it is easier to design the contact points using wheels/rollers. The wheels will produce a locking system so called "rolling self-locking". This locking principle will be used in the designed climbing robot. The robot requires at least two rollers with powerful actuation closer to the centre of mass.

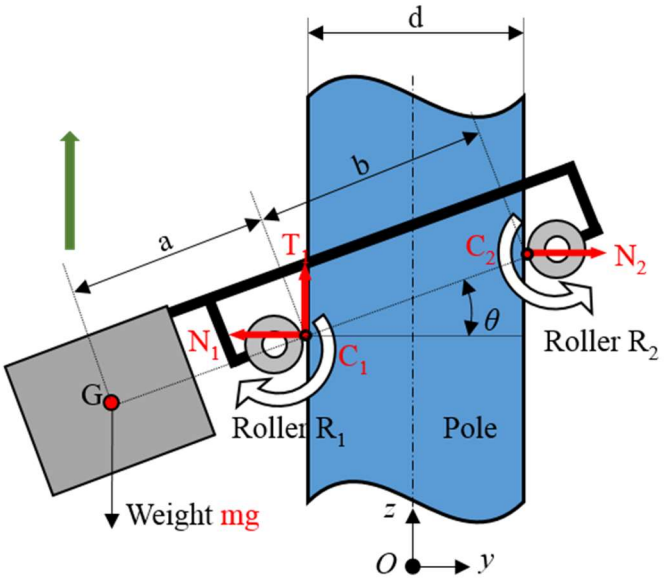

Figure 5.11: Rolling self-locking of climbing robot

Figure 5.11 shows the climbing robot with rolling self-locking. The Roller R_1 and roller R_2 are both designed to be actuated. Roller R_1 is in contact with the pole at C_1, which is transmitting a normal force N_1 and a tangential force T_1 from the pole to the robot. While roller R_2 is in contact with the pole at C_2, which is transmitting a normal force. Roller R_2 is actuated to provide very low resisting torque.

From the principle of statics, the rolling self-locking condition can be derived. The following results from *y* axis:

$$N_1 = N_2 \tag{5.12}$$

While in *z* axis yields

$$T_1 = mg \tag{5.13}$$

where, *m* and *g* are the mass of the robot and acceleration due to gravity respectively. At point C_1, the addition of torques around *x* axis yields,

$$mga\cos(\theta) = b\sin(\theta)N_2 \tag{5.14}$$

where, *a* is the distance between G and C_1 , *b* is the distance between the contact points C_1 and C_2, and θ the tilting angle of the robot. At point C_1, the non-slipping condition is derived based on Coulomb friction law with friction coefficient μ ,

$$T_1 \le \mu N_1 \tag{5.15}$$

Substituting for T_1 from equation (5.13) into equation (5.15) and rearranging yields

$$N_1 \ge mg/\mu \tag{5.16}$$

Using equations (5.12) and (5.14) the following expression is obtained for N_1:

$$N_1 = \frac{amg}{b\tan(\theta)} \tag{5.17}$$

Finally, the rolling self-locking condition is obtained from equations (5.16) and equation (5.17):

$$a \geq \frac{b\tan(\theta)}{\mu} \text{ with } \theta = \arccos(d/b) \tag{5.18}$$

Equation (5.18) shows that the geometry and friction properties are the factors that create the self-locking condition instead of the mass. If the distance of a is sufficiently long, it will create the self-locking. It follows from equation (5.18) that the friction property, μ is disproportional to the distance a. The locking condition will be retained when the tilt angle θ decreases, and this is proportional to the distance a. According to equation (5.17), when the angle, θ decreases, the normal forces will also increase. In practice for a climbing robot, it is impossible to keep a perfect horizontal level while climbing due to structure deformation. Therefore, the distance b will increase and cause the angle, θ to be increased as well. As a result, it creates a locking condition that can be verified in equation (5.18).

5.3.2 Climbing mode operation with PID controller

Climbing a pole using self-locking mechanism in the vertical angle, 90° requires the tilt angle, θ in Figure 5.11 to be retained at around 90°. In order to achieve this, a controller is needed to monitor the tilt angle and adjust the speed of the wheels accordingly to reduce the error in the tilt angle. Figure 5.12 shows the detailed configuration of the SR-X with PID controller.

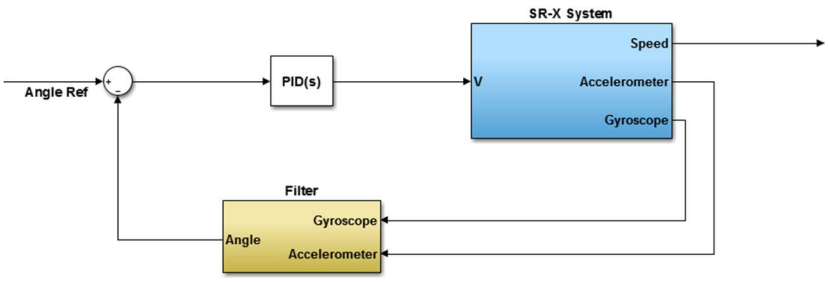

Figure 5.12: SR-X controller structure diagram for climbing mode operation.

The PID controller requires to be tuned properly according to the desired system output. Although methodologies for tuning the parameters exist such as Cohen-Coon and Ziegler-Nichols as well as some software tools, the controller parameters were manually tuned using a heuristic approach. In order to obtain a suitable combination of parameter values (*Kp, Ki* and *Kd*) to achieve satisfactory results, an online testing was carried out to investigate the system response. Table 5.3 shows the PID controller parameters set for the system in climbing mode.

Table 5.3: PID controller parameters for climbing mode operation.

Parameter	Value
Kp	7.0
Ki	1.0
Kd	1.0

In order to investigate the robustness of the PID setting, two tests were performed by pitch and roll assessment of the robot with respect to the wheels movement. Figure 5.13 and Figure 5.14 show the results of the tests for pitch and roll angle measurement respectively. The initial wheels speed of 40 mm/s (15 rpm) was used for this test.

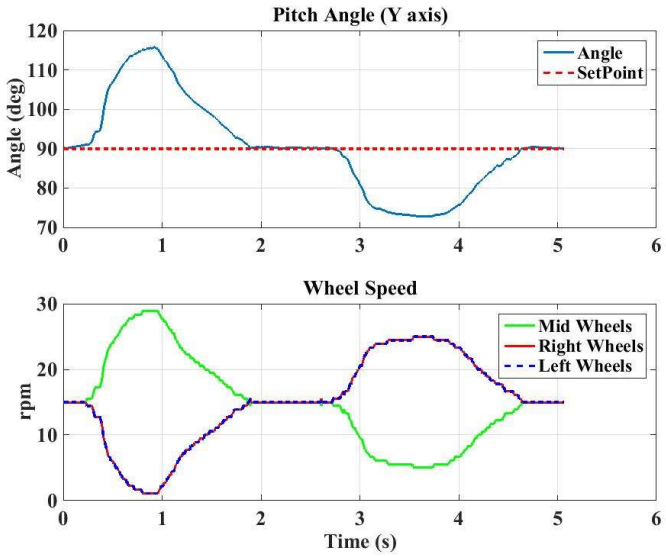

Figure 5.13: Pitch angle measurement

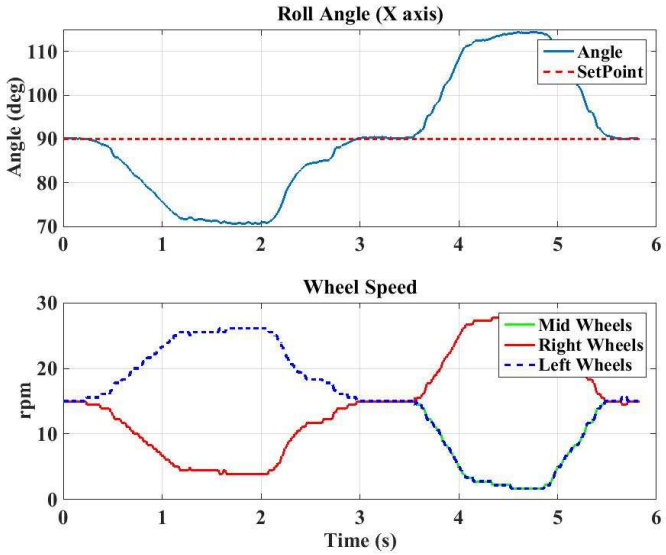

Figure 5.14: Roll angle measurement

The results show the response of the wheels speed whenever the sensor senses the deviation from the reference angle. Figure 5.13 represents the same position illustrated in Figure 5.11 where the error from pitch angle caused the middle wheel to accelerate and reduced the speed of left and right wheels and vice versa. On the other hand, the error from roll angle will cause either left or right wheel to accelerate while the middle wheel follows the acceleration of the wheel with slower speed as in Figure 5.14. These tests verified how the actual locomotion of the robot while performing the climbing task.

5.4 Path Planning for Walking Mode

In walking mode operation, foot trajectory planning is a fundamental part in the gait planning. The aim of the trajectory is to describe the necessary motion of the leg relative to links location and derivatives of locations. The leg's movement is determined by two factors: the extremity workspace with its movement paths and the joint geometry. The trajectory generation is based in the kinematics of the leg and can change depending on the terrain, or specific applications. There are two types of trajectory shape for legged robot: parabolic trajectory and triangular trajectory as in Figure 5.15 (Carlos et. al., 2012). The trajectories focus on the position of the tip of the foot, or in this case the end-effector of the two links manipulator.

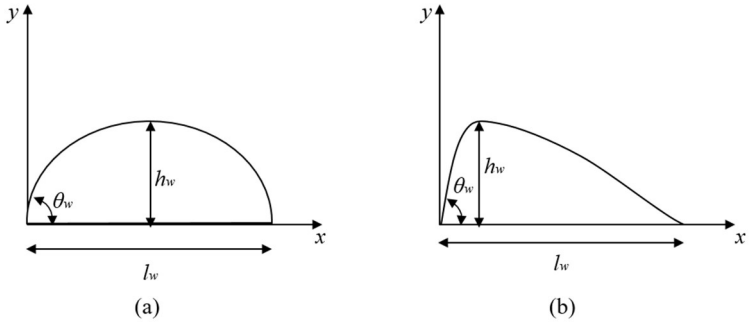

Figure 5.15: Foot trajectory shape; (a) Parabolic path; (b) Triangular path

In this project, the parabolic trajectory is considered as the path planning for SR-X leg in walking mode operation. The end-effector position trajectory can be represented by semi-circular path based on Figure 5.15 as follows:

$$x_w = r_w - r_w \cos(\pi(t)) \tag{5.19}$$

$$y_w = r_w \sin(\pi(t)) \tag{5.20}$$

where, $[x_w \quad y_w]$ is the end effector trajectory and r_w is the radius of the trajectory. A simulation was carried out to ensure the end-effector tracks the trajectory. Figure 5.16 shows the result of the single step simulation using parabolic path. Figure 5.17 and Figure 5.18 show the measurement angle of the each link for SR-X leg. The radius, r_w used in this simulation was 2 *cm*.

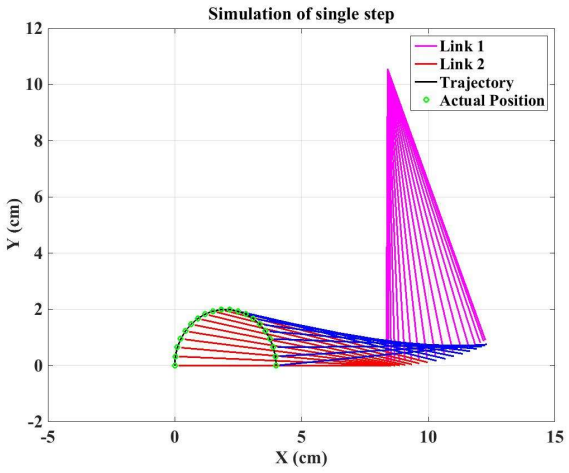

Figure 5.16: Simulation of single step using parabolic path

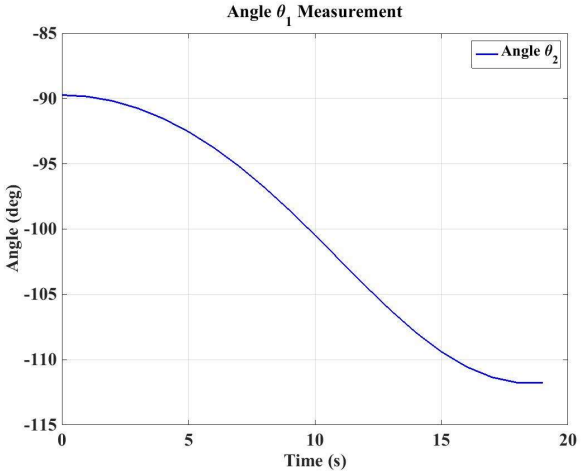

Figure 5.17: Angle, θ_1 measurement from simulation of single step using parabolic path

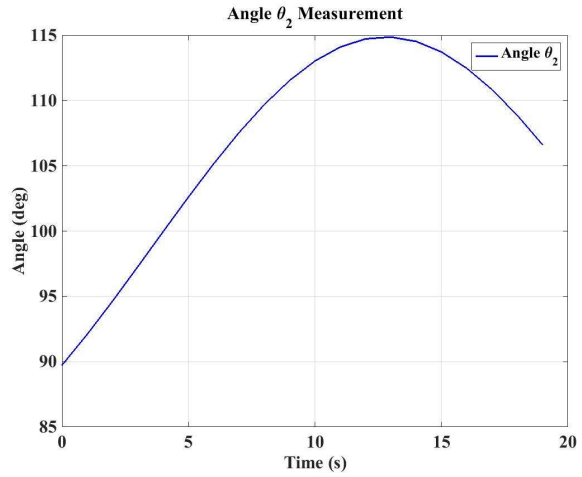

Figure 5.18: Angle, θ_2 measurement from simulation of single step using parabolic path

The simulation was verified with implementation in the actual hardware to investigate the performance of the SR-X leg action. Figure 5.19 shows the trajectory tracking of the end effector on one of the SR-X legs in the actual system. Figure 5.20 and Figure 5.21 show the tracking angle of link 1 and link 2 on SR-X leg respectively.

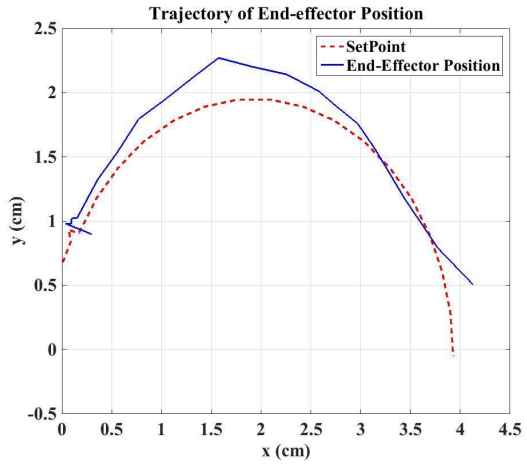

Figure 5.19: Actual experiment of single step using parabolic path

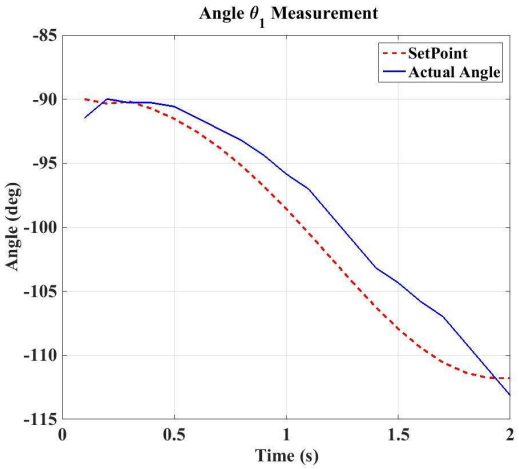

Figure 5.20: Angle, θ_1 measurement from real experiment of single step

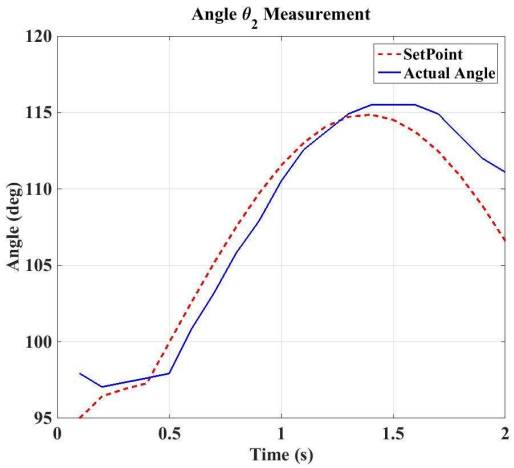

Figure 5.21: Angle, θ_2 measurement from actual experiment of single step

5.5 Path Planning for Steering Mode

In steering mode operation with skid steering system, there are three possible scenarios that occur while moving; move in straight line, turn left or right, and point turn. The robot moves in straight line if both set of drive wheels turn in tandem. If one set of wheel rotates faster than the other, the robot follows a curved path inward toward the slower wheel. However, if the wheels turn at equal speed, but in opposite directions, the robot pivots and it is known as point turn. According to those scenarios, the path trajectory of skid steering system is realised relative to the speed of the drive wheels.

In order to derive the functions for the robot's trajectory, the wheels have to be considered traveling at different speeds. Figure 5.22 shows the equivalent geometry for skid steering robot from Figure 4.11 in chapter 4.

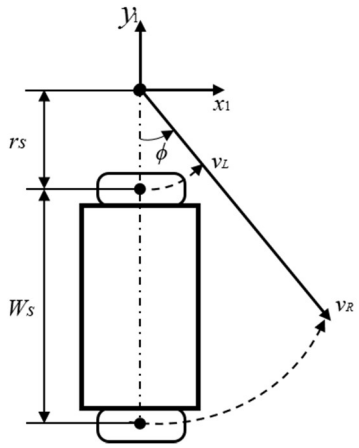

Figure 5.22: Geometric equivalent of four wheels skid steering configuration

From Figure 5.22, the differential equation describing the change in orientation with respect to time (angular speed) can be derived as follows:

$$\frac{d\phi}{dt} = \frac{(v_R - v_L)}{W_s} \tag{5.21}$$

where, $v_L = r_s\phi$ and $v_R = (r_s + W_s)\phi$ are the linear velocities of left and right wheels respectively. The change in orientation also applies to the absolute frame of reference. This change depends on the velocity at the COM. The velocity of the mobile platform is the average of both wheels speed and the differential equations for velocities are derived as follows:

$$\frac{dx_1}{dt} = \left[(v_R + v_L)/2\right]\sin(\phi(t)) \tag{5.22}$$

$$\frac{dy_1}{dt} = \left[(v_R + v_L)/2\right]\cos(\phi(t)) \tag{5.23}$$

By integrating equation (5.21), equation (5.22), and equation (5.23) with zero initial position and orientation, $x(0) = y(0) = \phi(0) = 0$ the position and orientation of the platform are obtained as:

$$x_1 = \frac{W_s(v_R + v_L)}{2(v_R - v_L)}\left[\cos(\phi)\right] \tag{5.24}$$

$$y_1 = \frac{W_s(v_R + v_L)}{2(v_R - v_L)}\left[\sin(\phi)\right] \tag{5.25}$$

$$\phi = (v_R - v_L)/W_s \tag{5.26}$$

The term $(W_s/2)(v_R + v_L)/(v_R - v_L)$ is the turn radius for the circular trajectory. It confirms that when the wheels turn at fixed speeds, the mobile platform follows a circular path. Equation (5.24) and equation (5.25) have the possibility to become infinitely large if their denominators equal zero where both wheels speed are equal. In order to avoid this situation, (Borenstein et al., 1996) proposed solution by removing the denominator term, $(v_R - v_L)$ for both equations as follows:

$$x_1 = \frac{W_s(v_R + v_L)}{2}\left[\cos(\phi)\right] = v_x\cos(\phi) \tag{5.27}$$

$$y_1 = \frac{W_s(v_R + v_L)}{2}\left[\sin(\phi)\right] = v_y\sin(\phi) \tag{5.28}$$

Note that, $v_1 = \begin{bmatrix} v_x & v_y \end{bmatrix}$ is the linear velocity and v_2 is the angular velocity of the robot from equation (4.63) in chapter 4.

5.5.1 Steering mode operation with PID controller

A simple trajectory tracking controller can reduce the error that occurs during the steering operation. In this project, a PID controller was used to minimise the position and orientation errors while implementing the steering operation. Arslan et al. (2011),

Malu et al. (2014) and Salem (2013) have successfully implemented PID controllers in skid steering mobile robot system. From Figure 5.22, the kinematic model at COM is given by,

$$\dot{x} = \frac{r(\omega_r + \omega_l)}{2}\sin\phi \tag{5.29}$$

$$\dot{y} = \frac{r(\omega_r + \omega_l)}{2}\cos\phi \tag{5.30}$$

$$\dot{\phi} = \frac{r(\omega_r - \omega_l)}{W_s} \tag{5.31}$$

where (x, y) is the position at COM, ω_r and ω_l are angular velocity of right and left wheels respectively, and *r* is the wheel radius.

For purposes of control, consider the new position vector, $q_r = [X_r \quad Y_r]^T \in \Re^2$ at the COM. The error vector between the set point and the platform location can be expressed, as follows:

$$e = \begin{bmatrix} X_r - X \\ Y_r - Y \end{bmatrix} \tag{5.32}$$

From equation (5.32), PID controller can be applied as follow,

$$u(t) = k_p e(t) + k_d \frac{d}{dt} e(t) + k_i \int e(t) dt \tag{5.33}$$

By using the tracking error in equation (5.33), the PID controller can be implemented in the skid steering configuration as shown in Figure 5.23. The model was simulated to evaluate the kinematics and dynamics of the system. The parameters in Table 5.4 were used to simulate the system.

Table 5.4: Simulation parameters for SR-X in steering mode

Sign	Description	Value
m	Mass of robot (kg)	2.70
r	Radius of the wheels (m)	0.025
W_s	Distance between left and right wheel (m)	0.0406
L	Distance between front and rear wheel (m)	0.1427
$L-a_s$	Distance between front wheel to COM (m)	0.0541
μ_x	Coefficient of friction in *x*-axis	0.9
μ_y	Coefficient of friction in *y*-axis	0.1
X_0, Y_0, ϕ_0	Initial position of the robot (m)	$[0 \quad 0 \quad \pi/2]$
X_r, Y_r	Desired position of the robot (m)	$[0.8 \quad 0.4]$
k_{Rp}	Proportional gain for right wheel	6.000
k_{Ri}	Integral gain for right wheel	0.001
k_{Rd}	Derivative gain for right wheel	11.000
k_{Lp}	Proportional gain for left wheel	2.055
k_{Li}	Integral gain for left wheel	0.004
k_{Ld}	Derivative gain for left wheel	0.045

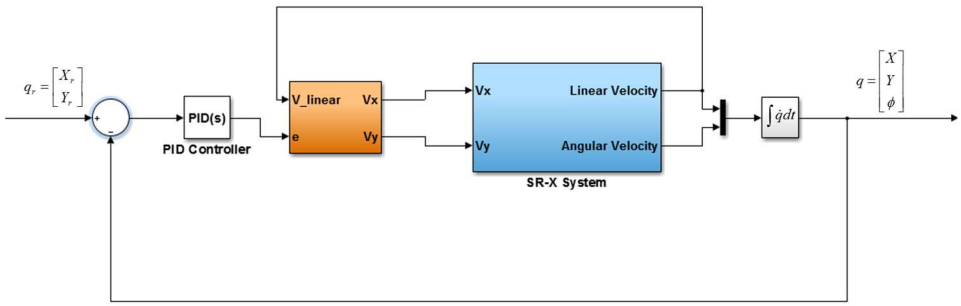

Figure 5.23: PID controller structure diagram for steering mode operation.

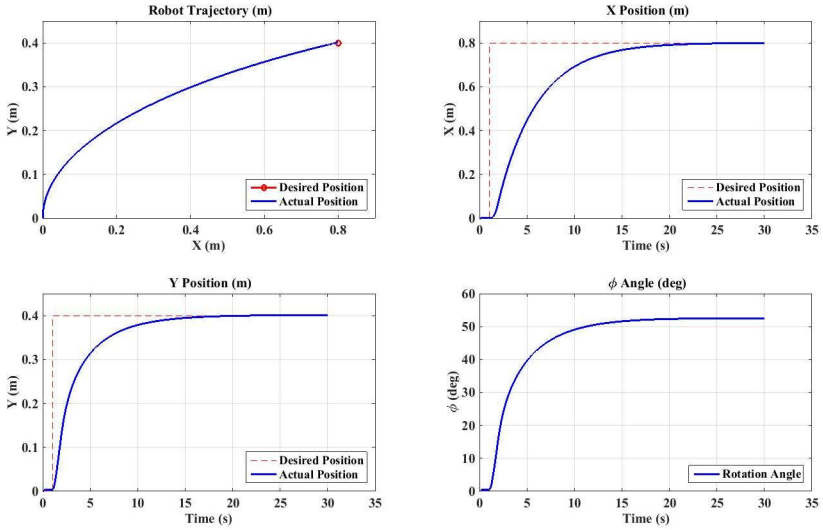

Figure 5.24: Simulation result of SR-X trajectory tracking position

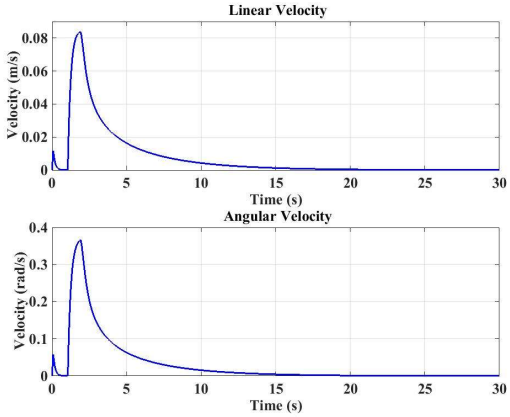

Figure 5.25: Simulation result of SR-X linear and angular velocity

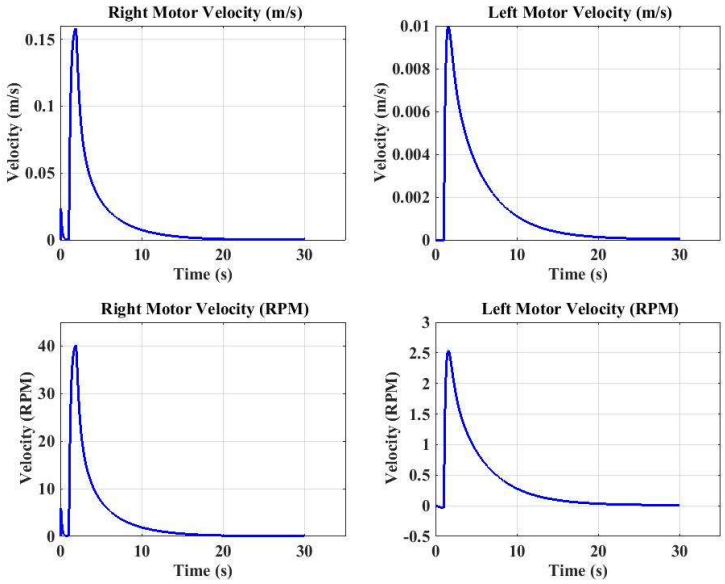

Figure 5.26: Simulation result of SR-X left and right wheels velocity

The simulation results for skid steering control obtained are shown in Figure 5.24, Figure 5.25 and Figure 5.26. The robot has successfully reached the desired position at $q_r = [0.8 \quad 0.4]^T$ using the set values for PID gains. The gains were heuristically tuned to achieve a satisfactory performance. In Figure 5.26, the speed for left and right wheels indicate the performance within the limitation of the motor with maximum speed of 114 RPM.

The real time experiment of skid steering for SR-X in steering mode operation will be discussed in chapter 6.

5.6 Summary

This chapter described the path planning and PID control system utilised in SR-X system in different configurations. The control system is divided into two levels: low level control for Dynamixel servo motor and high level control for motion algorithm. From the simulation, the system has successfully implemented the desired trajectory tracking. For climbing mode and walking mode, the initial experiment has been carried out to validate the motion trajectory as well as parameters tuning. Next chapter will discuss real-time experimental investigations carried out with the system.

CHAPTER 6

Real Time Implementation of SR-X

6.1 Introduction

This chapter will discuss the experiments conducted in actual hardware of SR-X system. The proposed design of versatile scansorial robot, SR-X was tested by simulation in chapter 5. The experimental results in this chapter demonstrate and verify the design and kinematics computations for different configurations mentioned in chapter 2. There are three experiments considered and implemented in this project: First, the locomotion of SR-X in climbing mode for pole climbing task; Second, the locomotion of SR-X in walking mode for step climbing, and; Third, the locomotion of SR-X in steering mode for inclined slope climbing.

6.2 Real time Implementation

The purpose of the experiments is to test the versatility of SR-X in real time implementation. A more specific aim is to validate the locomotion control of SR-X in different configuration modes namely climbing mode, walking mode and steering mode. For each individual mode, an appropriate motion control algorithm based on PID control is implemented to track the trajectory designed and discussed in chapter 4. The following section will discuss the results obtained from the experiments conducted during the process.

6.2.1 Experiment I: Climbing mode configuration

This experiment was intended to demonstrate the SR-X ability to perform the climbing task on straight pole. The combination of previous derivation of two links manipulator and self-locking mechanism in chapter 4 and chapter 5 provides enough information to implement the climbing task for SR-X. The arms of SR-X will be used as a grasping/gripping mechanism (adhesion mechanism) while, the friction force generated between the wheels and the pole surface will permit the robot to ascend

toward the upper pole. Figure 6.1 shows the real implementation of the robot grasping position on the pole.

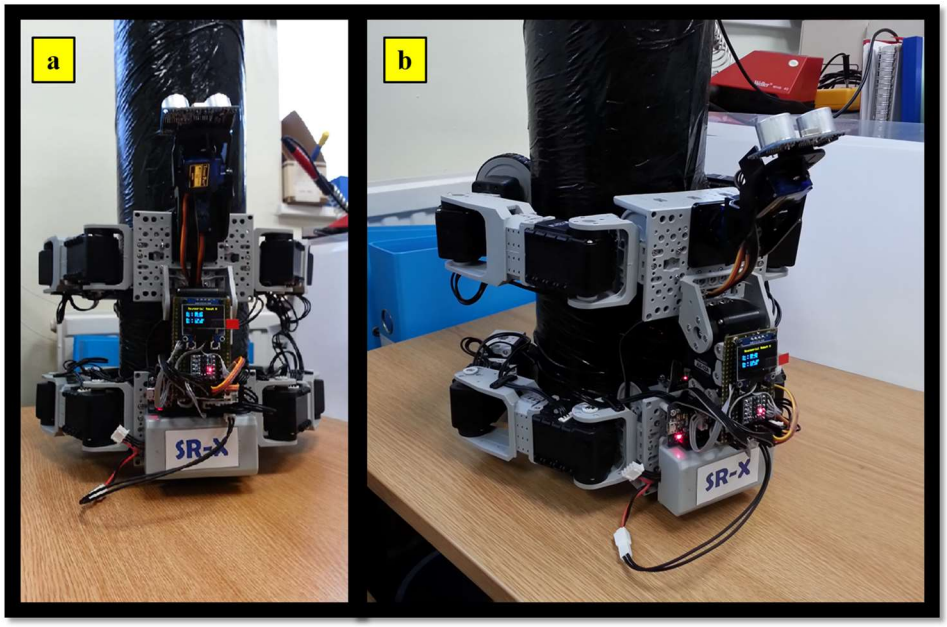

Figure 6.1: Real time implementation of SR-X grips on pole in climbing mode operation.

In order for the robot to grip on the pole properly, the angle of the grasping position should be critically considered. For optimal grip around the pole, the angle should be at least 120 degrees for both arms as shown in Figure 5.5 in chapter 5. This will produce sufficient gripping position to avoid the robot slipping from the pole due to the centre of gravity of the robot as illustrated in Figure 5.11. The initial speed used in this experiment was 15 rpm (40 mm/s).

Holding Force

Another point to be considered in climbing mode is the holding force. Since the adhesion mechanism used in the climbing robot is a grasping/gripping mechanism, the holding force produced by the robot should be measured. The dynamixel AX-12 servo motor used in the robot has the capability to generate the load feedback which is essentially important to calculate the force for the servo. A simple test was performed to measure the force produced by the servo motor using force gauge. Table 6.1 shows the result of the force measurement.

Table 6.1: Force measurement for Dynamixel AX-12A

Force Applied, F (N)	**Load Reading, L*d***	**Ratio, F/L*d***
6.10	160.00	0.038
6.75	192.00	0.035
7.30	256.00	0.029
8.00	288.00	0.028

Taking the average of the ratio will give the value of 0.032. This value will then multiply by 10 bits (1024 steps) to produce the actual force of 66.34 N. The force produced by the gripping is adequate to overcome the weight of the robot and eventually allows the robot to ascend on the pole.

Figure 6.2 shows the sequence diagram of climbing operation during the experiment. From the initial position Figure 6.2 (a), the robot performed a grasp with both left and right arms. Once the grip on the pole is secured, the robot initiated the climbing task operation shown in Figure 6.2 (b). The robot climbed at a steady speed as in Figure 6.2 (c, d, e, f) while PID controlled the robot position level at minimum tilt angle deviation. Figure 6.3, Figure 6.4 and Figure 6.5 show the speed measurement, holding force measurement and tilt angle measurement from the experiment in Figure 6.2.

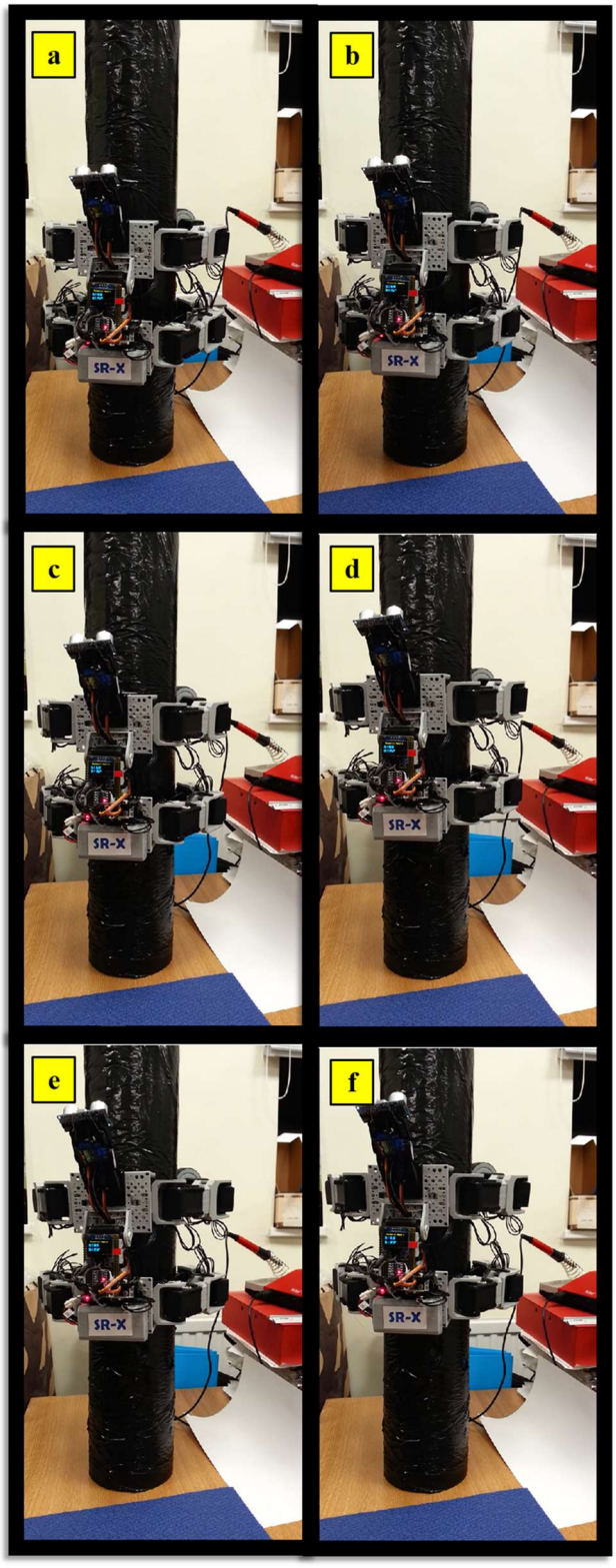

Figure 6.2: Real time implementation of SR-X in climbing mode operation.

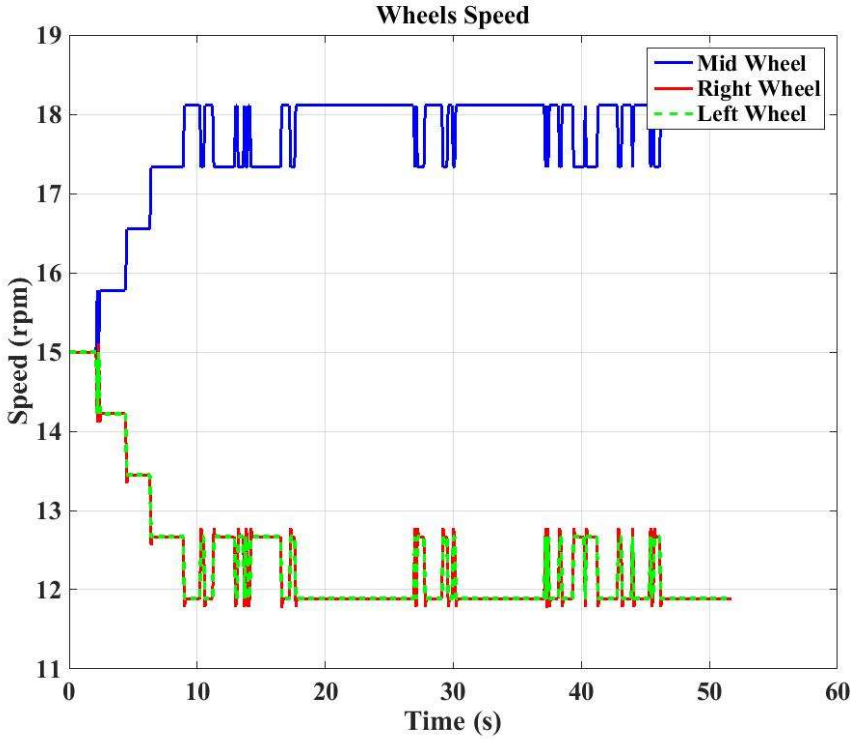

Figure 6.3: Wheels speed while climbing operation

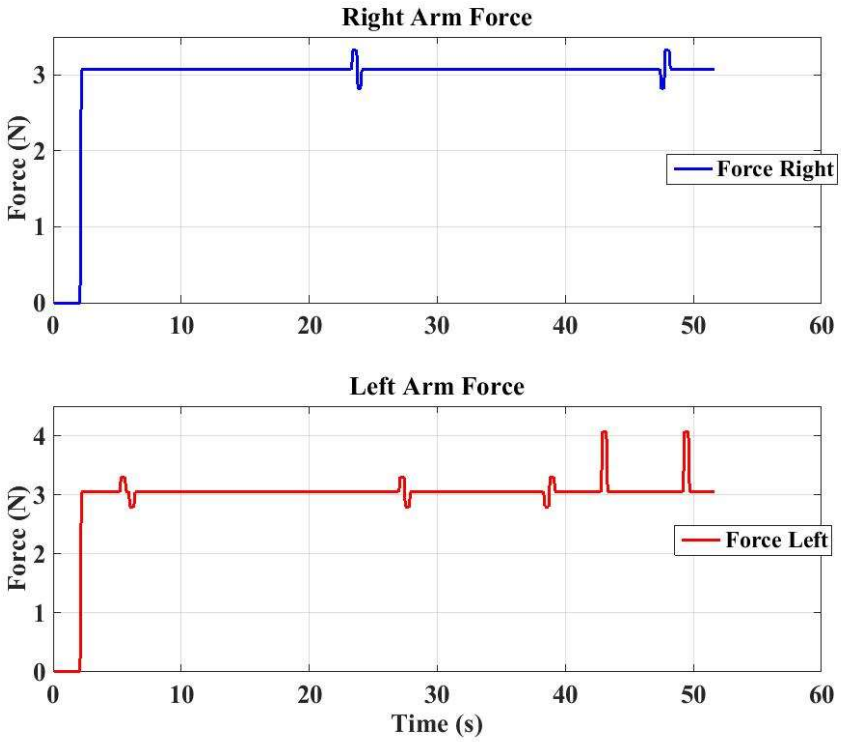

Figure 6.4: Holding force while climbing operation

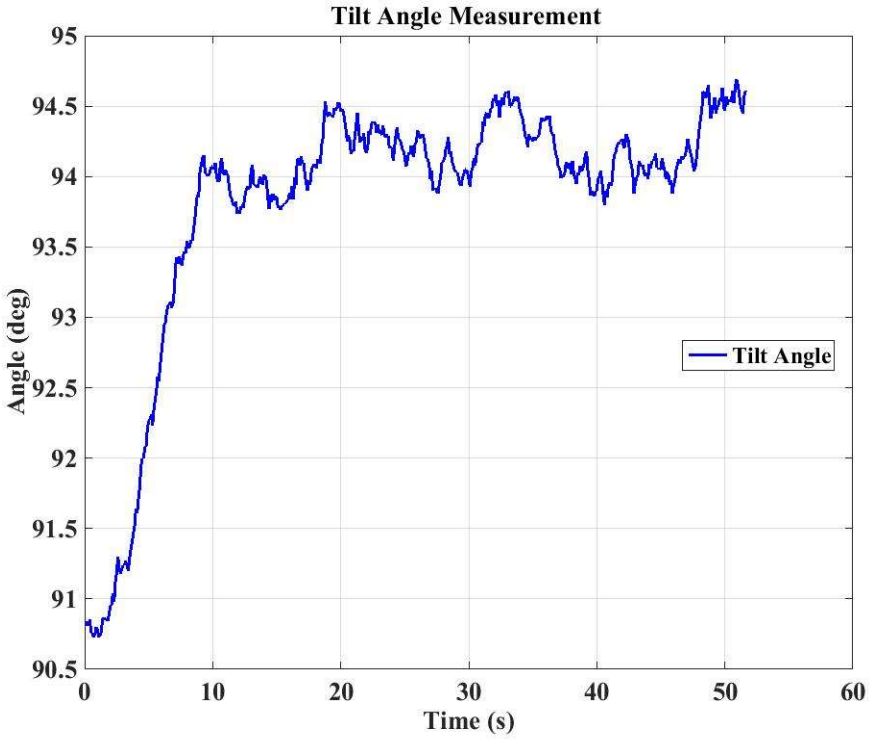

Figure 6.5: Tilt angle measurement while climbing operation

Figure 6.3 shows the implementation result from the experiment. It indicates that the middle wheel increased speed while left and right wheels decreased the speed to ensure the level position of the robot. Figure 6.4 shows the holding forces from both left and right arms while performing the climbing operation. Figure 6.5 shows the tilt angle (pitch angle) about ± 5 degrees from the actual angle set point of 90 degrees. In practice, the SR-X in climbing mode operation will not be able to keep a perfect horizontal level due to the structure deformation. However, this position actually provides a good grip for the robot since it can be considered as self-locking to pole.

6.2.2 Experiment II: Walking Mode Configuration

In order to implement this experiment, SR-X was configured into walking mode as shown in Figure 4.6 in chapter 4. The SR-X arms were configured into legs for walking mode operation. All the wheels servo were disabled as they are not used in this mode. This experiment is divided into two scenarios. First scenario is the implementation of SR-X in normal walking operation. Second scenario is more challenging by implementing step climbing in walking mode.

Scenario 1: Normal Walking Operation

This scenario was implemented to investigate the complete cycle of walking gait shown in Figure 2.7 in chapter 2 using the path planning from Figure 5.15 in chapter 5. SR-X successfully realised the walking gait as shown in Figure 6.6. Figure 6.6 shows snapshots of one of SR-X legs performing the trajectory.

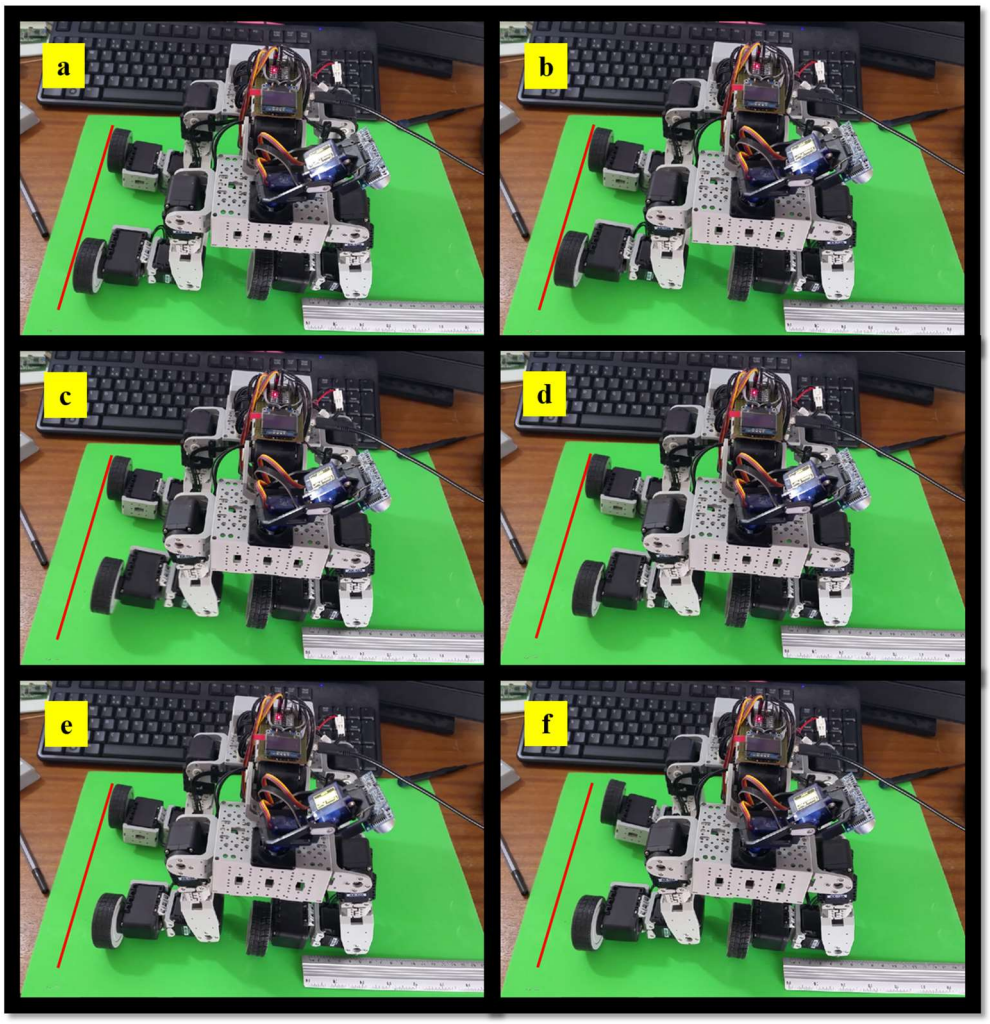

Figure 6.6: Real time implementation of SR-X in walking mode operation

Figure 6.6 (a) shows the initial position of the leg. Second snapshot, Figure 6.6 (b) shows the leg lifted off the ground at a quarter of the given trajectory. The leg position was at half of the trajectory with maximum height in Figure 6.6 (c). In Figure 6.6 (d), the position of the leg was at third quarter before it touched the ground in Figure 6.6 (e). Finally in Figure 6.6 (f), the subsequent leg performed the same trajectory to complete the walking gait. Figure 6.7 shows the trajectory of each leg performed by SR-X in walking mode operation.

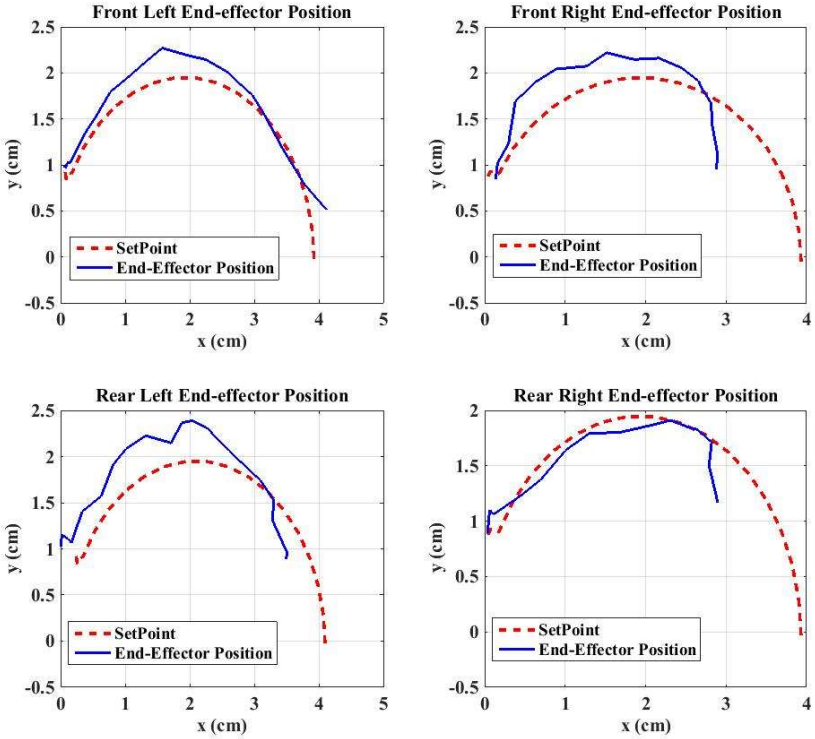

Figure 6.7: Trajectory tracking of real time implementation of SR-X leg in walking mode operation.

The reading of each leg's angle has been measured to investigate the tracking of the trajectory. Figure 6.8 and Figure 6.9 show the angle measurement of hip and knee respectively. Each leg took around one second to implement the trajectory. Therefore, for complete walking gait the time taken was four seconds in total.

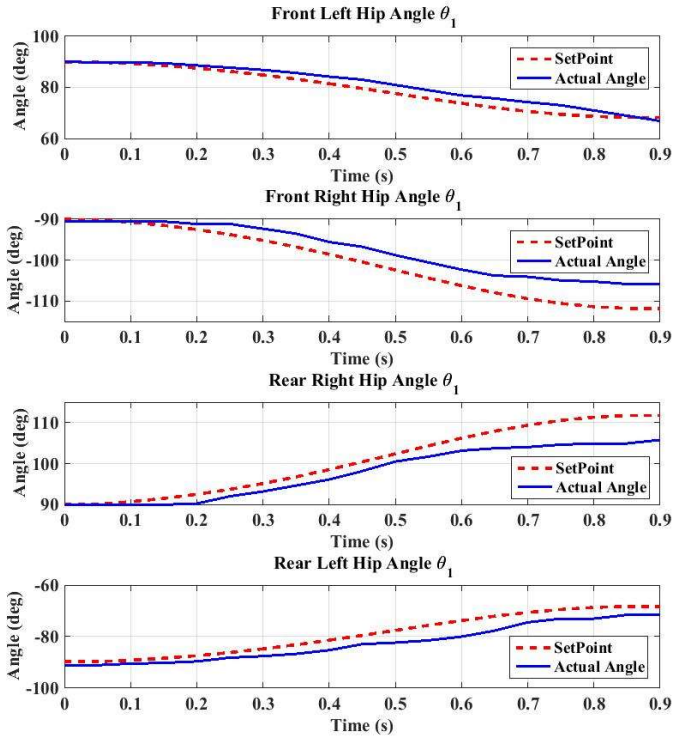

Figure 6.8: Hip angle measurement of real time implementation SR-X leg.

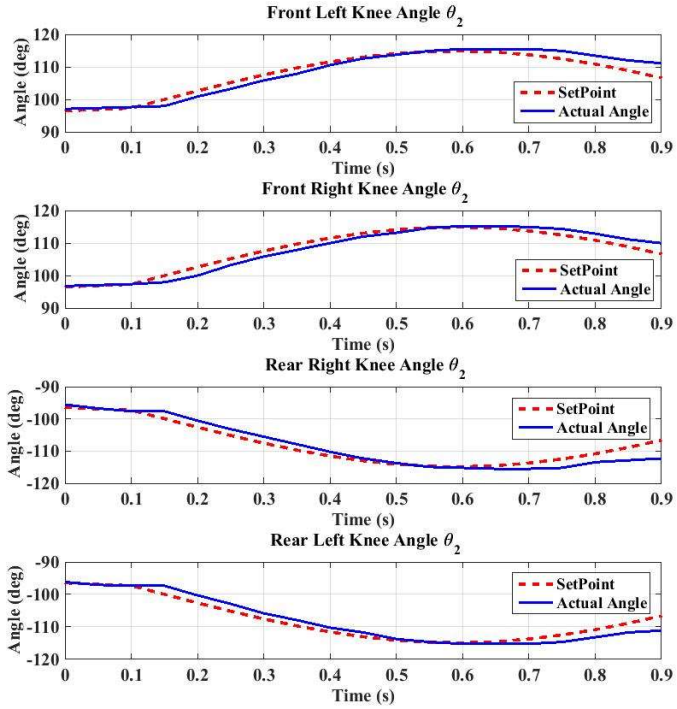

Figure 6.9: Knee angle measurement of real time implementation SR-X leg.

Scenario 2: Step Climbing in Walking Mode Operation

The second scenario for SR-X in walking mode operation is step climbing. In this experiment, a height of 10 *mm* from ground was chosen for SR-X to climb. Figure 6.10 shows the real implementation of step climbing in walking mode operation.

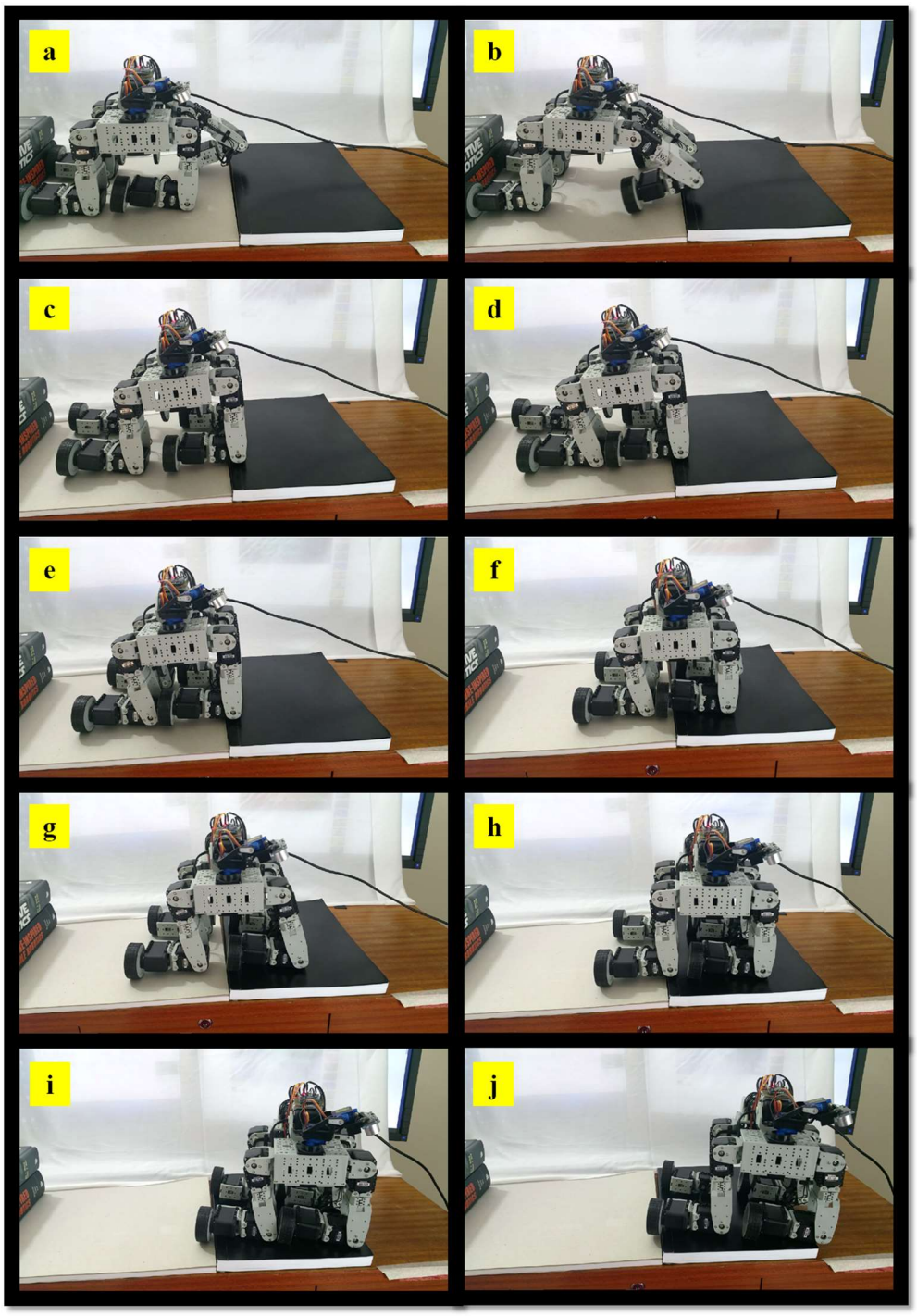

Figure 6.10: Real time implementation of SR-X step climbing in walking mode operation.

Figure 6.10 (a) shows the left leg lifted above the step and then followed by right leg as in Figure 6.10 (b). Next step was to move the SR-X body on the step as shown in Figure 6.10 (c). Once half of the body above the step, the normal walking operation took over as in Figure 6.10 (d, e, f, g, h, i, j) for the rest of the climbing task. From scenario 1 in walking mode operation, the trajectory of end-effector of the leg rose about 20 mm and therefore SR-X managed to implement the step climbing successfully.

6.2.3 Experiment III: Steering Mode Operation

For experiment III, SR-X was configured in steering mode as in Figure 4.9 in chapter 4. The SR-X arms were configured as the suspension in skid steering operation. All four wheels at the end of the link were enabled while the other two on the body were disable as they were not in contact with the surface. This experiment is divided into two scenarios. First scenario is the implementation of SR-X on flat surface. Second scenario is implementing the inclined slope climbing in steering mode operation.

Scenario 1: Manoeuvre on Flat Surface in Steering Mode Operation

This scenario was implemented to investigate the SR-X capability to perform skid steering on flat surface. It is also to verify the simulation done in chapter 5 for steering mode operation. In this experiment, the same parameters as in Table 5.4 in chapter 5 were used to implement in real time. Figure 6.11 shows the snapshots of SR-X performing skid steering operation on the flat surface. SR-X successfully executed the skid steering in steering mode operation. Figure 6.11 (a) shows the initial position of SR-X at origin coordinates, $q = \begin{bmatrix} 0 & 0 \end{bmatrix}^T$. In Figure 6.11 (b, c, d, e, f, g) shows the SR-X executing skid steering by increasing the speed of right wheels toward final position. Figure 6.11 (h, i, j) shows the SR-X moving in straight line forward and eventually stopping at desired position, $q_r = \begin{bmatrix} 0.8 & 0.4 \end{bmatrix}^T$.

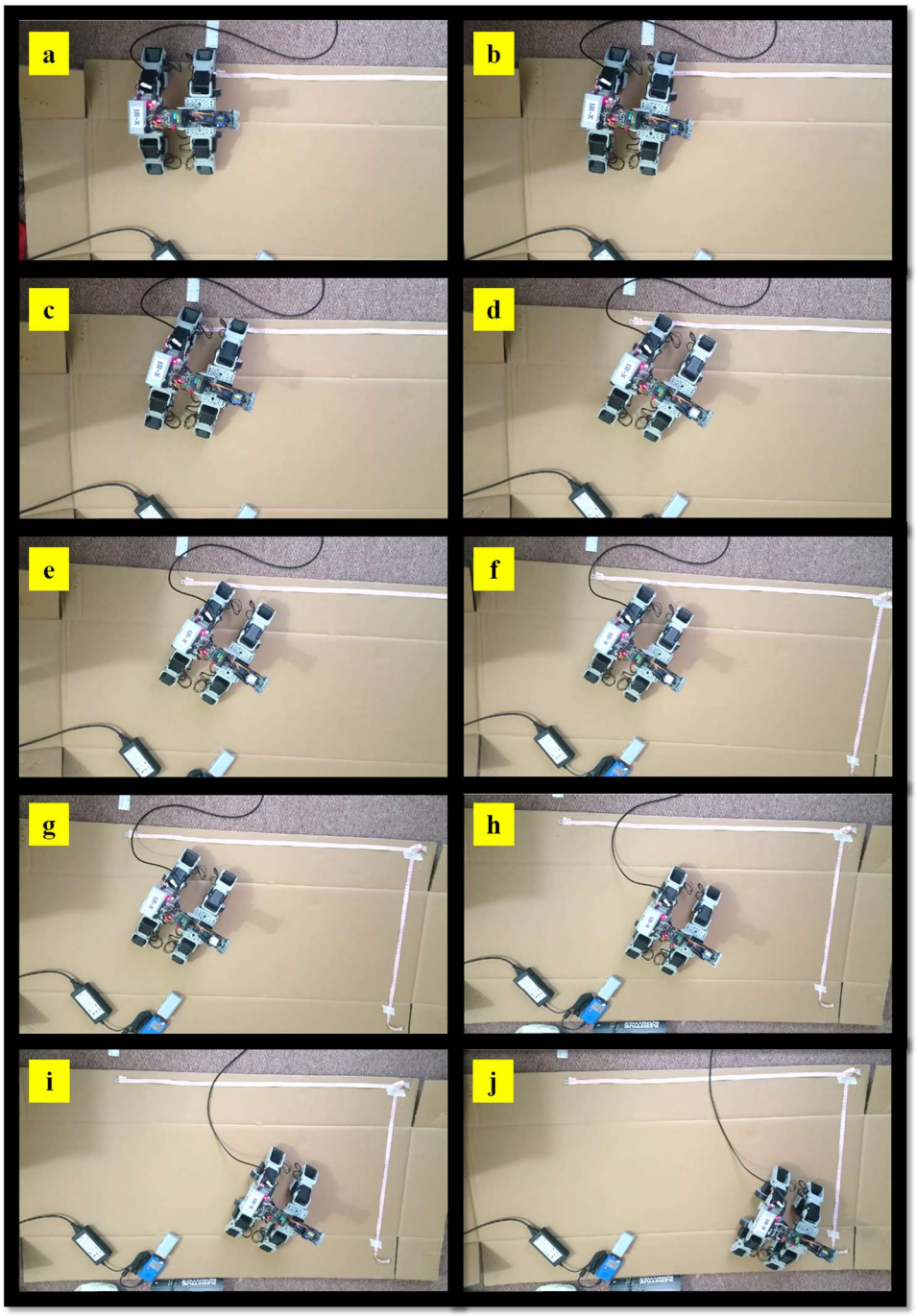

Figure 6.11: Real time implementation skid steering of SR-X in steering mode operation.

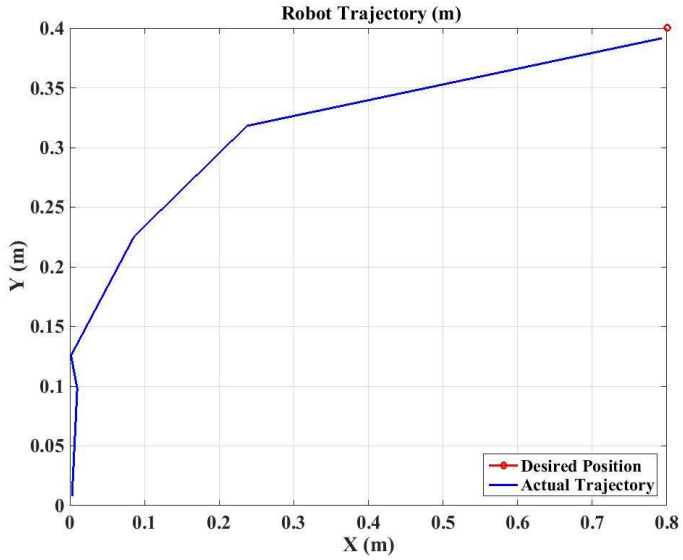

Figure 6.12: Real time implementation of SR-X trajectory position in steering mode operation.

Figure 6.12 shows that SR-X was successfully realised the skid steering operation to reach the desired position. The trajectory of SR-X was calculated based on the displacement of the wheels. The slightest slip on the wheels may cause the position error. Figure 6.12 shows 3 percent position error at the end of the experiment.

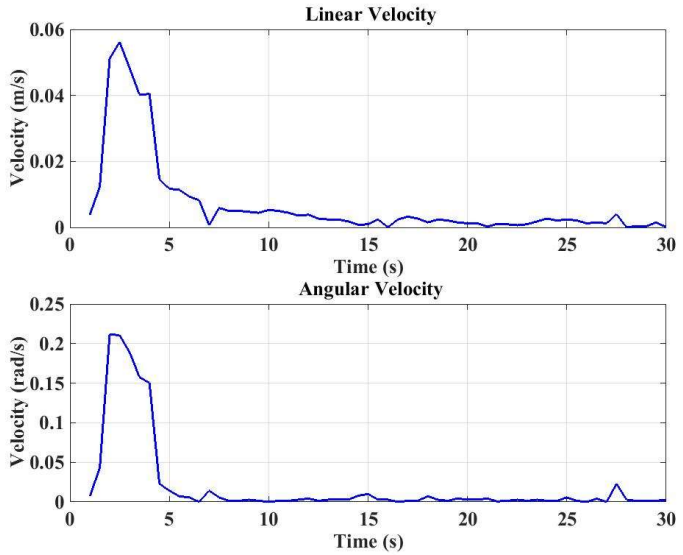

Figure 6.13: Real time implementation of SR-X linear and angular velocity

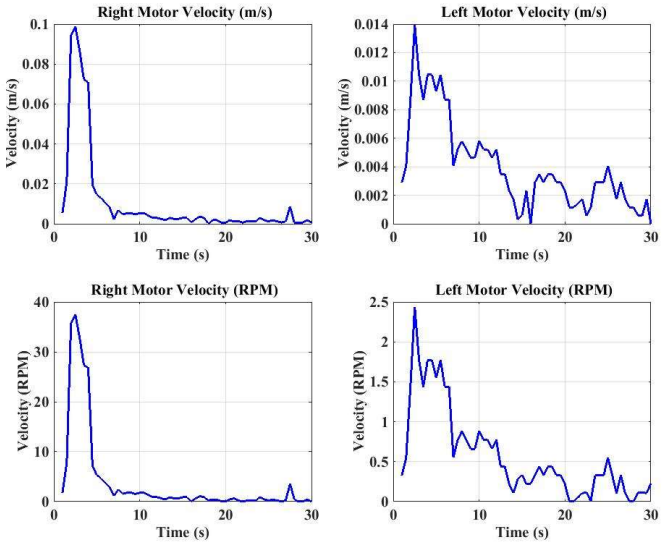

Figure 6.14: Real time implementation of SR-X left and right wheels velocity

Figure 6.13 shows the linear velocity and angular velocity of SR-X and Figure 6.14 shows the left and right velocity of the SR-X wheels for the skid steering operation. The figures that show the right wheels increased the speed by 30 percent compare to left wheels. This situation enables the SR-X to implement the skid steering.

Scenario 2: Inclined Slope Climbing in Steering Mode Operation

This experiment demonstrates the ability of SR-X to climb the inclined slope. In this experiment, the inclined slope of 10 degrees was used to investigate the climbing capability of SR-X in steering mode. The trajectory of this experiment was changed to straight line from initial position of $q = [0 \quad 0]^T$ and the final position $q_r = [0 \quad 0.5]^T$ *m*. Figure 6.15 shows snapshots of SR-X performing the climbing on inclined slope of 10 degrees. The experiment was successfully executed without a problem of slipping on the inclined surface. Figure 6.15 (a) shows the initial position of the SR-X before implementing the climbing task. Figure 6.15 (b, c, d, e) show the interval for every 0.1 *m* displacement of SR-X position on the inclined slope. Finally Figure 6.15 (f) shows SR-X stopping by position 0.5 *m*.

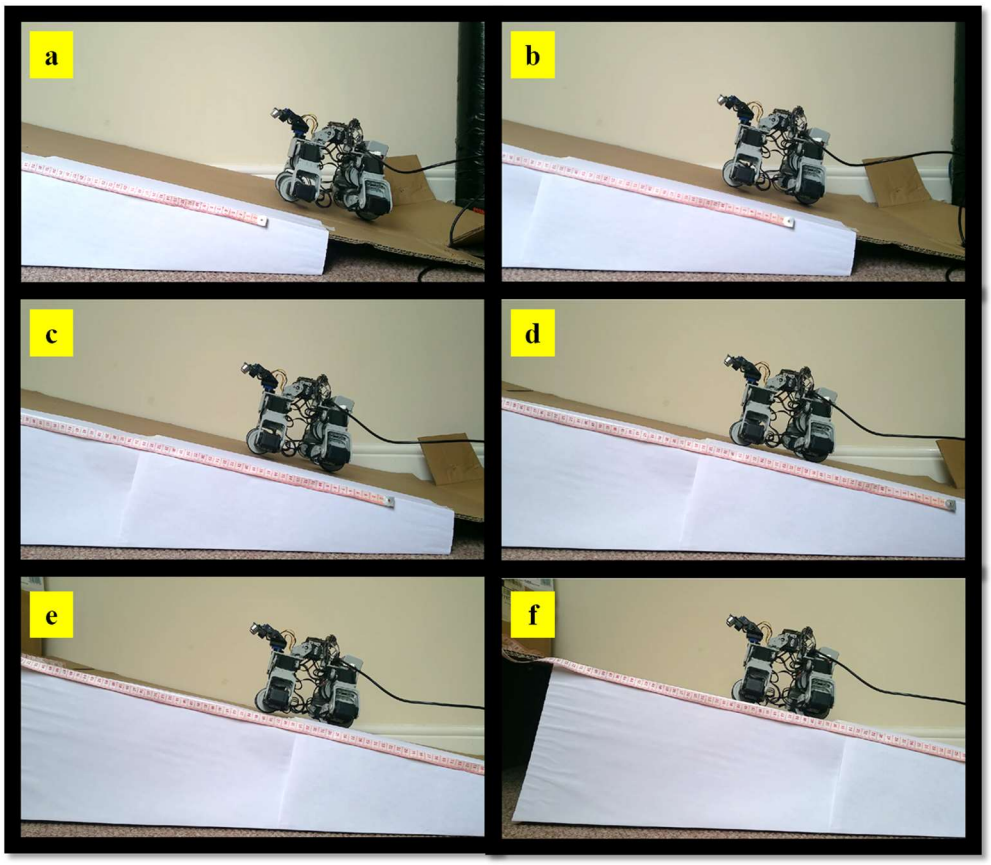

Figure 6.15: Real time implementation inclined slope climbing of SR-X in steering mode operation.

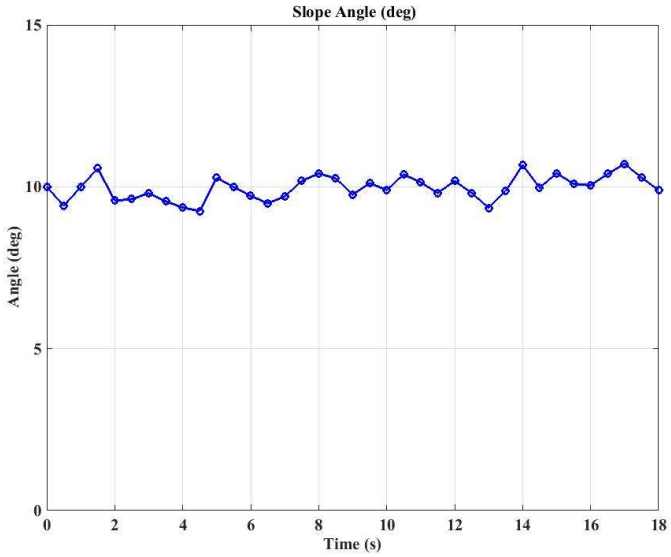

Figure 6.16: Angle measurement of inclined slope while SR-X implement climbing task in steering mode operation.

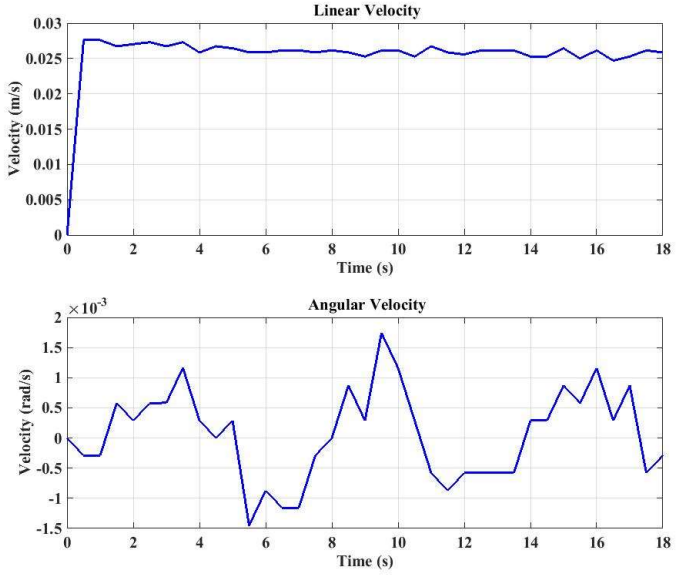

Figure 6.17: Real time implementation of SR-X linear and angular velocity on 10° inclined slope

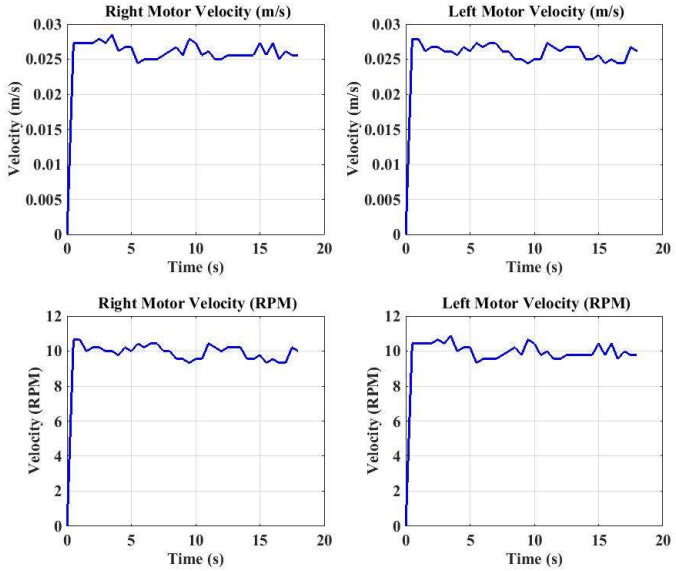

Figure 6.18: Real time implementation of SR-X left and right wheels velocity on 10° inclined slope

Figure 6.16 shows the angle measurement of the slope while SR-X realises the climbing task. It indicates the angle almost constant at 10 degrees across the whole experiment. The speed of SR-X as measured is shown in Figure 6.17 and Figure 6.18. The average linear velocity of SR-X was at 0.025 *m/s* which indicates both left and right wheels had the same speed as in Figure 6.18 for straight line manoeuvre. The

angular velocity of SR-X was measured to determine that there was no skid while executing straight line manoeuvre. It indicates the angular speed measured around zero value which means that SR-X realised straight line manoeuvre on 10 degrees inclined slope.

6.3 Summary

This chapter discussed experiments of real-time hardware implementation of SR-X in different modes namely climbing mode, walking mode and steering mode. SR-X has successfully implemented all three experiments. In climbing mode, SR-X has successfully performed the climbing task on a straight pole. In walking mode, there were two scenarios considered; normal walking operation and step climbing operation. While in steering mode, SR-X managed to implement the skid steering mode on a flat surface and also climb an inclined surface. Therefore, the experiments have validated the versatility of the scansorial robot proposed for the project.

CHAPTER 7

Conclusion and Future Work

7.1 Summary and Conclusion

The objective of the project was to develop a versatile scansorial robot (SR-X) to perform the climbing task in different environments namely pole, step and inclined surfaces. In order to implement the tasks the SR-X adapts the locomotion mode for each surface as such climbing mode for pole climbing, walking mode for normal walking operation and step climbing, and steering mode for skid steering manoeuvre and inclined slope climbing operation. The project has realised a flexible new scansorial robot that has the capability to be configured into different operation modes to achieve this objective.

The new design approach presented in this thesis is based on the hybrid leg-wheel mobile robot. The design was derived from a function-oriented analysis of the state-of-the-art scansorial robot capable of executing either climbing, walking or steering. The hybrid robot with leg and wheel attached allows the robot to implement walking locomotion by using the leg and steering ability from wheels. However, the design has to be innovative to deal with the requirements of the project. The new approach adopted in the new scansorial robot design along with other design characteristics provide solutions to the different configurations related to the operations of SR-X over different environments. Hence, the proposed design approach provided a systematic and practical development method that addressed the overall design according to the required configuration and locomotion operation. The versatile scansorial robot development outlined in this thesis allows the new design concepts to adapt to different environments with the configurable design to implement the locomotion operation according to the surface.

In order to analyse the SR-X capability, a 3D virtual prototype of the complete system was developed in Autodesk Inventor Professional 2014 Student version. The 3D design has been used to study the flexibility of the robot in different configurations and the outcomes of the analysis have become the deciding factor for the robot

locomotion operation. Moreover, the design has allowed limitation analysis of the robot to ensure the configurations applied are within operating limit in the actual hardware. Another benefit of virtual design is the project cost estimation; the cost of the actual robot can be estimated within the available budget and the time taken for trial and error process can be eliminated.

From the virtual design of actual robot, the measurement needed for further analysis can be obtained. As the design of the SR-X arm implicates two link manipulator, the link measurement has been used to simulate the system in MATLAB for locomotion analysis. This project has focused on the robot configuration that allows a certain locomotion to be applied. Hence, in climbing mode the arm of SR-X was simulated to grip the pole at a certain angle for each link. Similarly in walking mode, the arms were converted into legs to allow the walking locomotion be implemented. However, in steering mode the link was set at constant angle to act as a suspension for skid steering operation. The simulation has been carried out before implementing the control algorithms on the actual system so as to avoid any mistake that may cause damage to the hardware. Following completion of the simulation phase and ensuring that the results adhere to the operating limits of the hardware, the motion algorithm has been coded in C programming and implemented on the microcontroller. In this project, each mode of operation is run individually and an automatic transformation mechanism between configurations has not been developed, and this will form part of the future recommended work.

The first mode of operation of the robot comprises climbing for which the implementation of grasping mechanism has been presented with experimental verification. A PID control mechanism has been developed to control the tilt angle with respect to the movement of the wheels. By controlling the angle, the robot can provide a good grip while climbing as well as maintain the climbing stability. The experimental results have shown the ability of the robot to grasp/grip the pole and climb steadily. The sensory system incorporated into the SR-X allows to sense the distance between the robot and surfaces and keep track of the distance to avoid climb further at top of the pole and similarly stop descend when near the ground.

The second mode of operation of the robot is walking, and this has been successfully executed. The required walking gait of the robot has been verified as in simulations and experimentally. By implementing the motion sequence of SR-X legs with the

trajectory tracking, the SR-X has managed to perform the complete walking gait locomotion within 4 seconds. SR-X also successfully implemented step climbing. The stability of the robot during step climbing has been ensured by carefully distributing the body mass inside the support polygon and by using short step trajectory to counteract with any foreseeable instability problem.

Steering as the third mode of operation of the SR-X has successfully performed the skid steering manoeuvre by applying different speeds for left and right wheels. In this mode, PID control has been used to reduce the position error by tracking the desired position, and satisfactory trajectory tracking performance has been achieved. The position error has been translated into wheels speed and therefore, the SR-X has managed to execute the skid steering effectively. The robot has also successfully performed the inclined slope climbing. Given enough friction between wheels and the climbed surface, the SR-X has managed to climb the inclined slope without slipping down.

In conclusion, SR-X has accomplished the objectives set by the project as a versatile scansorial robot. The robot has managed to implement all three modes of operation namely climbing mode, walking mode and steering mode. PID control mechanism for each of the operating modes have allowed to achieve satisfactory trajectory tracking performance.

7.2 Recommendation for Future work

The main objectives of this research have been successfully achieved in real time for the versatile scansorial robot (SR-X) using PID control for trajectory tracking with an acceptable performance. However, there are many areas that can be explored further. The following suggestions can be pursued for further development of the current SR-X. The robot has been equipped with LCD display and two buttons (cursor and select buttons) for in-situ operations. Due to the limited time for this project, the fully or partially autonomous operation cannot be performed in time. Figure 7.1 shows snapshots of the LCD display with all configurations investigated in this research. Figure 7.1 (a) shows the boot-up screen of SR-X whenever the power is turned ON or when the microcontroller is reset.

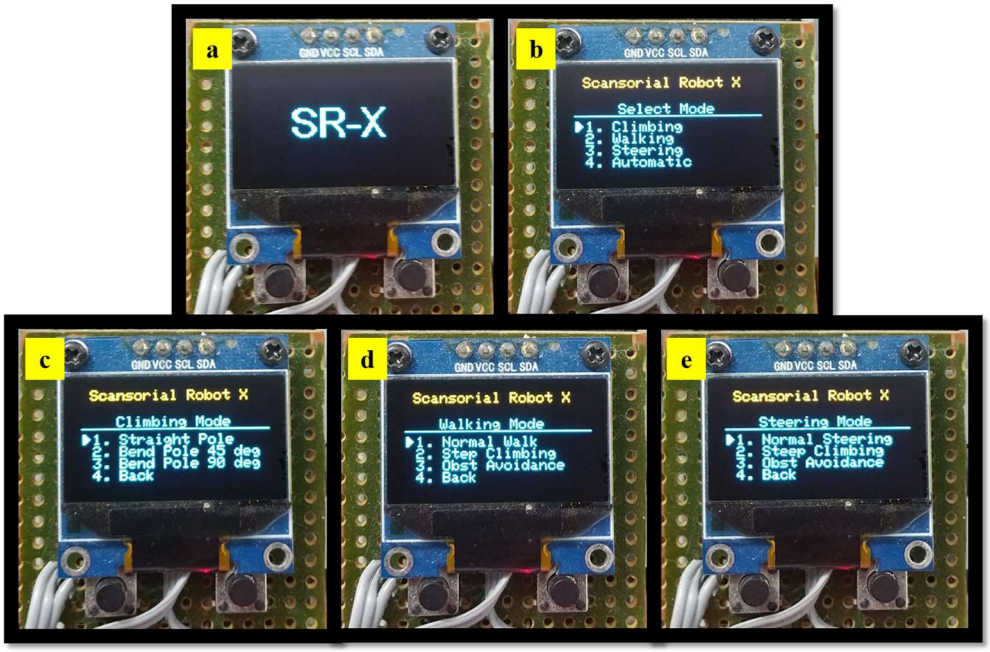

Figure 7.1: Menu on LCD display on board of SR-X

The main menu of SR-X program can be seen as in Figure 7.1 (b). This menu is the mode selection and includes the climbing mode (Figure 7.1 (c)), walking mode (Figure 7.1 (d)), steering mode (Figure 7.1 (e)) and automatic. The program can be selected by pressing the cursor button on the left side. The desired program can be selected by pressing the right button.

7.2.1 Future work for climbing mode

The LCD display shows the climbing mode operation in Figure 7.1 (c) with a sub-menu which includes the sub-program for this mode. For this research, the first program has been completed. However, further two sub-programs were not completed due to time constraints. SR-X has been designed to have flexible body joint where it is possible to implement the pole climbing operation of 45 degrees and 90 degrees bend. Theoretically the operation can be done but the actual experiment needs to be implemented to ensure the capability of SR-X for those operations. Figure 7.2 shows an illustration of climbing operation on 45 degrees bent pole and Figure 7.3 shows an illustration of climbing operation on 90 degrees bent pole.

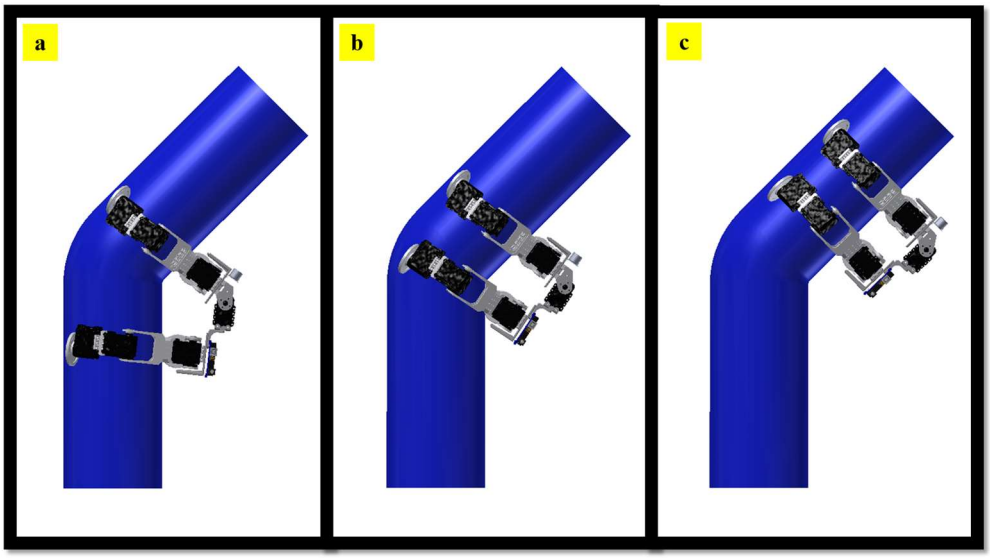

Figure 7.2: An illustration of SR-X climb on 45 degrees angle bend pole

From the illustration, in order to sense the bend on the pole, the ultrasonic sensor on board can measure the current distance between the robot and pole. Using this measurement as an input for bend operation, the body joint can be programmed accordingly.

The specification on roughness of the surface should also be investigated to ensure the robot does not slip while performing the climbing task. As the robot relies on friction forces to adhere on the pole, it is recommended to use a material with highest friction coefficient for better performance.

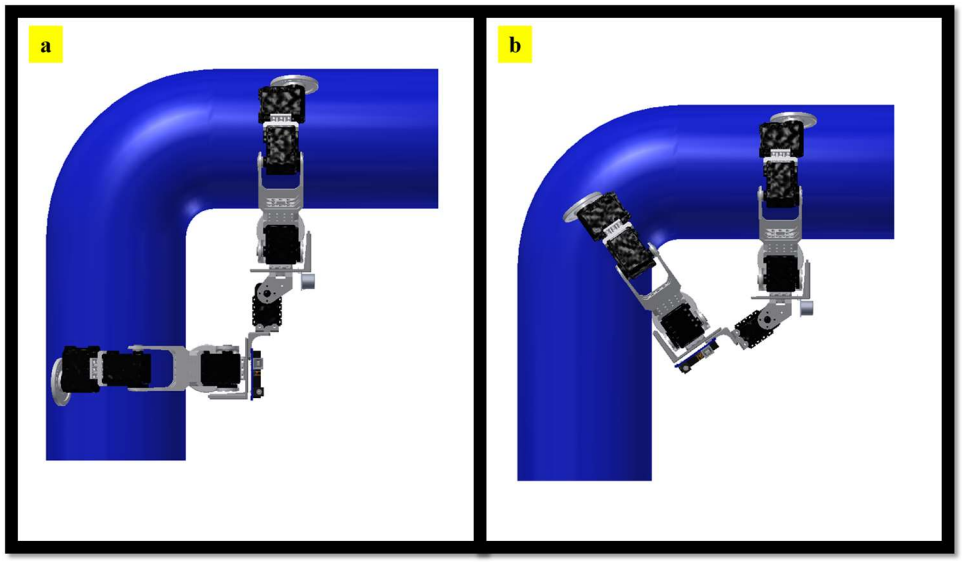

Figure 7.3: An illustration of SR-X climb on 90 degrees angle bend pole

Another suggestion in climbing mode is to implement different types of controller to minimise the tilt angle error during climbing operation. Optimisation of the current PID controller may reduce the error. However, online optimisation is not recommended due to time consumption during the operation and actual hardware may not be able to cope with the on board computation. It is recommended to do offline optimisation, and later apply the final tuned result to the motion algorithm.

7.2.2 Future work for walking mode

Figure 7.1 (d) shows the walking mode sub-menu and includes the sub-program for this mode of operation. The first (normal walking) and second (step climbing) sub-program have been successfully executed individually for this research. Automatic transformation from normal walking mode to step climbing was not realised due to the time constraints. There are several improvements that can be made in this mode such as improve the stability of SR-X while executing the walking and step climbing. By varying the step distance and with help of the accelerometer on board, the body mass distribution of SR-X can be done through dynamic stability system. This option may take long time to program as every time the leg lifts off the ground and swings to make the step, the body mass shifts significantly outside the support polygon. Short distance step is recommended while implementing this operation.

Another recommendation for walking mode is obstacle avoidance which is the third option in Figure 7.1 (d). The ultrasonic sensor can measure the distance to an obstacle in front of SR-X up to 400 *cm* apart. This distance allows the robot to make a turn with a specific motion algorithm for turning in walking mode. Due to no yaw rotation on the hip, the turning for SR-X can be challenging.

7.2.3 Future work for steering mode

Figure 7.1 (e) shows steering mode sub-menu operation, and includes the sub-program for SR-X. The first (normal steering) and second (steep climbing) sub-program have been successfully executed individually in this research. There are a number of future works that can be done in steering such as multiple waypoint for SR-X to manoeuvre and avoidance obstacles. The ultrasonic sensor can measure the distance of the obstacle and calculate the turning point to avoid the obstacle.

Apart from the sub-program, the controller used to track the trajectory can be improved by using offline optimisation of the PID controller. The optimised controller can be applied on the system. Furthermore, a different type of controller can be implemented in SR-X provided that the program is written in microcontroller language.

7.2.4 Inside duct system (pipe) manoeuvre

Another capability of SR-X is manoeuvring inside the duct system. Similarly to the climbing pole by grasping the outer pole, this manoeuvre can be implemented by grasping the duct system outward. Figure 7.4 shows an illustration of SR-X grasping inside duct system or pipe provided that the diameter of the pipe is bigger than the configuration in this mode.

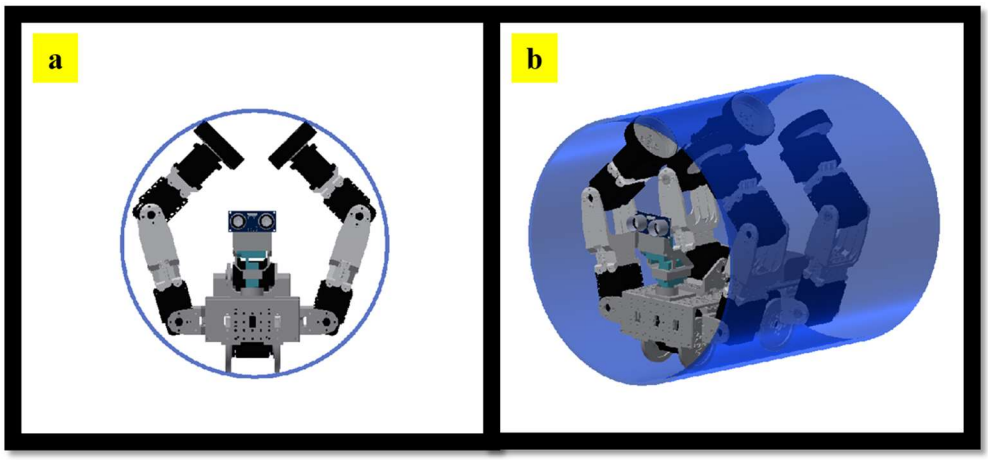

Figure 7.4: An illustration of SR-X manoeuvre inside duct system or pipe

7.3 Hardware

The current SR-X system uses USB to communicate with the computer to send the data for analysis. A wireless communication module can be equipped in SR-X system for future work. This module will allow the robot to send the data wirelessly to the main computer and a very effective solution to avoid tangle cable during the experiment. It will also allow the robot to fully standalone and controlled by gamepad for manual operation. Figure 7.5 shows the wireless module and gamepad for microcontroller used in SR-X.

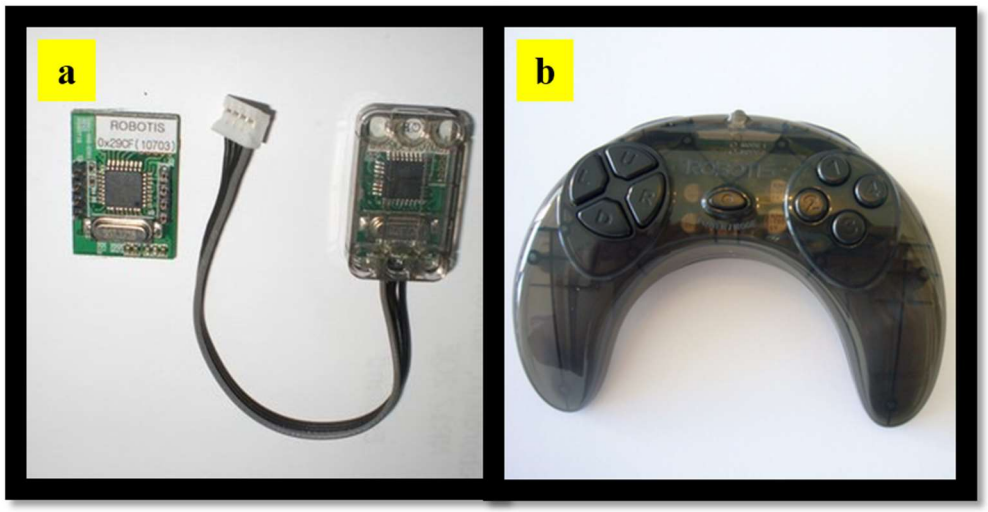

Figure 7.5: (a) Wireless module and (b) gamepad for microcontroller used in SR-X

APPENDIX

Denavit Hartenberg representation

The basic transformations via Denavit Hartenberg convention equation are

$$A_i = R_{z,\theta_i} Trans_{x,a_i} R_{x,a_i}$$

$$= \begin{bmatrix} c_{\theta_i} & -s_{\theta_i} & 0 & 0 \\ s_{\theta_i} & c_{\theta_i} & 0 & 0 \\ 0 & 0 & 1 & 0 \\ 0 & 0 & 0 & 1 \end{bmatrix} \begin{bmatrix} 1 & 0 & 0 & 0 \\ 0 & 1 & 0 & 0 \\ 0 & 0 & 1 & d_i \\ 0 & 0 & 0 & 1 \end{bmatrix} \begin{bmatrix} 1 & 0 & 0 & a_i \\ 0 & 1 & 0 & 0 \\ 0 & 0 & 1 & 0 \\ 0 & 0 & 0 & 1 \end{bmatrix} \begin{bmatrix} 1 & 0 & 0 & 0 \\ 0 & c_{\alpha_i} & -s_{\alpha_i} & 0 \\ 0 & s_{\alpha_i} & c_{\alpha_i} & 0 \\ 0 & 0 & 0 & 1 \end{bmatrix}$$

$$= \begin{bmatrix} c_{\theta_i} & -s_{\theta_i} c_{\alpha_i} & s_{\theta_i} s_{\alpha_i} & a_i c_{\theta_i} \\ s_{\theta_i} & c_{\theta_i} c_{\alpha_i} & -c_{\theta_i} s_{\alpha_i} & a_i c_{\theta_i} \\ 0 & s_{\alpha_i} & c_{\alpha_i} & d_i \\ 0 & 0 & 0 & 1 \end{bmatrix}$$

REFERENCES

Ahn, H. S., Lee, D. W., Choi, D., Lee, D. Y., Lee, H. G., & Baeg, M. H. (2013). Development of an incarnate announcing robot system using emotional interaction with humans. *International Journal of Humanoid Robotics*, 10(02).

Arikawa, K., & Hirose, S. (2007). Mechanical design of walking machines.*Philosophical Transactions of the Royal Society of London A: Mathematical, Physical and Engineering Sciences*, *365*(1850), 171-183.

Arslan, S., & Temelta, H. (2011, December). Robust motion control of a four wheel drive skid-steered mobile robot. In *Electrical and Electronics Engineering (ELECO), 2011 7th International Conference on* (pp. II-415). IEEE.

Asbeck, A. T., Kim, S., Cutkosky, M. R., Provancher, W. R., & Lanzetta, M. (2006). Scaling hard vertical surfaces with compliant microspine arrays. *The International Journal of Robotics Research*, *25*(12), 1165-1179.

Autodesk. 2014. Inventor Professional. [ONLINE] Available at: http://www.autodesk.com/education/free-software/inventor-professional. [Accessed 1 January 2014].

Balaguer, C., Gimenez, A., & Jardón, A. (2005). Climbing robots' mobility for inspection and maintenance of 3D complex environments. *Autonomous Robots*, *18*(2), 157-169.

Bell, M., & Balkcom, D. (2006, May). A toy climbing robot. In *Proc. of the 2006 IEEE International Conference on Robotics and Automation* (pp. 4366-4368).

Berns, K., Braun, T., Hillenbrand, C., & Luksch, T. (2005). Developing climbing robots for education. In *Climbing and Walking Robots* (pp. 981-988). Springer Berlin Heidelberg.

Bicchi, A., & Kumar, V. (2000, April). Robotic grasping and contact: A review. In *ICRA* (pp. 348-353).

Borenstein, J., Everett, H. R., & Feng, L. (1996). Where am I? Systems and methods for mobile robot positioning. *Ann Arbor: University of Michigan Press*.

Botelho, W. T., Okada, T., & Shimizu, T. (2008, August). Smooth switching phases of a mobile robot from leg-type to wheel-type and vice versa. In *SICE Annual Conference, 2008* (pp. 687-690). IEEE.

Boulevard, J., Renaud, J.C. (2008), "POBOT: pole climbing robot", *IFMA Project, IFMA*, Houston, TX.

Calderon, C.A.A., Mohan, E.R. and Ng, B.S., (2015). Development of a hospital mobile platform for logistics tasks. *Digital Communications and Networks,* 1(2), pp.102-111.

Caracciolo, L., De Luca, A., & Iannitti, S. (1999). Trajectory tracking control of a four-wheel differentially driven mobile robot. In *Robotics and Automation, 1999. Proceedings. 1999 IEEE International Conference on* (Vol. 4, pp. 2632-2638). IEEE.

Chen, H., Sheng, W., Xi, N., & Tan, J. (2005, April). Motion control of a micro biped robot for nondestructive structure inspection. In *Robotics and Automation, 2005. ICRA 2005. Proceedings of the 2005 IEEE International Conference on* (pp. 478-483). IEEE.

Chen, S. C., Ko, C. C., Li, C. H., & Lin, P. C. (2012). Stair climbing in a quadruped robot. *International Journal of Automation and Smart Technology*, *2*(1), 11-20.

Chen, S. C., Huang, K. J., Li, C. H., & Lin, P. C. (2011, May). Trajectory planning for stair climbing in the leg-wheel hybrid mobile robot quattroped. In *Robotics and Automation (ICRA), 2011 IEEE International Conference on* (pp. 1229-1234). IEEE.

Clark, J., Goldman, D., Lin, P. C., Lynch, G., Chen, T., Komsuoglu, H., Full, R.J. and Koditschek, D.E., (2007, June). Design of a Bio-inspired Dynamical Vertical Climbing Robot. In *Robotics: Science and Systems*.

Dang V. N., Nguyen V. Q. K., (2010). Trajectory tracking control for four wheel skid-steering mobile robot. *Science and Technology Development Journal*, Vol 13.

Duan, X., Huang, Q., Rahman, N., Li, J., & Du, Q. (2006, October). Kinematic modeling of a small mobile robot with multi-locomotion modes. In *Intelligent Robots and Systems, 2006 IEEE/RSJ International Conference on* (pp. 5582-5587). IEEE.

Elliott, M., Morris, W., Calle, A., & Xiao, J. (2007, April). City-climbers at work. In *Robotics and Automation, 2007 IEEE International Conference on* (pp. 2764-2765). IEEE.

Fauroux, J. C., & Morillon, J. (2010). Design of a climbing robot for cylindro-conic poles based on rolling self-locking. *Industrial Robot: An International Journal*, *37*(3), 287-292.

García-López, M. C., Gorrostieta-Hurtado, E., Vargas-Soto, E., Ramos-Arreguín, J. M., Sotomayor-Olmedo, A., & Morales, J. M. (2012). Kinematic analysis for trajectory generation in one leg of a hexapod robot. *Procedia Technology*, *3*, 342-350.

Guo, J. L., Justham, L., Jackson, M., & Parkin, R. (2015). A concept selection method for designing climbing robots. *In Key Engineering Materials* (Vol. 649, pp. 22-29).

Haynes, G. C., Khripin, A., Lynch, G., Amory, J., Saunders, A., Rizzi, A. A., & Koditschek, D. E. (2009, May). Rapid pole climbing with a quadrupedal robot. In *Robotics and Automation, 2009. ICRA'09. IEEE International Conference on* (pp. 2767-2772). IEEE.

Hardt, M., & Von Stryk, O. (2000, October). Towards optimal hybrid control solutions for gait patterns of a quadruped. In *CLAWAR: Int. Conf. on Climbing and Walking Robots* (pp. 385-392).

Hirose, S. (1984). A study of design and control of a quadruped walking vehicle. *The International Journal of Robotics Research*, *3*(2), 113-133.

Hirose, S., Fukuda, Y., Yoneda, K., Nagakubo, A., Tsukagoshi, H., Arikawa, K., Endo, G., Doi, T. & Hodoshima, R. (2009). Quadruped walking robots at tokyo institute of technology: design, analysis, and gait control methods. *IEEE Robotics and Automation Magazine*, *16*(2), 104-114.

Hirose, S., Nagakubo, A., & Toyama, R. (1991, June). Machine that can walk and climb on floors, walls and ceilings. In *Advanced Robotics, 1991.'Robots in Unstructured Environments', 91 ICAR, Fifth International Conference on* (pp. 753-758). IEEE.

Howlader, M. O. F., & Sattar, T. P. (2015, September). Development of magnetic adhesion based climbing robot for non-destructive testing. *In Computer Science and Electronic Engineering Conference* (CEEC), 2015 7th (pp. 105-110). IEEE.

Indiveri, G. (2009). Swedish wheeled omnidirectional mobile robots: kinematics analysis and control. *IEEE transactions on robotics*, *25*(1), 164-171.

Inoue, K., Tsurutani, T., Takubo, T., & Arai, T. (2006, October). Omni-directional gait of limb mechanism robot hanging from grid-like structure. In *Intelligent Robots and Systems, 2006 IEEE/RSJ International Conference on* (pp. 1732-1737). IEEE.

InvenSense, 2013, MPU-6050 Six-Axis (Gyro + Accelerometer) MEMS Motion tracking Devisea [Online], Available: http://invensense.com/index.html [Accessed 21 January 13].

Kamen, D. (2001). The Segway® Personal Transporter (PT), the first self-balancing, zero emissions personal transportation vehicle.

Kawasaki, S., & Kikuchi, K. (2014). Development of a small legged wall climbing robot with passive suction cups. *In Proceedings of the 3rd International conference on design engineering and science*–ICDES (pp. 112-16).

Kim, S., Asbeck, A. T., Cutkosky, M. R., & Provancher, W. R. (2005, July). SpinybotII: climbing hard walls with compliant microspines. In *Advanced Robotics, 2005. ICAR'05. Proceedings, 12th International Conference on* (pp. 601-606). IEEE.

Kim, S., Jung, S. H., Lee, S. U., Kim, C. H., Shin, H. C., Seo, Y. C., Lee, N.H. & Jung, K. M. (2010, October). Application of robotics for the nuclear power plants in Korea. In *Applied Robotics for the Power Industry (CARPI), 2010 1st International Conference on* (pp. 1-5). IEEE.

Kubota, T., Kuroda, Y., Kunii, Y., & Nakatani, I. (2003). Small, light-weight rover "Micro5" for lunar exploration. *Acta Astronautica*, *52*(2), 447-453.

Lauria, M., Conti, F., Maeusli, P. A., Van Winnendael, M., Bertrand, R., & Siegwart, R. (1998). Design and control of an innovative micro-rover. In *None* (No. LSA-CONF-1998-010).

Leon-Rodriguez, H., Hussain, S., & Sattar, T. (2012, October). A compact wall-climbing and surface adaptation robot for non-destructive testing. *In Control, Automation and Systems (ICCAS), 2012 12th International Conference on* (pp. 404-409). IEEE.

Liu, J., Wan, Y., Ma, S., & Li, B. (2005, June). Analysis of stairs-climbing ability for a tracked reconfigurable modular robot. In *Safety, Security and Rescue Robotics, Workshop, 2005 IEEE International* (pp. 36-41). IEEE.

Longo, D., & Muscato, G. (2006). The Alicia 3 climbing robot: a three-module robot for automatic wall inspection. *Robotics & Automation Magazine, IEEE*, *13* (1), 42-50.

Lu, D., Dong, E., Liu, C., Xu, M., & Yang, J. (2013, November). Design and development of a leg-wheel hybrid robot "HyTRo-I". In *Intelligent Robots and Systems (IROS), 2013 IEEE/RSJ International Conference on* (pp. 6031-6036). IEEE.

Mahdavi, S., Noohi, E., & Ahmadabadi, M. N. (2006, December). Path planning of the nonholonomic pole climbing robot ut-pcr. In *Robotics and Biomimetics, 2006. ROBIO'06. IEEE International Conference on* (pp. 1517-1522). IEEE.

Malu, S. K., & Majumdar, J. (2014). Kinematics, Localization and Control of Differential Drive Mobile Robot. *Global Journal of Research and Engineering-GJRE-H*, *14*(1).

Mason, R., Rimon, E., & Burdick, J. (1997, April). Stable poses of 3-dimensional objects. In *Robotics and Automation, 1997. Proceedings, 1997 IEEE International Conference on* (Vol. 1, pp. 391-398). IEEE.

Menon, C., Murphy, M., & Sitti, M. (2004, August). Gecko inspired surface climbing robots. In *Robotics and Biomimetics, 2004. ROBIO 2004. IEEE International Conference on* (pp. 431-436). IEEE.

McGhee, R. B. (1985a). Vehicular legged locomotion. *Advances in Automation and Robotics*, *1*, 259-284.

McGhee, R. B., Orin, D. E., Pugh, D. R., & Patterson, M. R. (1985, May). A hierarchically-structured system for computer control of a hexapod walking machine. In *Theory and Practice of Robots and Manipulators, Proceedings of RoManSy-84 Symposium, A. Morecki, Ed. London: Hermes Publishing Co* (pp. 375-381).

Miyanaka, H., Wada, N., Kamegawa, T., Sato, N., Tsukui, S., Igarashi, H., & Matsuno, F. (2007, April). Development of an unit type robot" KOHGA2" with stuck avoidance ability. In *Robotics and Automation, 2007 IEEE International Conference on* (pp. 3877-3882). IEEE.

Murphy, F.E., Donovan, M., Cunningham, J., Jezequel, T., Garc, E., Jaeger, A., McCarthy, J. and Popovici, E.M., (2015), November. i4Toys: Video technology in toys for improved access to play, entertainment, and education. *In 2015 IEEE International Symposium on Technology and Society* (ISTAS) (pp. 1-6). IEEE.

Murphy, M. P., Kute, C., Mengüç, Y., & Sitti, M. (2011). Waalbot II: Adhesion recovery and improved performance of a climbing robot using fibrillar adhesives. *The International Journal of Robotics Research*, 30(1), 118-133.

Murphy, M. P., & Sitti, M. (2007). Waalbot: An agile small-scale wall-climbing robot utilizing dry elastomer adhesives. *Mechatronics, IEEE/ASME Transactions on*, *12*(3), 330-338.

NASA. (2009). Mars Science Laboratory: Integrating Science and Engineering Teams. [ONLINE] Available at: http://appel.nasa.gov/2009/03/01/mars-science-laboratory-integrating-science-and-engineering-teams/. [Accessed 21 January 16].

Nieto-Granda, C., Rogers, J. G., & Christensen, H. I. (2014). Coordination strategies for multi-robot exploration and mapping. *The International Journal of Robotics Research.*

Niku, S. B. (2001). *Introduction to robotics: analysis, systems, applications* (Vol. 7). New Jersey: Prentice Hall.

Nish, A., & Miyagi, H. (1994, September). Mechanism and control of propeller type wall-climbing robot. In *Intelligent Robots and Systems' 94.'Advanced Robotic Systems and the Real World', IROS'94. Proceedings of the IEEE/RSJ/GI International Conference on* (Vol. 3, pp. 1724-1729). IEEE.

Nourbaskhsh, I. R., & Siegwart, R. (2004). Introduction to autonomous mobile robots. *The MIT Press, Cambridge, Massachusetts, England, ISBN 0*, *262*(19502), 142-150.

Ogata, K. (2001). *Modern control engineering*. Prentice Hall PTR.

Ota, Y., Yoneda, K., Ito, F., Hirose, S., & Inagaki, Y. (2001a). Design and control of 6-DOF mechanism for twin-frame mobile robot. *Autonomous Robots*, *10*(3), 297-316.

Ota, Y., Yoneda, K., Muramatsu, Y., & Hirose, S. (2001b). Development of walking and task performing robot with bipedal configuration. In *Intelligent Robots and Systems, 2001. Proceedings. 2001 IEEE/RSJ International Conference on* (Vol. 1, pp. 247-252). IEEE.

Ota, Y., Yoneda, K., Tamaki, T., & Hirose, S. (2002). A walking and wheeled hybrid locomotion with twin-frame structure robot. In *Intelligent Robots and Systems, 2002. IEEE/RSJ International Conference on* (Vol. 3, pp. 2645-2651). IEEE.

Ota, Y., Tamaki, T., Yoneda, K., & Hirose, S. (2003, September). Development of walking manipulator with versatile locomotion. In *Robotics and Automation, 2003. Proceedings. ICRA'03. IEEE International Conference on* (Vol. 1, pp. 477-483). IEEE.

Park, S., Jeong, H. D., & Lim, Z. S. (2003, October). Design of a mobile robot system for automatic integrity evaluation of large size reservoirs and pipelines in industrial fields. In *Intelligent Robots and Systems, 2003. (IROS 2003). Proceedings. 2003 IEEE/RSJ International Conference on* (Vol. 3, pp. 2618-2623). IEEE.

Qian, Z. Y., Zhao, Y. Z., & Fu, Z. (2006, October). Development of wall-climbing robots with sliding suction cups. In *Intelligent Robots and Systems, 2006 IEEE/RSJ International Conference on* (pp. 3417-3422). IEEE.

Rimon, E., & Burdick, J. (1996, April). On force and form closure for multiple finger grasps. In *Robotics and Automation, 1996. Proceedings, 1996 IEEE International Conference on* (Vol. 2, pp. 1795-1800). IEEE.

Robotics Online. (2011). Robotics in Security and Military Applications. [ONLINE] Available at: http://www.robotics.org/content-detail.cfm/Industrial-Robotics-Industry-Insights/Robotics-in-Security-and-Military-Applications/content_id/3112. [Accessed 21 January 16].

Robotis. (2006). Open Source Project. [ONLINE] Available at: http://en.robotis.com/index/index.php. [Accessed 1 January 2014].

Şahin, E. (2004). Swarm robotics: From sources of inspiration to domains of application. In *Swarm robotics* (pp. 10-20). Springer Berlin Heidelberg.

Salem, F. A. (2013). Dynamic and Kinematic Models and Control for Differential Drive Mobile Robots. *International Journal of Current Engineering and Technology*, *3*(2), 253-263.

Sánchez, J., Vázquez, F., & Paz, E. (2006). Machine vision guidance system for a modular climbing robot used in shipbuilding. In *Climbing and Walking Robots* (pp. 893-900). Springer Berlin Heidelberg.

Santos, D., Kim, S., Spenko, M., Parness, A., & Cutkosky, M. (2007, April). Directional adhesive structures for controlled climbing on smooth vertical surfaces. In *Robotics and Automation, 2007 IEEE International Conference on* (pp. 1262-1267). IEEE.

Santos, P. G., Garcia, E., & Estremera, J. (2007). *Quadrupedal locomotion: an introduction to the control of four-legged robots*. Springer Science & Business Media.

Sato, M., Kanda, A., & Ishii, K. (2007, October). An environmental adaptive control system of a wheel type mobile robot for the rough terrain movement. In *Intelligent Robots and Systems, 2007. IROS 2007. IEEE/RSJ International Conference on* (pp. 3962-3967). IEEE.

Sitti, M., & Fearing, R. S. (2003, September). Synthetic gecko foot-hair micro/nano-structures for future wall-climbing robots. In *Robotics and Automation, 2003. Proceedings. ICRA'03. IEEE International Conference on* (Vol. 1, pp. 1164-1170). IEEE.

Song, S. M., & Waldron, K. J. (1989). *Machines that walk: the adaptive suspension vehicle*. MIT press.

Stoeter, S. A., Rybski, P. E., Gini, M., & Papanikolopoulos, N. (2002). Autonomous stair-hopping with scout robots. In *Intelligent Robots and Systems, 2002. IEEE/RSJ International Conference on* (Vol. 1, pp. 721-726). IEEE.

Tanaka, Y.; Arai, M.; Hirose, S. & Tsukui, S. (2006). Development of "Souryu-V" with MonoTread-Crawlers and Elastic-Rods Joint. *Proceedings of IEEE International Workshop on Safety Security and Rescue Robotics (SSRR2006)*.

Tavakoli, M., Viegas, C., Marques, L., Pires, J. N., & De Almeida, A. T. (2013). OmniClimbers: Omni-directional magnetic wheeled climbing robots for inspection of ferromagnetic structures. *Robotics and Autonomous Systems*, *61*(9), 997-1007.

Tedeschi, F., & Carbone, G. (2014, September). Towards the design of a leg-wheel walking hexapod. In *Mechatronic and Embedded Systems and Applications (MESA), 2014 IEEE/ASME 10th International Conference on* (pp. 1-6). IEEE.

Thueer, T., Lamon, P., & Krebs, A. (2006). *CRAB-Exploration rover with advanced obstacle negotiation capabilities*. Swiss Federal Institute of Technology (ETHZ), Autonomous Systems Lab.

Ting, L. H., Blickhan, R., & Full, R. J. (1994). Dynamic and static stability in hexapedal runners. *Journal of Experimental Biology*, *197*(1), 251-269.

Tsai, L. W. (1999). *Robot analysis: the mechanics of serial and parallel manipulators*. John Wiley & Sons.

Van Winnendael, M., Visentin, G., Bertrand, R., & Rieder, R. (1999). Nanokhod microrover heading towards Mars. *EUROPEAN SPACE AGENCY-PUBLICATIONS-ESA SP*, *440*, 69-76.

Wang, R., & Kawamura, Y. (2014, June). A magnetic climbing robot for steel bridge inspection. *In Intelligent Control and Automation (WCICA), 2014 11th World Congress on* (pp. 3303-3308). IEEE.

Wang, W., Zhang, H. X., Wang, K., Zhang, J. W., & Chen, W. H. (2009, July). Gait control of modular climbing caterpillar robot. *In 2009 IEEE/ASME International Conference on Advanced Intelligent Mechatronics* (pp. 957-962). IEEE.

Xiao, J., Sadegh, A., Elliott, M., & Calle, A. (2005). Design of mobile robots with wall climbing capability. In *Advanced Intelligent Mechatronics. Proceedings, 2005 IEEE/ASME International Conference on* (pp. 438-443). IEEE.

Yim, M., Duff, D. G., & Roufas, K. (2000, January). Modular reconfigurable robots, an approach to urban search and rescue. In *Proceedings of the 1st International Workshop on Human-friendly Welfare Robotics Systems, Taejon, Korea*.

Yoneda, K. (1987). The development of biped walking robot for HC-plane. In *Proc. of 5th Annual Conf. of RSJ* (pp. 585-586).

Yoshida, Y., & Ma, S. (2010, December). Design of a wall-climbing robot with passive suction cups. In *Robotics and Biomimetics (ROBIO), 2010 IEEE International Conference on* (pp. 1513-1518). IEEE.

Zhang, H., Zhang, J., Wang, W., Liu, R., & Zong, G. (2007). A series of pneumatic glass-wall cleaning robots for high-rise buildings. *Industrial Robot: An International Journal*, 34(2), 150-160.

Zhu, J., Sun, D., & Tso, S. K. (2002). Development of a tracked climbing robot. *Journal of Intelligent and Robotic Systems,* 35(4), 427-443.